

Weierstraß-Institut
für Angewandte Analysis und Stochastik
Leibniz-Institut im Forschungsverbund Berlin e. V.

Preprint

ISSN 2198-5855

**On the divergence constraint in mixed finite element methods
for incompressible flows**

Volker John¹, Alexander Linke², Christian Merdon², Michael Neilan³,

Leo G. Rebholz⁴

submitted: November 11, 2015

¹ Weierstrass Institute
Mohrenstr. 39, 10117 Berlin, Germany
and Free University of Berlin
Dep. of Mathematics and Computer Science
Arnimallee 6, 14195 Berlin, Germany
email: volker.john@wias-berlin.de

² Weierstrass Institute
Mohrenstr. 39, 10117 Berlin
Germany
email: alexander.linke@wias-berlin.de
christian.merdon@wias-berlin.de

³ University of Pittsburgh
Department of Mathematics
USA
email: neilan@pitt.edu

⁴ Clemson University
Department of Mathematical Sciences
USA
email: rebholz@clemson.edu

No. 2177
Berlin 2015



2010 *Mathematics Subject Classification.* 65N30, 76M10.

Key words and phrases. incompressible Navier–Stokes and Stokes equations, divergence-free properties, mixed finite elements, pressure-robust discretization.

Michael Neilan is partially supported by the National Science Foundation grant DMS–1417980 and the Alfred Sloan Foundation.

Leo G. Rebholz is partially supported by U.S. Army grant 65294-MA and National Science Foundation grant DMS–1522191.

Edited by
Weierstraß-Institut für Angewandte Analysis und Stochastik (WIAS)
Leibniz-Institut im Forschungsverbund Berlin e. V.
Mohrenstraße 39
10117 Berlin
Germany

Fax: +49 30 20372-303
E-Mail: preprint@wias-berlin.de
World Wide Web: <http://www.wias-berlin.de/>

Abstract. The divergence constraint of the incompressible Navier–Stokes equations is revisited in the mixed finite element framework. While many stable and convergent mixed elements have been developed throughout the past four decades, most classical methods relax the divergence constraint and only enforce the condition discretely. As a result, these methods introduce a pressure-dependent consistency error which can potentially pollute the computed velocity. These methods are not robust in the sense that a contribution from the right-hand side, which influences only the pressure in the continuous equations, impacts both velocity and pressure in the discrete equations. This paper reviews the theory and practical implications of relaxing the divergence constraint. Several approaches for improving the discrete mass balance or even for computing divergence-free solutions will be discussed: grad-div stabilization, higher order mixed methods derived on the basis of an exact de Rham complex, $\mathbf{H}(\text{div})$ -conforming finite elements, and mixed methods with an appropriate reconstruction of the test functions. Numerical examples illustrate both the potential effects of using non-robust discretizations and the improvements obtained by utilizing pressure-robust discretizations.

CONTENTS

1	The Navier–Stokes and the Stokes equations, goals and contents of the review	2
1.1	Examples that demonstrate difficulties of standard methods	2
1.2	Goals of the review	4
1.3	Outline of the review	6
1.4	Nomenclature	7
2	Variational formulation, Helmholtz–Hodge decomposition and the momentum balance	8
3	The lack of pressure-robustness for standard mixed methods	11
4	Pressure-robustness of weakly divergence-free mixed finite element methods	14
4.1	Stability and accuracy of pressure-robust mixed methods for the Stokes equations	15
4.2	The formal and the discrete vorticity equation	17
4.3	A tool to develop divergence-free elements: the de Rham Complex	19
4.4	$\mathbf{H}(\text{div})$ -conforming finite element methods	23
5	Improving the pressure-robustness of standard mixed finite elements	28
5.1	Grad-div stabilization	29
5.2	Using appropriate reconstructions of test functions	32
5.3	Post-processing of low order velocity fields computed with non-inf-sup stable methods	35
6	Numerical studies	35
7	Outlook	45

1. The Navier–Stokes and the Stokes equations, goals and contents of the review.

The Navier–Stokes equations are a fundamental model of incompressible Newtonian flows. They are used to model flows in pipes and channels, flows around objects such as the wing of a plane, and weather and climate, to name just a few. Developed in the mid 19th century, these equations have garnered great interest from mathematicians, engineers, and scientists. In their simplest form, and assuming constant fluid density, the equations are given in a domain $\Omega \subset \mathbb{R}^d$, $d \in \{2, 3\}$, and a time interval $(0, T)$, $T < \infty$, by

$$(1.1a) \quad \partial_t \mathbf{u} - \nu \Delta \mathbf{u} + (\mathbf{u} \cdot \nabla) \mathbf{u} + \nabla p = \mathbf{f},$$

$$(1.1b) \quad \nabla \cdot \mathbf{u} = 0,$$

where \mathbf{u} denotes the velocity of the fluid, p denotes the pressure, and ν is the kinematic viscosity. The nonlinear term $\mathbf{u} \cdot \nabla \mathbf{u} = (\mathbf{u} \cdot \nabla) \mathbf{u}$ represents the inertial force, while the term with the Laplace operator $\Delta \mathbf{u} := \sum_{i=1}^d \partial_{ii} \mathbf{u}$ encodes the viscous effects of the fluid. The given function \mathbf{f} takes into account external forces, e.g., gravity, buoyancy, and centrifugal forces, and the divergence constraint $\nabla \cdot \mathbf{u} = 0$ represents the incompressibility of the fluid, or equivalently in this setting, the conservation of mass.

The fact that the Navier–Stokes equations are a constrained system of partial differential equations poses fundamental mathematical and numerical difficulties. A basic model for studying the impact of the divergence constraint are the steady-state (scaled) Stokes equations, given by

$$(1.2a) \quad -\nu \Delta \mathbf{u} + \nabla p = \mathbf{f},$$

$$(1.2b) \quad -\nabla \cdot \mathbf{u} = g,$$

$$(1.2c) \quad \mathbf{u}|_{\partial\Omega} = \mathbf{0},$$

with the last equation representing no-slip boundary conditions. The divergence constraint $-\nabla \cdot \mathbf{u} = g$ originates, e.g., from transforming inhomogeneous Dirichlet boundary conditions to no-slip boundary conditions. One notes immediately that the analysis of the Stokes equations is simpler than for the Navier–Stokes equations, since the Stokes equations form a linear system and are not time-dependent.

A main goal of this review is to highlight and elaborate a type of non-robustness of many standard finite element methods for the Stokes and Navier–Stokes equations. This non-robustness is connected to the discretization of the divergence constraint (and not to the nonlinearity nor to dominating convection). The intended type of robustness is called pressure-robustness, which means that some mixed methods are robust with respect to large and complicated pressures and some are not. To avoid technicalities which do not concern the divergence constraint and its discretization, the numerical analysis presented herein is limited to the Stokes equations. However, it is directly relevant to more complex systems, and the fundamental ideas presented herein for the Stokes equations are extendable. The numerical studies consider the Stokes and Navier–Stokes equations, and also multiphysics systems.

1.1. Examples that demonstrate difficulties of standard methods. In the following, three simple numerical examples are presented which illustrate the lack of pressure-robustness in the numerical simulation of incompressible flow problems with standard finite element methods. All simulations were performed on uniformly refined grids using classical pairs of mixed finite elements: the mini element proposed in [4], the Taylor–Hood element from [42], and the non-conforming

Crouzeix–Raviart element [26].

EXAMPLE 1.1. No-flow problem for the Stokes equations. Consider the Stokes equations with $\nu = 1$ in $\Omega = (0, 1)^2$, no-slip boundary conditions and the right-hand side $\mathbf{f} = (0, \text{Ra}(1 - y + 3y^2))^T$, where $\text{Ra} > 0$ is a parameter. One finds that $\mathbf{u} = \mathbf{0}$, $p = \text{Ra}(y^3 - y^2/2 + y - 7/12)$ is the solution of this equation. Changing the parameter Ra in the right-hand side changes only the pressure. On the other hand, applying standard mixed finite element methods, one can also see an influence of this parameter on the discrete velocity, see Fig. 1.1. For both considered pairs of finite element spaces, the Taylor–Hood space $\mathcal{P}_2/\mathcal{P}_1$ and the non-conforming Crouzeix–Raviart space, the discrete velocity is far from being equal to zero, even for $\text{Ra} = 1$.

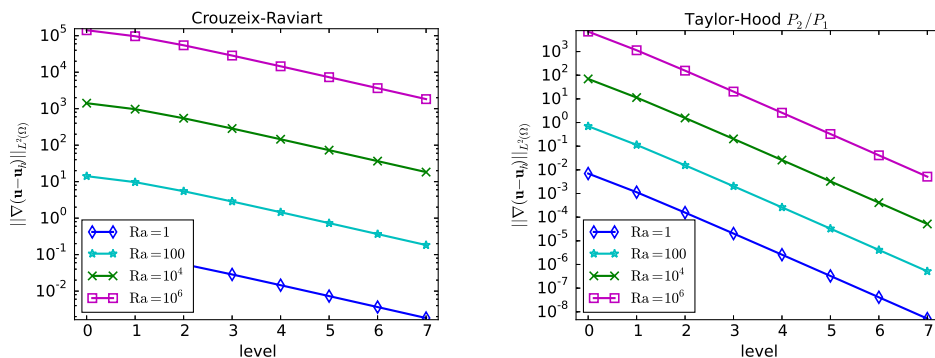


FIG. 1.1. *Example 1.1. Velocity errors in the no-flow problem for the Stokes equations.*

The impact on the discrete velocity of a term which only influences the pressure in the continuous case is one type of non-robustness which is studied here. By the construction of this example, this lack of robustness cannot be due to dominating convection or to the nonlinearity of the problem. It is clarified in this review that this lack of robustness is connected with the discretization of the divergence-free constraint in mixed finite element methods. Based on studying this issue carefully, a remedy which removes this instability for the Crouzeix–Raviart pair of finite element spaces was proposed in [50]. The underlying idea of this remedy is explained in Section 5.2 and the result of its application is shown in Example 6.1.

EXAMPLE 1.2. Stationary vortex. Consider the Navier–Stokes equations (1.1) with $\nu = 1$ in $\Omega = (-1, 1)^2$ with the prescribed solution

$$\mathbf{u} = \begin{pmatrix} -y \\ x \end{pmatrix}, \quad p = \text{Re} \left(\frac{x^2 + y^2}{2} - \frac{1}{3} \right), \quad \text{Re} > 0,$$

where Re is the Reynolds number, and with Dirichlet boundary conditions. The flow field has the form of a vortex and a direct calculation shows that $\mathbf{f} = \mathbf{0}$. Clearly, $\partial_t \mathbf{u} = \mathbf{0}$ and $\Delta \mathbf{u} = \mathbf{0}$. Hence, there is a balance of the nonlinear term of the Navier–Stokes equations and the pressure gradient.

In standard finite element error estimates, some norm of the solution appears on the right-hand side. In this example, one could think that the velocity errors are uniformly bounded since the velocity does not depend on Re . Instead, one observes in Fig. 1.2 that the errors are proportional to Re , i.e., the velocity error has the same scaling as the pressure.

This example shows that there is a negative impact of the pressure onto the discrete velocity. This influence is also a kind of non-pressure-robustness which by construction is not due to domi-

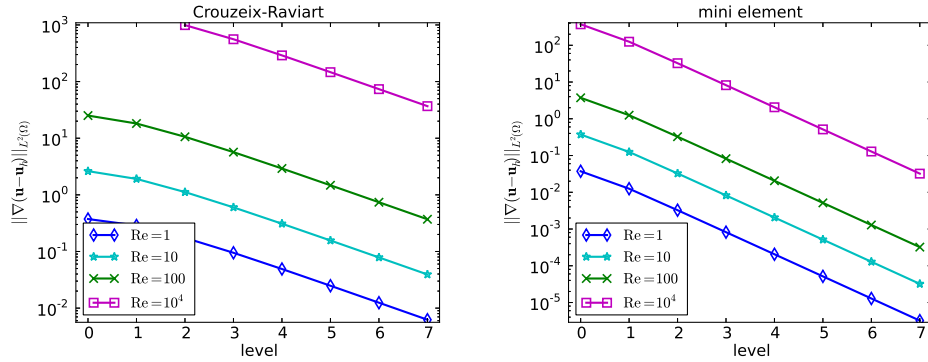


FIG. 1.2. *Example 1.2. Velocity errors for the stationary vortex.*

nating convection. A remedy in the case of the Crouzeix–Raviart finite element pair was proposed in [50], see Section 5.2 for the basic idea and Example 6.1 for numerical results.

EXAMPLE 1.3. Flow with Coriolis force. In some applications, such as meteorology, the Coriolis force acting on the flow field is of the utmost importance. The Coriolis force is modeled with the additional term $2\mathbf{w} \times \mathbf{u}$ on the left-hand side of the momentum balance of the Navier–Stokes equations (1.1), where \mathbf{w} is the vector of angular momentum.

Consider a flow field which is two-dimensional, i.e., $\mathbf{u} = (u_1, u_2, 0)$, $\mathbf{w} = y(0, 0, \omega/2)^T$, $\omega \in \mathbb{R}$, and assume that none of the functions of the problem depends on the third coordinate. Then one obtains a two-dimensional model, similar to the Navier–Stokes equations. In this model, the left-hand side of (1.1) contains the additional term $\omega y(-u_2, u_1)^T$. The y -dependence of the Coriolis force models in meteorology a latitude-dependence in a so-called β -plane approximation [64]. Here, a part of the Earth’s surface is approximated by a tangent plane and vertical velocities are neglected.

This problem is considered for the Navier–Stokes equations in $\Omega = (0, 10) \times (0, 1)$ with $\nu = 1$ and the prescribed solution

$$\mathbf{u} = \begin{pmatrix} 1 \\ 0 \end{pmatrix}, \quad p = \omega \left(-\frac{y^2}{2} + \frac{1}{6} \right) \quad \implies \quad \mathbf{f} = \mathbf{0},$$

and with Dirichlet boundary conditions. In meteorology, this situation would model a constant ocean current from west to east. For this solution, the first three terms of the momentum balance of the Navier–Stokes equations (1.1) vanish, while ∇p is balanced by the additional Coriolis force $2\mathbf{w} \times \mathbf{u}$.

Once again this is a problem where in the continuous setting the velocity does not depend on the parameter ω , but the pressure does. The numerical results presented in Fig. 1.3 show that this property is not inherited by standard pairs of mixed finite elements. The discrete velocity depends on ω and the error scales linearly with this parameter, i.e., it scales the same way as the pressure.

1.2. Goals of the review. A pressure-robust method in the sense studied in this review is a method for which modifications of the continuous problem that only affect the pressure lead to changes of the discrete solution that only affect the discrete pressure. Otherwise, the method is said to be non-pressure-robust. In Examples 1.1 – 1.3 it was shown that for non-pressure-robust methods there might be a large impact on the discrete velocity from modifications that only affect the pressure in the continuous equations.

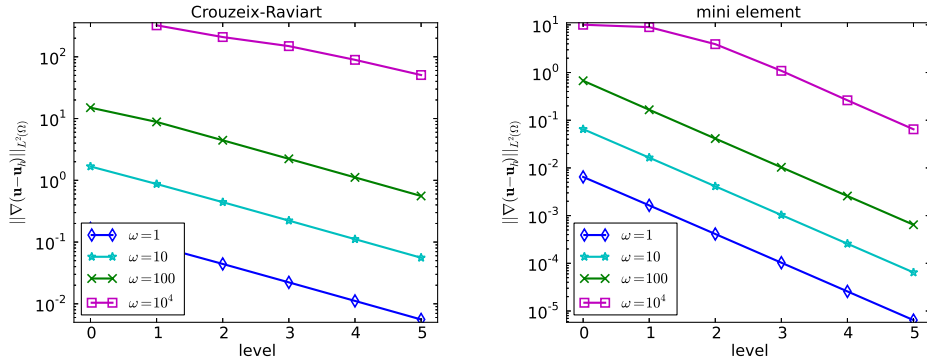


FIG. 1.3. Example 1.3. Velocity errors for the flow with Coriolis force.

Two fundamental observations concerning the Stokes (1.2) and Navier–Stokes equations (1.1) can be made immediately:

1. For solutions to exist, the divergence operator must possess a certain surjectivity property, the fundamental inf-sup compatibility condition: There exists a constant β such that

$$(1.3) \quad \inf_{q \in L_0^2(\Omega) \setminus \{0\}} \sup_{\mathbf{v} \in H_0^1(\Omega)^d \setminus \{\mathbf{0}\}} \frac{(\nabla \cdot \mathbf{v}, q)}{\|\nabla \mathbf{v}\|_{L^2(\Omega)} \|q\|_{L^2(\Omega)}} \geq \beta > 0.$$

Otherwise, the constraint $-\nabla \cdot \mathbf{u} = g$ cannot hold.

2. A fundamental invariance property holds: changing the external force by a gradient field changes only the pressure solution, and not the velocity; in symbols,

$$(1.4) \quad \mathbf{f} \rightarrow \mathbf{f} + \nabla \psi \quad \implies \quad (\mathbf{u}, p) \rightarrow (\mathbf{u}, p + \psi),$$

since the additional force field $\nabla \phi$ is balanced by the pressure gradient, and the no-slip boundary conditions do not involve the pressure.

These issues not only affect the continuous equations but also their discretizations. In this review, the effect of the second observation on finite element discretizations will be elaborated.

The significance of the first observation is well known, and forms a cornerstone of numerical analysis for the Stokes and Navier–Stokes equations. It comprises the fundamental finding that numerical schemes for approximating the Stokes and Navier–Stokes equations should satisfy a certain compatibility criterion between the discrete velocity and pressure spaces, in order to fulfill an appropriate surjectivity of the discrete divergence operator: the so-called discrete inf-sup stability. The need for discrete inf-sup stability results from the fact that the discrete velocity trial functions are constrained. The great practical value of discrete inf-sup stability is due to the fact that it provides a recipe for the construction of discretization schemes which lead to well posed problems, and whose solutions have (asymptotically) optimal convergence rates.

The significance of the second observation for the discretization of the Navier–Stokes equations has only recently begun to be realized [36]. As it is explained in detail in Section 4.2, the discrete divergence constraint induces a discrete rotation operator via the velocity test functions, since divergence-free vector test functions have a vector potential. Therefore, in every mixed finite element discretization for the Stokes problem (1.2) a *discrete vorticity equation* is hidden. For

discretization schemes satisfying (1.4) it holds exactly that $\nabla \times \nabla \psi \equiv 0$ for any differentiable ψ . However, classical mixed methods, which satisfy the discrete inf-sup condition, satisfy $\nabla \times \nabla \psi \equiv 0$ only approximately, up to some order of accuracy. In addition, (1.4) can be explained using the Helmholtz–Hodge projection, see Section 2, which is mathematically more rigorous.

The violation of (1.4) by a discretization might have severe consequences.

- As it is discussed in Section 3, the violation of (1.4) results in finite element error bounds for the velocity which depend on the pressure. Thus, large pressures may lead to large velocity errors, which has already been observed in Examples 1.1 – 1.3. Indeed, there are important applications, e.g., natural convection problems, where the pressure is larger than the velocity by orders of magnitude. In such situations, one cannot expect to compute accurate velocity fields with classical mixed methods.
- In the case $\nabla \cdot \mathbf{u} = 0$, one often expects in applications that the discrete computed velocity field is also divergence-free. Otherwise, the conservation of mass is violated. A violation of this conservation law is not tolerable in many applications.

It turns out that so-called *divergence-free mixed methods*, i.e., methods whose discrete velocity \mathbf{u}_h is in a sufficiently strong sense divergence-free (or in the general case $\nabla \cdot \mathbf{u}_h = g$ in a sufficiently strong sense), satisfy (1.4) and thus belong to the class of pressure-robust methods.

Another main goal is to review the construction of pressure-robust mixed methods that satisfy simultaneously the discrete inf-sup stability and (1.4). In the last decade, tremendous progress has been achieved in approaching this goal, though it seemingly was believed for more than thirty years that it would be (practically) impossible to construct such schemes. Indeed, the first pressure-robust mixed method on 3d tetrahedral grids was published only recently in 2005 [77]. Pressure-robust mixed methods in 2d reach back to 1983 [72], although they were rarely used in practice. Nowadays, three different approaches exist for the construction of pressure-robust mixed methods.

- The first approach, which is the most classical one, constructs *divergence-free mixed Galerkin schemes* such that the discrete velocity is H^1 -conforming and divergence-free. Here, novel ideas from the finite element exterior calculus have delivered a tremendous breakthrough, see Section 4.3.
- The second approach is due to recent Discontinuous Galerkin (DG) methods. Here, novel mixed schemes for (1.2) look for divergence-free, $H(\text{div})$ -conforming velocities, see Section 4.4. This regularity suffices to assure (1.4). Due to the relaxation of the H^1 -conformity of the velocity, the tangential velocity components are discretized in the DG framework.
- The third approach is very recent, and it is based on the observation that velocity trial and velocity test functions play a different role in order to guarantee discrete inf-sup stability and (1.4), see Section 5.2. Therefore, the resulting schemes are not of Galerkin type. For (1.2) a variational crime in the right-hand side of the momentum balance is applied, in order to replace discretely divergence-free velocity test functions by divergence-free ones. In the case of the Navier–Stokes equations, the variational crime must be applied also to the test function of the convective term and if a Coriolis force term is present, also to this term.

In addition, an approach for improving the pressure-robustness of classical mixed methods, the so-called grad-div stabilization, is presented in Section 5.1.

1.3. Outline of the review. An outline of this review paper is now given, and is immediately followed by a list of notation used throughout the manuscript. To focus on the goals of the review and to avoid technical details, this review will concentrate on the Stokes equations (1.2).

Section 2 recalls the variational formulation of the Stokes equations and presents the fundamen-

tal associated results. The momentum balance is discussed in detail, as is the invariance property that ‘changes to the irrotational part of the forcing only affect the pressure and do not alter the velocity’. The standard mixed finite element method for Stokes is given in Section 3, along with results for well-posedness under an inf-sup condition, and a general error estimate. It is discussed here that common element choices only enforce the divergence constraint discretely, and how this leads to pressure-dependent error estimates for the velocity.

Section 4 discusses pressure-robust mixed finite element methods for the Stokes equations. In particular, it is shown here that for special element choices, the divergence constraint is enforced exactly, and the velocity error does not depend on the pressure. Such methods are deemed *pressure-robust mixed methods* herein, as this property does not hold in most commonly used elements. Discrete invariance properties which are analogues of those found at the continuous level are also discussed in this section, and it is shown that they hold for pressure-robust mixed methods. A detailed description of the de Rham complex is then given, which is a tool to develop pressure-robust mixed methods. The section is concluded with a discussion of (non-conforming) $H(\text{div})$ mixed methods and how they can be used in a pressure-robust way.

The focus of Section 5 is on techniques that improve, or even fix, standard (non-pressure-robust) mixed methods. The topics discussed are grad-div stabilization and appropriate modification of test functions, which all serve the purpose of reducing or eliminating the pressure from the velocity error. Moreover, a kind of post-processing approach is discussed that produces divergence-free $H(\text{div})$ -conforming velocities from discretely divergence-free velocity fields. Such a post-processing is related to the discussed modification of test functions, and is interesting for the discretization of tracers described by convection-diffusion equations, see, e.g., [34]. Results and discussion for several numerical studies presented are presented in Section 6. The aim of this section is to show the types of problems where the methods discussed in this paper can make a significant improvement in solution accuracy, as well as problems where they do not make a difference.

1.4. Nomenclature. Throughout this review, standard notations will be used for function spaces.

$a(\cdot, \cdot)$	velocity-velocity bilinear form	$b(\cdot, \cdot)$	velocity-pressure bilinear form
C_F	Fortin operator constant	C_P	constant in Poincaré’s estimate
curl	vector curl operator	div	divergence operator
grad	gradient operator	β	continuous inf-sup constant
β_h	discrete inf-sup constant	Ra	Rayleigh number
\mathcal{T}_h	triangulation of Ω	Re	Reynolds number
\mathcal{E}_h	set of edges of \mathcal{T}_h	γ	parameter in grad-div stabilization
T	mesh cell of \mathcal{T}_h	ν	kinematic viscosity
e	mesh cell of \mathcal{E}_h	\mathbf{f}	body force
g	right-hand side of continuity equation	h	maximal value of h_T for given mesh
h_T	diameter of T	\mathbf{n}	outward unit normal to $\partial\Omega$
\mathbf{n}_T	outward unit normal to T	$\mathbb{P}(\cdot)$	Helmholtz–Hodge projector
p	pressure	p_h	finite element pressure
\mathcal{P}_k	space of globally continuous scalar-valued piecewise polynomials of degree not exceeding k	\mathcal{P}_k	space of globally continuous vector-valued piecewise polynomials of degree not exceeding k
\mathbf{u}	velocity	\mathbf{u}_h	finite element velocity

\mathcal{V}_h	set of vertices of \mathcal{T}_h	\mathbf{W}_h	non-conforming finite element velocity space
\mathbf{X}	velocity space, $\mathbf{H}_0^1(\Omega)$	\mathbf{X}_h	conforming finite element velocity space
\mathbf{X}_{div}	subspace of \mathbf{X} , containing the weakly divergence-free functions	$\mathbf{X}_{h,\text{div}}$	space of discretely divergence-free functions
$\mathbf{X}_{h,\text{div}}(g)$	manifold of functions with divergence equal to g	Y	pressure space, $L_0^2(\Omega)$
Y_h	finite element pressure space	π_F	Fortin operator
π	L^2 -projection to some space	Ω	domain
$\boldsymbol{\omega}$	vorticity	$\partial\Omega$	boundary of Ω
$\nabla \cdot_h$	discrete divergence operator	$[\![\cdot]\!]_\tau$	jump across edges/faces in 2d/3d

2. Variational formulation, Helmholtz–Hodge decomposition and the momentum balance. In this section, the variational formulation of the Stokes problem is introduced and the Helmholtz projector is discussed and its significance is emphasized for the (Navier–)Stokes momentum balance. The Helmholtz projector is of central importance for understanding the results obtained with mixed finite element methods, yet is generally not emphasized in the numerical analysis literature, or only in a posteriori error control [1, 21].

A weak solution to the incompressible Stokes equations (1.2) is defined as a pair $(\mathbf{u}, p) \in \mathbf{X} \times Y := \mathbf{H}_0^1(\Omega) \cap L_0^2(\Omega)$ satisfying

$$(2.1a) \quad a(\mathbf{u}, \mathbf{v}) + b(\mathbf{v}, p) = (\mathbf{f}, \mathbf{v}) \quad \forall \mathbf{v} \in \mathbf{X},$$

$$(2.1b) \quad b(\mathbf{u}, q) = (g, q) \quad \forall q \in Y,$$

where $L_0^2(\Omega)$ is the space of square integrable functions with vanishing mean. The bilinear forms are given by $a(\mathbf{w}, \mathbf{v}) = \nu(\nabla \mathbf{w}, \nabla \mathbf{v})$ and $b(\mathbf{v}, q) = -(\nabla \cdot \mathbf{v}, q)$, and (\cdot, \cdot) denotes the L^2 inner product over Ω . Note that vector-valued functions and vector-valued function spaces are denoted in boldface, e.g., $\mathbf{H}_0^1(\Omega) = (H_0^1(\Omega))^d$.

To analyze (2.1), the following partial integration formula for the divergence is recalled which allows the introduction of a *distributional divergence* and a *weak divergence*.

LEMMA 2.1. *For all $\psi \in H^1(\Omega)$ and $\mathbf{w} \in \mathbf{H}^1(\Omega)$ there holds*

$$\int_{\Omega} \psi \nabla \cdot \mathbf{w} \, d\mathbf{x} = - \int_{\Omega} \nabla \psi \cdot \mathbf{w} \, d\mathbf{x} + \int_{\partial\Omega} \psi \mathbf{w} \cdot \mathbf{n} \, ds.$$

The surface integral is understood as a duality pairing between the spaces $H^{\frac{1}{2}}(\partial\Omega)$ and $H^{-\frac{1}{2}}(\partial\Omega)$.

Proof. For smooth functions $\psi \in C^\infty(\Omega)$ and $\mathbf{w} \in \mathbf{C}^\infty(\Omega)$, the proof is a direct consequence of the vector calculus identity $\nabla \cdot (\psi \mathbf{w}) = \psi \nabla \cdot \mathbf{w} + \nabla \psi \cdot \mathbf{w}$ and the divergence theorem (integration by parts of the divergence term). Using the density of $C^\infty(\Omega)$ and $\mathbf{C}^\infty(\Omega)$ in $H^1(\Omega)$ and $\mathbf{H}^1(\Omega)$, respectively, gives the statement of the lemma. \square

This lemma motivates the introduction of the notion of a *distributional divergence*.

DEFINITION 2.2. *For a vector field $\mathbf{w} \in \mathbf{L}^1(\Omega)$ the mapping $C_0^\infty(\Omega) \rightarrow \mathbb{R}$ given by*

$$\psi \mapsto - \int_{\Omega} \nabla \psi \cdot \mathbf{w} \, d\mathbf{x}$$

is called the distributional divergence of \mathbf{w} .

The *weak divergence* is defined in the usual way of defining weak derivatives.

DEFINITION 2.3. *If for a vector field $\mathbf{w} \in \mathbf{L}^p(\Omega)$ with $p \geq 1$ there exists a function $\rho \in L^1_{\text{loc}}(\Omega)$ such that the distributional divergence can be represented in the form*

$$-\int_{\Omega} \nabla \psi \cdot \mathbf{w} \, d\mathbf{x} = \int_{\Omega} \psi \rho \, d\mathbf{x} \quad \forall \psi \in C_0^\infty(\Omega),$$

the function ρ is called the *weak divergence* of \mathbf{w} , abbreviated as $\rho := \nabla \cdot \mathbf{w}$. In particular, for divergence-free vector fields \mathbf{w} there holds

$$(2.2) \quad \int_{\Omega} \nabla \psi \cdot \mathbf{w} \, d\mathbf{x} = 0 \quad \forall \psi \in C_0^\infty(\Omega).$$

REMARK 2.4. *Loosely speaking, divergence-free vector fields are characterized by the fact that they are orthogonal in the $L^2(\Omega)$ scalar product to all gradient fields (with compact support). Classical mixed methods, whose construction is guided by the discrete inf-sup condition (3.2), usually violate this essential property. Its violation might lead to the lack of pressure-robustness as demonstrated in Examples 1.1 – 1.3.*

Considering in the divergence constraint (2.1b) a test function $q \in Y \cap C_0^\infty(\Omega)$, one obtains with the divergence theorem

$$\int_{\Omega} \nabla q \cdot \mathbf{u} \, d\mathbf{x} = \int_{\Omega} qg \, d\mathbf{x}.$$

Following Definition 2.3, $-g$ is the weak divergence of \mathbf{u} . This statement can be made more precise. Since \mathbf{u} satisfies no-slip boundary conditions, one finds by the divergence theorem that $0 = \int_{\partial\Omega} \mathbf{u} \cdot \mathbf{n} \, ds = \int_{\Omega} \nabla \cdot \mathbf{u} \, d\mathbf{x}$. Combining this identity with $\mathbf{u} \in \mathbf{H}^1(\Omega)$ implies that $\nabla \cdot \mathbf{u} \in Y$. Hence one can choose $q = \nabla \cdot \mathbf{u} - g$ in (2.1b), such that

$$(2.3) \quad \|\nabla \cdot \mathbf{u} + g\|_{L^2(\Omega)} = 0.$$

Thus $\nabla \cdot \mathbf{u} = -g$ in the sense of $L^2(\Omega)$.

DEFINITION 2.5. *The Hilbert space of vector fields that possess a weak divergence is defined by*

$$(2.4) \quad \mathbf{H}(\text{div}, \Omega) := \{\mathbf{w} \in \mathbf{L}^2(\Omega) : \nabla \cdot \mathbf{w} \in L^2(\Omega)\}.$$

Here, $\nabla \cdot \mathbf{w}$ is understood in the sense of Definition 2.3.

These definitions and lemmas allow to prove the Helmholtz–Hodge decomposition, a fundamental result for understanding the lack of pressure-robustness in classical mixed methods.

LEMMA 2.6 (Helmholtz–Hodge decomposition). *Let Ω be a connected domain. For every vector field $\mathbf{f} \in \mathbf{L}^2(\Omega)^d$, there exist a vector field $\mathbf{f}_0 \in \mathbf{H}(\text{div}, \Omega)$ and a scalar function $\phi \in H^1(\Omega)/\mathbb{R}$ with*

1. $\mathbf{f} = \mathbf{f}_0 + \nabla \phi$,
2. $\nabla \cdot \mathbf{f}_0 = 0$,
3. $(\mathbf{f}_0, \nabla \phi) = 0$.

The decomposition is unique.

Proof. The following Neumann problem is well-posed [37, pp. 40]: find $\phi \in H^1(\Omega)/\mathbb{R}$ such that

$$(2.5) \quad (\nabla \phi, \nabla \psi) = (\mathbf{f}, \nabla \psi) \quad \forall \psi \in H^1(\Omega)/\mathbb{R}.$$

Since $\mathbf{f} \in L^2(\Omega)^d$ and $\phi \in H^1(\Omega)$, it follows that $\mathbf{f}_0 := \mathbf{f} - \nabla\phi$ is in $L^2(\Omega)$. The uniqueness of ϕ implies also the uniqueness of \mathbf{f}_0 . By construction, it holds

$$(2.6) \quad (\mathbf{f}_0, \nabla\psi) = 0 \quad \forall \psi \in H^1(\Omega)/\mathbb{R}.$$

Since $C_0^\infty(\Omega)/\mathbb{R} \subset H^1(\Omega)/\mathbb{R}$, it follows that \mathbf{f}_0 is weakly divergence-free in the sense of Definition 2.3. In particular, $\nabla \cdot \mathbf{f}_0 = 0 \in L^2(\Omega)$ so that $\mathbf{f}_0 \in \mathbf{H}(\text{div}, \Omega)$. Choosing $\psi = \phi$ in (2.6) gives the third property stated in the lemma. \square

DEFINITION 2.7 (Helmholtz–Hodge projector). *The function $\mathbf{f}_0 =: \mathbb{P}(\mathbf{f})$ is called the Helmholtz–Hodge projector of \mathbf{f} .*

Using the Helmholtz–Hodge projector, the following existence, uniqueness, and stability estimates can be derived.

LEMMA 2.8. *Let $\mathbf{f} \in L^2(\Omega)$ and $g \in Y$. Then the Stokes problem (2.1) has a unique solution for which the following stability estimates hold*

$$(2.7a) \quad \|\nabla\mathbf{u}\|_{L^2(\Omega)} \leq \frac{C_P}{\nu} \|\mathbb{P}(\mathbf{f})\|_{L^2(\Omega)} + \frac{1}{\beta} \|g\|_{L^2(\Omega)},$$

$$(2.7b) \quad \|p\|_{L^2(\Omega)} \leq \frac{C_P}{\beta} \|\mathbf{f}\|_{L^2(\Omega)} + \frac{\nu}{\beta^2} \|g\|_{L^2(\Omega)},$$

where β is the inf-sup constant defined in (1.3).

Proof. Assume that there is a velocity solution $\mathbf{u} \in \mathbf{X}$. Define the divergence-free subspace

$$\mathbf{X}_{\text{div}} := \{\mathbf{v} \in \mathbf{X} : b(\mathbf{v}, q) = 0 \quad \forall q \in Y\}.$$

Then, \mathbf{u} can be orthogonally decomposed $\mathbf{u} = \mathbf{u}^0 + \mathbf{u}^\perp$ with respect to the scalar product $a(\cdot, \cdot)$ with $\mathbf{u}^0 \in \mathbf{X}_{\text{div}}$ and $\mathbf{u}^\perp \in \mathbf{X}_{\text{div}}^\perp$. It will be shown that both parts of this decomposition exist and are uniquely defined. Hence, \mathbf{u} also exists and is unique.

Due to the continuous inf-sup condition, the divergence operator is bijective from $\mathbf{X}_{\text{div}}^\perp$ to Y . Thus, there exists a unique $\mathbf{w}^\perp \in \mathbf{X}_{\text{div}}^\perp$ with $-\nabla \cdot \mathbf{w}^\perp = g$ and $\|\nabla\mathbf{w}^\perp\|_{L^2(\Omega)} \leq \frac{1}{\beta} \|g\|_{L^2(\Omega)}$. Since $\nabla \cdot \mathbf{u} = \nabla \cdot \mathbf{u}^\perp$, condition (2.1b) enforces $\mathbf{u}^\perp = \mathbf{w}^\perp$. Consequently \mathbf{u}^\perp is uniquely given and

$$(2.8) \quad \|\nabla\mathbf{u}^\perp\|_{L^2(\Omega)} \leq \frac{1}{\beta} \|g\|_{L^2(\Omega)}.$$

The divergence-free part \mathbf{u}^0 is determined by testing (2.1a) with an arbitrary divergence-free function $\mathbf{v}^0 \in \mathbf{X}_{\text{div}}$. One obtains, using on the left-hand side the a -orthogonality and on the right-hand side the L^2 -orthogonality against \mathbf{X}_{div}

$$(2.9) \quad a(\mathbf{u}, \mathbf{v}^0) + b(p, \mathbf{v}^0) = (\mathbf{f}, \mathbf{v}^0) \quad \iff \quad a(\mathbf{u}^0, \mathbf{v}^0) = (\mathbb{P}(\mathbf{f}), \mathbf{v}^0).$$

Applying the Lax–Milgram theorem, it follows that \mathbf{u}^0 is uniquely defined due to the coercivity of $a(\cdot, \cdot)$. The Cauchy–Schwarz inequality and Poincaré’s inequality for $\mathbf{v}^0 = \mathbf{u}^0$ yield

$$\nu \|\nabla\mathbf{u}^0\|_{L^2(\Omega)}^2 \leq \|\mathbb{P}(\mathbf{f})\|_{L^2(\Omega)} \|\mathbf{u}^0\|_{L^2(\Omega)} \leq C_P \|\mathbb{P}(\mathbf{f})\|_{L^2(\Omega)} \|\nabla\mathbf{u}^0\|_{L^2(\Omega)}.$$

Division by $\|\nabla\mathbf{u}^0\|_{L^2(\Omega)}$, the decomposition of \mathbf{u} and estimate (2.8) give (2.7a).

The pressure p is now obtained by testing (2.1a) with arbitrary functions $\mathbf{v}^\perp \in \mathbf{X}_{\text{div}}^\perp$, yielding

$$(2.10) \quad a(\mathbf{u}, \mathbf{v}^\perp) + b(p, \mathbf{v}^\perp) = (\mathbf{f}, \mathbf{v}^\perp) \quad \iff \quad (p, \nabla \cdot \mathbf{v}^\perp) = -(\mathbf{f}, \mathbf{v}^\perp) + a(\mathbf{u}^\perp, \mathbf{v}^\perp).$$

Again, since $\nabla \cdot : \mathbf{X}_{\text{div}}^\perp \rightarrow Y$ is a bijection, p is uniquely determined by (2.10). For proving the stability estimate of the pressure, one chooses the unique $\mathbf{v}_p \in \mathbf{X}_{\text{div}}^\perp$ such that holds $\nabla \cdot \mathbf{v}_p = p$ and $\|\nabla \mathbf{v}_p\|_{L^2(\Omega)} \leq \frac{1}{\beta} \|p\|_{L^2(\Omega)}$. Inserting \mathbf{v}_p into (2.10), using the Cauchy–Schwarz and Poincaré estimates, and (2.8) yields

$$\begin{aligned} \|p\|_{L^2(\Omega)}^2 &\leq C_P \|\mathbf{f}\|_{L^2(\Omega)} \|\nabla \mathbf{v}_p\|_{L^2(\Omega)} + \nu \|\nabla \mathbf{u}^\perp\|_{L^2(\Omega)} \|\nabla \mathbf{v}_p\|_{L^2(\Omega)} \\ &\leq \frac{C_P}{\beta} \|\mathbf{f}\|_{L^2(\Omega)} \|p\|_{L^2(\Omega)} + \frac{\nu}{\beta^2} \|g\|_{L^2(\Omega)} \|p\|_{L^2(\Omega)}, \end{aligned}$$

which proves (2.7b). \square

The Helmholtz–Hodge projector allows to justify the fundamental invariance property (1.4) in a mathematically rigorous way. First, the following corollary is proved:

COROLLARY 2.9. *The Helmholtz projector $\mathbb{P}(\nabla\phi)$ of a gradient field $\nabla\phi$ with $\phi \in H^1(\Omega)/\mathbb{R}$ vanishes, i.e., $\mathbb{P}(\nabla\phi) = \mathbf{0}$.*

Proof. Taking $\mathbf{f} = \nabla\phi$, it follows from the first property given in Lemma 2.6 that $\mathbf{f}_0 = \mathbf{0}$ and consequently $\mathbb{P}(\mathbf{f}) = \mathbb{P}(\nabla\phi) = \mathbf{0}$. \square

This corollary allows to conclude the fundamental invariance property (1.4) rigorously.

LEMMA 2.10. *Let $\mathbf{f} \in \mathbf{L}^2(\Omega)$, then it holds for the Stokes problem (2.1) that changing the right-hand side by $\mathbf{f} \rightarrow \mathbf{f} + \nabla\psi$, with $\psi \in H^1(\Omega)/\mathbb{R}$, leads to a change of the solution by $(\mathbf{u}, p) \rightarrow (\mathbf{u}, p + \psi)$.*

Proof. Let the Stokes solutions for the forcings \mathbf{f} and $\mathbf{f} + \nabla\psi$ be denoted by (\mathbf{u}, p) and $(\mathbf{u}_\psi, p_\psi)$, respectively. Both solutions are decomposed, $\mathbf{u} = \mathbf{u}^0 + \mathbf{u}^\perp$ and $\mathbf{u}_\psi = \mathbf{u}_\psi^0 + \mathbf{u}_\psi^\perp$ with $\mathbf{u}^0, \mathbf{u}_\psi^0 \in \mathbf{X}_{\text{div}}$ and $\mathbf{u}^\perp, \mathbf{u}_\psi^\perp \in \mathbf{X}_{\text{div}}^\perp$. Since (2.1b) is satisfied in both cases, it follows that $b(\mathbf{u}^\perp - \mathbf{u}_\psi^\perp, q) = 0$ for all $q \in Y$ such that from the continuous inf-sup condition (1.3) it follows that $\mathbf{u}^\perp = \mathbf{u}_\psi^\perp$. The divergence-free parts \mathbf{u}^0 and \mathbf{u}_ψ^0 are determined by (2.9) and they are equal, since it holds $\mathbb{P}(\mathbf{f} + \nabla\psi) = \mathbb{P}(\mathbf{f})$ according to corollary 2.9. Using $\mathbf{u}^\perp = \mathbf{u}_\psi^\perp$, equation (2.10) for (\mathbf{u}, p) , and integration by parts gives the following pressure equation for the forcing

$$(p_\psi, \nabla \cdot \mathbf{v}^\perp) = -(\mathbf{f} + \nabla\psi, \mathbf{v}^\perp) + a(\mathbf{u}^\perp, \mathbf{v}^\perp) = (p + \psi, \nabla \cdot \mathbf{v}^\perp) \quad \forall \mathbf{v}^\perp \in \mathbf{X}_{\text{div}}^\perp.$$

Therefore, the fundamental invariance property (1.4) holds. \square

3. The lack of pressure-robustness for standard mixed methods. This section presents the basic finite element formulation for the Stokes problem and the error analysis for the velocity error $\|\nabla(\mathbf{u} - \mathbf{u}_h)\|_{L^2(\Omega)}$. In particular, it is pointed out why the pressure cannot be removed from the a priori velocity error bound for standard mixed methods.

A *finite element method* poses the variational formulation (2.1) onto a pair of finite-dimensional spaces consisting of piecewise polynomials. In particular, if $\mathbf{X}_h \times Y_h \subset \mathbf{X} \times Y$ denotes a pair of conforming piecewise polynomial spaces with respect to a partition \mathcal{T}_h of Ω (parameterized by h), then a Galerkin finite element method for the Stokes equations seeks $(\mathbf{u}_h, p_h) \in \mathbf{X}_h \times Y_h$ such that

$$(3.1a) \quad a(\mathbf{u}_h, \mathbf{v}_h) + b(\mathbf{v}_h, p_h) = (\mathbf{f}, \mathbf{v}_h) \quad \forall \mathbf{v}_h \in \mathbf{X}_h,$$

$$(3.1b) \quad b(\mathbf{u}_h, q_h) = (g, q_h) \quad \forall q_h \in Y_h.$$

The discrete problem (3.1) is an example of a *mixed finite element method* in which two finite element spaces are present in the formulation. In such methods, the finite element spaces \mathbf{X}_h and Y_h must be *compatible* in order to guarantee the existence and uniqueness of a solution as well as

convergence as the discretization parameter tends to zero. In the case of the Stokes (and Navier–Stokes) equations, the compatibility requirement is a surjective property of the divergence operator. In particular, a necessary condition for the existence and stability of a solution of problem (3.1) is the discrete inf-sup condition

$$(3.2) \quad \inf_{q_h \in Y_h \setminus \{0\}} \sup_{\mathbf{v}_h \in \mathbf{X}_h \setminus \{\mathbf{0}\}} \frac{(\nabla \cdot \mathbf{v}_h, q_h)}{\|\nabla \mathbf{v}_h\|_{L^2(\Omega)} \|q_h\|_{L^2(\Omega)}} \geq \beta_h > 0.$$

For stability and optimal order convergence, it is required that $\beta_h \geq \beta_0 > 0$ as $h \rightarrow 0^+$.

Setting $\mathbf{v}_h = \mathbf{u}_h$ in (3.1a), $q_h = -p_h$ in (3.1b), and adding the two equations gives

$$\nu \|\nabla \mathbf{u}_h\|_{L^2(\Omega)}^2 = (\mathbf{f}, \mathbf{u}_h) - (g, p_h),$$

which implies that zero data $\mathbf{f} \equiv \mathbf{0}$ and $g = 0$ yield a zero solution $\mathbf{u}_h \equiv \mathbf{0}$. Since the problem is linear, uniqueness of the discrete velocity solution is guaranteed, independent of the choice of finite element spaces. With uniqueness of the velocity established, the uniqueness of the pressure follows immediately by assuming two solutions and inserting the corresponding finite element problems into the discrete inf-sup condition (3.2). The existence of solutions follows from the uniqueness, since the problem is linear and finite-dimensional.

The discrete divergence operator $\nabla \cdot_h : \mathbf{X}_h \rightarrow Y_h$ is defined with the help of the L^2 -projection

$$(\nabla \cdot_h \mathbf{v}_h, q_h) = (\nabla \cdot \mathbf{v}_h, q_h) \quad \forall q_h \in Y_h.$$

Condition (3.2) implies that this operator is surjective from \mathbf{X}_h onto Y_h , with a bounded right-inverse. Many finite element pairs have been developed that satisfy the discrete inf-sup condition (3.2) with $\beta_h \geq \beta_0 > 0$ as $h \rightarrow 0^+$. A popular example is the family of Taylor–Hood finite element pairs $\mathcal{P}_k/\mathcal{P}_{k-1}$, $k \geq 2$. In the mini element [4], it is $Y_h = \mathcal{P}_1$ and the velocity space consists of continuous linear functions that are enriched with local bubble functions to satisfy (3.2). An enrichment of the velocity space with bubble functions for the same reason is also used for the Bernardi–Raugel element [14], where the base polynomial spaces are \mathcal{P}_2 for the velocity and discontinuous piecewise linears for the pressure. A first-order variant in the same paper is based on piecewise constant pressures and \mathcal{P}_1 for the velocity enriched by normal-weighted face bubbles.

In the finite element problem, the divergence-free condition is enforced only by (3.1b). Note that the pairs of spaces just mentioned satisfy $\nabla \cdot_h \mathbf{X}_h = Y_h$ but lack the inclusion $\nabla \cdot \mathbf{X}_h \subset Y_h$. If $\nabla \cdot \mathbf{X}_h \not\subset Y_h$, it cannot be expected that $\|\nabla \cdot \mathbf{u}_h\|_{L^2(\Omega)} = 0$. In fact it is known that this quantity can become quite large in simulations with common element choices such as the Taylor–Hood pair $\mathcal{P}_2/\mathcal{P}_1$, see [22].

To derive finite element error estimates, under the assumptions that the discrete inf-sup condition (3.2) holds for the pair $\mathbf{X}_h \times Y_h$ and that $\nabla \cdot \mathbf{X}_h \not\subset Y_h$, consider the manifold

$$(3.3) \quad \mathbf{X}_{h,\text{div}}(g) := \{\mathbf{v}_h \in \mathbf{X}_h : (\nabla \cdot \mathbf{v}_h, q_h) = (g, q_h) \quad \forall q_h \in Y_h\}.$$

In the case $g = 0$, the abbreviation $\mathbf{X}_{h,\text{div}} = \mathbf{X}_{h,\text{div}}(0)$ will be used, i.e., $\mathbf{X}_{h,\text{div}}$ is the space of *discretely divergence-free functions*, which is the kernel of the discrete divergence operator. Note that, because of $\nabla \cdot \mathbf{X}_h \not\subset Y_h$, functions from $\mathbf{X}_{h,\text{div}}$ are generally not divergence-free in the sense of $L^2(\Omega)$ and hence it follows that $\mathbf{X}_{h,\text{div}} \not\subset \mathbf{X}_{\text{div}}$. Since $\mathbf{X}_{h,\text{div}} \subset \mathbf{X}_h \subset \mathbf{X}$, test functions from $\mathbf{X}_{h,\text{div}}$ can be used as test functions in the continuous problem (2.1a) as well as in the finite element

problem (3.1). Taking such test functions, $q_h = 0$, and subtracting both equations gives the error equation

$$(3.4) \quad a(\mathbf{u} - \mathbf{u}_h, \mathbf{v}_h) + b(\mathbf{v}_h, p - p_h) = 0 \quad \forall \mathbf{v}_h \in \mathbf{X}_{h,\text{div}}.$$

Because of the special choice of test function there holds $b(\mathbf{v}_h, p_h) = 0$, and therefore the discrete pressure can be removed from the error equation. However, since $\mathbf{X}_{h,\text{div}} \not\subset \mathbf{X}_{\text{div}}$, the continuous pressure does not vanish in general. At this point it is not possible to remove the dependency of the velocity error on the pressure. The best that can be done is to add $b(\mathbf{v}_h, q_h) = 0$ for arbitrary $q_h \in Y_h$ to the left-hand side of the error equation. Decomposing the error into

$$\mathbf{u} - \mathbf{u}_h = (\mathbf{u} - I_h \mathbf{u}) - (\mathbf{u}_h - I_h \mathbf{u}) =: \boldsymbol{\eta} - \boldsymbol{\phi}_h$$

for arbitrary $I_h \mathbf{u} \in \mathbf{X}_{h,\text{div}}$, inserting this decomposition into (3.4), and taking as test function $\mathbf{v}_h = \boldsymbol{\phi}_h$ yields

$$\nu \|\nabla \boldsymbol{\phi}_h\|_{L^2(\Omega)}^2 = \nu(\nabla \boldsymbol{\eta}, \nabla \boldsymbol{\phi}_h) - (\nabla \cdot \boldsymbol{\phi}_h, p - q_h) \quad \forall q_h \in Y_h.$$

The terms on the right-hand side are estimated by the Cauchy–Schwarz inequality and the estimate $\|\nabla \cdot \boldsymbol{\phi}_h\|_{L^2(\Omega)} \leq \|\nabla \boldsymbol{\phi}_h\|_{L^2(\Omega)}$ (which holds with constant 1 for functions with homogeneous Dirichlet boundary conditions). Dividing by $\nu \|\nabla \boldsymbol{\phi}_h\|_{L^2(\Omega)} \neq 0$ (the other case is trivial), one obtains

$$\|\nabla \boldsymbol{\phi}_h\|_{L^2(\Omega)} \leq \|\nabla \boldsymbol{\eta}\|_{L^2(\Omega)} + \nu^{-1} \|p - q_h\|_{L^2(\Omega)} \quad \forall q_h \in Y_h.$$

Finally, one gets with the triangle inequality

$$(3.5) \quad \|\nabla(\mathbf{u} - \mathbf{u}_h)\|_{L^2(\Omega)} \leq 2 \inf_{I_h \mathbf{u} \in \mathbf{X}_{h,\text{div}}} \|\nabla(\mathbf{u} - I_h \mathbf{u})\|_{L^2(\Omega)} + \nu^{-1} \inf_{q_h \in Y_h} \|p - q_h\|_{L^2(\Omega)}.$$

The error estimate (3.5) shows that the bound for the velocity error $\|\nabla(\mathbf{u} - \mathbf{u}_h)\|_{L^2(\Omega)}$ depends on the best approximation error of the pressure which is scaled with the inverse of the viscosity. This term becomes large if ν is small or if the best approximation error is large. Estimating the best approximation error with some interpolation error, one obtains a bound which contains the norm of the pressure in some Sobolev space. Examples 1.1 – 1.3 already show that the bound obtained in this way is sharp in the sense that large norms of the pressure dominate the velocity error and the error scales the same way as the pressure does.

REMARK 3.1. *It is useful to summarize the different meanings of a function being ‘divergence-free’ introduced so far. In the strong form the the Navier–Stokes equations (1.1) classical derivatives are used and \mathbf{u} is pointwise divergence-free. The property of a vector field to be weakly divergence-free is given in (2.2). For functions $\mathbf{v} \in \mathbf{X}$, this property is equivalent to $\|\nabla \cdot \mathbf{v}\|_{L^2(\Omega)} = 0$, see (2.3) for $g = 0$. Finally, (conforming) discretely divergence-free vector fields are defined in (3.3). Clearly, a pointwise divergence-free field is weakly and discretely divergence-free. Also, a weakly divergence-free field from \mathbf{X} is discretely divergence-free. However, a discretely divergence-free field is usually neither pointwise nor weakly divergence-free.*

REMARK 3.2. *Since discretely divergence-free vector fields are generally not weakly divergence-free, the question of the error in the divergence arises. From $\|\nabla \cdot (\mathbf{u} - \mathbf{u}_h)\|_{L^2(\Omega)} \leq \|\nabla(\mathbf{u} - \mathbf{u}_h)\|_{L^2(\Omega)}$ one gets that this error is bounded with the same order as the error of the gradient of the velocity.*

In particular for $g = 0$, this estimate means $\|\nabla \cdot \mathbf{u}_h\|_{L^2(\Omega)} \leq \|\nabla(\mathbf{u} - \mathbf{u}_h)\|_{L^2(\Omega)}$. In numerical simulations one finds that both sides of this estimate possess in fact generally the same order of

convergence. Thus, large errors $\|\nabla(\mathbf{u} - \mathbf{u}_h)\|_{L^2(\Omega)}$ usually induce a bad (local) conservation of mass.

REMARK 3.3. Consider the case $g = 0$. Then, one gets with the divergence theorem that

$$(3.6) \quad 0 = \int_{\partial\Omega} \mathbf{u}_h \cdot \mathbf{n} \, ds = \int_{\Omega} \nabla \cdot \mathbf{u}_h \, d\mathbf{x},$$

such that mass is conserved in this global sense.

If discontinuous pressure spaces $Y_h \subset Y$ are used, one has even a more local mass conservation. Since the piecewise constant functions are usually a subspace of a discontinuous pressure finite element space, one obtains from (2.1b)

$$(3.7) \quad 0 = \sum_{T \in \mathcal{T}_h} \int_T (\nabla \cdot \mathbf{u}_h) q_h \, d\mathbf{x} = \sum_{T \in \mathcal{T}_h} q_h \int_T \nabla \cdot \mathbf{u}_h \, d\mathbf{x}$$

for all $q_h \in \mathcal{P}_0$. Considering an arbitrary mesh cell T_1 and another arbitrary mesh cell $T_2 \neq T_1$. Then one can choose

$$q_h = \begin{cases} 1 & \text{in } T_1, \\ -\frac{|T_1|}{|T_2|} & \text{in } T_2, \\ 0 & \text{else.} \end{cases}$$

With this choice, $q_h \in Y_h$. One gets with (3.7)

$$\int_{T_2} \nabla \cdot \mathbf{u}_h \, d\mathbf{x} = \frac{|T_2|}{|T_1|} \int_{T_1} \nabla \cdot \mathbf{u}_h \, d\mathbf{x} \quad \forall T_2 \in \mathcal{T}_h.$$

It follows that

$$(3.8) \quad \begin{aligned} \int_{\Omega} \nabla \cdot \mathbf{u}_h \, d\mathbf{x} &= \sum_{T \in \mathcal{T}_h} \int_T \nabla \cdot \mathbf{u}_h \, d\mathbf{x} = \sum_{T \in \mathcal{T}_h} \frac{|T|}{|T_1|} \int_{T_1} \nabla \cdot \mathbf{u}_h \, d\mathbf{x} \\ &= \frac{1}{|T_1|} \int_{T_1} \nabla \cdot \mathbf{u}_h \, d\mathbf{x} \sum_{T \in \mathcal{T}_h} |T| = \frac{|\Omega|}{|T_1|} \int_{T_1} \nabla \cdot \mathbf{u}_h \, d\mathbf{x}. \end{aligned}$$

From (3.6) one concludes that the last factor on the right-hand side of (3.8) vanishes. Since T_1 was chosen to be arbitrary, one obtains the local mass conservation

$$(3.9) \quad \int_T \nabla \cdot \mathbf{u}_h \, d\mathbf{x} = 0 \quad \forall T \in \mathcal{T}_h.$$

Note that the local mass conservation (3.9) does not necessarily imply that the error $\|\nabla \cdot \mathbf{u}_h\|_{L^2(\Omega)}$ is smaller in comparison with methods which use a continuous space Y_h .

4. Pressure-robustness of weakly divergence-free mixed finite element methods.

4.1. Stability and accuracy of pressure-robust mixed methods for the Stokes equations. In this section, mixed finite element error estimates for the discrete incompressible Stokes equations (3.1) are derived for inf-sup stable conforming element pairs $\mathbf{X}_h \subset \mathbf{X}$, $Y_h \subset Y$ that satisfy $\nabla \cdot \mathbf{X}_h \subset Y_h$. It will be shown that the condition $\nabla \cdot \mathbf{X}_h \subset Y_h$ ensures pressure-robustness in the sense that the discrete velocity error does not depend on the pressure. Due to this condition it holds $\mathbf{X}_{h,\text{div}} \subset \mathbf{X}_{\text{div}}$. The inf-sup stability of the element pair (\mathbf{X}_h, Y_h) ensures the existence of a so-called Fortin operator $\pi_F : \mathbf{X} \rightarrow \mathbf{X}_h$ such that for all $\mathbf{v} \in \mathbf{X}$ and for all $q_h \in Y_h$ holds $(\nabla \cdot \mathbf{v}, q_h) = (\nabla \cdot \pi_F(\mathbf{v}), q_h)$ with $\|\nabla \pi_F(\mathbf{v})\|_{L^2(\Omega)} \leq C_F \|\nabla \mathbf{v}\|_{L^2(\Omega)}$, see [32].

REMARK 4.1. *Standard reasoning shows that the discrete inf-sup stability is indeed equivalent to the existence of a Fortin interpolator. However, the same standard reasoning can only show that the stability constant of the Fortin interpolator satisfies $C_F \leq 1/\beta_h$, which is usually too pessimistic [52, 75]. Note that the discrete inf-sup constant is in inverse proportion to the aspect ratio of the domain [23, 27, 28]. Likewise, classical mixed finite element error estimates, which involve the inverse of the discrete inf-sup constant, are very pessimistic on domains with large aspect ratio like channel domains – which occur often in computational practice. Estimates containing the stability constant C_F are much sharper [75], and will be preferred in the following.*

In perfect analogy to the continuous case, one obtains for the discrete solution of (3.1) the following results.

LEMMA 4.2. *Let the finite element spaces $\mathbf{X}_h \subset \mathbf{X}$ and $Y \subset Y_h$ satisfy the discrete inf-sup stability (3.2) and let $\nabla \cdot \mathbf{X}_h \subset Y_h$. Then, for $\mathbf{f} \in \mathbf{L}^2(\Omega)$ and $g \in Y$, the Stokes problem (3.1) has a unique discrete solution, for which the following stability estimates hold*

$$(4.1a) \quad \|\nabla \mathbf{u}_h\|_{L^2(\Omega)} \leq \frac{C_P}{\nu} \|\mathbb{P}(\mathbf{f})\|_{L^2(\Omega)} + \frac{1}{\beta_h} \|g\|_{L^2(\Omega)},$$

$$(4.1b) \quad \|p_h\|_{L^2(\Omega)} \leq \frac{C_P}{\beta_h} \|\mathbf{f}\|_{L^2(\Omega)} + \frac{\nu}{\beta_h^2} \|g\|_{L^2(\Omega)}.$$

Proof. The proof is line by line the same as in Lemma 2.8, i.e., replace \mathbf{X} by \mathbf{X}_h , change the words continuous inf-sup condition (with stability constant β) by discrete inf-sup condition (with stability constant β_h), and note that $\mathbf{X}_{h,\text{div}} \subset \mathbf{X}_{\text{div}}$ holds. The discrete space $\mathbf{X}_{h,\text{div}}^\perp$ is defined by a-orthogonality in the space \mathbf{X} . \square

LEMMA 4.3. *Let the finite element spaces $\mathbf{X}_h \subset \mathbf{X}$ and $Y \subset Y_h$ fulfill the discrete inf-sup stability (3.2) and $\nabla \cdot \mathbf{X}_h \subset Y_h$. Then, it holds for all $\mathbf{w} \in \mathbf{X}$ with $\mathbf{w} \in \mathbf{X}_{\text{div}}(g)$*

$$(4.2) \quad \inf_{\mathbf{w}_h \in \mathbf{X}_{h,\text{div}}(g)} \|\nabla(\mathbf{w} - \mathbf{w}_h)\|_{L^2(\Omega)} \leq (1 + C_F) \inf_{\mathbf{v}_h \in \mathbf{X}_h} \|\nabla(\mathbf{w} - \mathbf{v}_h)\|_{L^2(\Omega)}.$$

Proof. Let $\mathbf{v}_h \in \mathbf{X}_h$ be arbitrary and define $\mathbf{z}_h := \pi_F(\mathbf{w} - \mathbf{v}_h) \in \mathbf{X}_h$. Due to the properties of the Fortin interpolant one has $\|\nabla \mathbf{z}_h\|_{L^2(\Omega)} \leq C_F \|\nabla(\mathbf{w} - \mathbf{v}_h)\|_{L^2(\Omega)}$ and $(\nabla \cdot \mathbf{z}_h, q_h) = (\nabla \cdot (\mathbf{w} - \mathbf{v}_h), q_h)$ for all $q_h \in Y_h$. Then, it is $\mathbf{w}_h := \mathbf{z}_h + \mathbf{v}_h \in \mathbf{X}_{h,\text{div}}(g)$ since

$$\begin{aligned} (\nabla \cdot \mathbf{w}_h, q_h) &= (\nabla \cdot \mathbf{z}_h, q_h) + (\nabla \cdot \mathbf{v}_h, q_h) = (\nabla \cdot (\mathbf{w} - \mathbf{v}_h), q_h) + (\nabla \cdot \mathbf{v}_h, q_h) \\ &= -(g, q_h) \quad \forall q_h \in Y_h. \end{aligned}$$

Finally, the triangle inequality gives

$$\|\nabla(\mathbf{w} - \mathbf{w}_h)\|_{L^2(\Omega)} \leq \|\nabla(\mathbf{w} - \mathbf{v}_h)\|_{L^2(\Omega)} + \|\nabla \mathbf{z}_h\|_{L^2(\Omega)} \leq (1 + C_F) \|\nabla(\mathbf{w} - \mathbf{v}_h)\|_{L^2(\Omega)}.$$

□

LEMMA 4.4. *Let the finite element spaces $\mathbf{X}_h \subset \mathbf{X}$ and $Y \subset Y_h$ satisfy the discrete inf-sup stability (3.2) with $\nabla \cdot \mathbf{X}_h \subset Y_h$, and let $\pi_{Y_h} p \in Y_h$ be the L^2 -projection of p defined by*

$$(p - \pi_{Y_h} p, q_h) = 0 \quad \forall q_h \in Y_h.$$

Then, for the unique discrete solution (\mathbf{u}_h, p_h) of (3.1), there hold the following a-priori error estimates

$$(4.4a) \quad \begin{aligned} \|\nabla(\mathbf{u} - \mathbf{u}_h)\|_{L^2(\Omega)} &\leq 2 \inf_{\mathbf{w}_h \in \mathbf{X}_{h,\text{div}}(g)} \|\nabla(\mathbf{u} - \mathbf{w}_h)\|_{L^2(\Omega)} \\ &\leq 2(1 + C_F) \inf_{\mathbf{w}_h \in \mathbf{X}_h} \|\nabla(\mathbf{u} - \mathbf{w}_h)\|_{L^2(\Omega)}, \end{aligned}$$

$$(4.4b) \quad \|\pi_{Y_h} p - p_h\|_{L^2(\Omega)} \leq \frac{\nu}{\beta_h} \|\nabla(\mathbf{u} - \mathbf{u}_h)\|_{L^2(\Omega)},$$

$$(4.4c) \quad \|p - p_h\|_{L^2(\Omega)} \leq \|p - \pi_{Y_h} p\|_{L^2(\Omega)} + \frac{\nu}{\beta_h} \|\nabla(\mathbf{u} - \mathbf{u}_h)\|_{L^2(\Omega)}.$$

Proof. For an arbitrary $\mathbf{w}_h \in \mathbf{X}_{h,\text{div}}(g)$ it holds $\mathbf{v}_h^0 := \mathbf{u}_h - \mathbf{w}_h \in \mathbf{X}_{h,\text{div}}$. Using the Galerkin orthogonality and the Cauchy–Schwarz inequality yields

$$\begin{aligned} \nu \|\nabla \mathbf{v}_h^0\|_{L^2(\Omega)}^2 &= a(\mathbf{v}_h^0, \mathbf{v}_h^0) = a(\mathbf{u}_h - \mathbf{w}_h, \mathbf{v}_h^0) = a(\mathbf{u} - \mathbf{w}_h, \mathbf{v}_h^0) \\ &\leq \nu \|\nabla(\mathbf{u} - \mathbf{w}_h)\|_{L^2(\Omega)} \|\nabla \mathbf{v}_h^0\|_{L^2(\Omega)} \implies \|\nabla \mathbf{v}_h^0\|_{L^2(\Omega)} \leq \|\nabla(\mathbf{u} - \mathbf{w}_h)\|_{L^2(\Omega)}. \end{aligned}$$

Now, the triangle inequality gives

$$\|\nabla(\mathbf{u} - \mathbf{u}_h)\|_{L^2(\Omega)} \leq \|\nabla(\mathbf{u} - \mathbf{w}_h)\|_{L^2(\Omega)} + \|\nabla \mathbf{v}_h^0\|_{L^2(\Omega)} \leq 2\|\nabla(\mathbf{u} - \mathbf{w}_h)\|_{L^2(\Omega)},$$

which proves the first inequality of (4.4a), since $\mathbf{w}_h \in \mathbf{X}_{h,\text{div}}(g)$ was chosen arbitrarily. The second inequality is a direct consequence of Lemma 4.3.

The proof for (4.4b) exploits the assumption $\nabla \cdot \mathbf{X}_h \subset Y_h$. Hence, one obtains for all $\mathbf{v}_h \in \mathbf{X}_h$

$$(4.5) \quad (\pi_{Y_h} p - p_h, \nabla \cdot \mathbf{v}_h) = (\pi_{Y_h} p - p_h, q_h) = (p - p_h, q_h) = \nu(\nabla(\mathbf{u} - \mathbf{u}_h), \nabla \mathbf{v}_h),$$

where the last step uses the definitions of the continuous and discrete Stokes problem (2.1) and (3.1), respectively. Using the discrete inf-sup condition (3.2), (4.5), and the Cauchy–Schwarz inequality yields

$$\begin{aligned} \|\pi_{Y_h} p - p_h\|_{L^2(\Omega)} &\leq \frac{1}{\beta_h} \sup_{\mathbf{v}_h \in \mathbf{X}_h \setminus \{0\}} \frac{(\pi_{Y_h} p - p_h, \nabla \cdot \mathbf{v}_h)}{\|\nabla \mathbf{v}_h\|_{L^2(\Omega)}} \\ &\leq \frac{1}{\beta_h} \sup_{\mathbf{v}_h \in \mathbf{X}_h \setminus \{0\}} \frac{\nu \|\nabla(\mathbf{u} - \mathbf{u}_h)\|_{L^2(\Omega)} \|\nabla \mathbf{v}_h\|_{L^2(\Omega)}}{\|\nabla \mathbf{v}_h\|_{L^2(\Omega)}} = \frac{\nu}{\beta_h} \|\nabla(\mathbf{u} - \mathbf{u}_h)\|_{L^2(\Omega)}. \end{aligned}$$

Statement (4.4c) follows with the triangle inequality. □

REMARK 4.5. *The error estimates in Lemma 4.4 show that the discrete velocity converges with an asymptotically optimal order to the continuous velocity (in case of sufficiently regular velocity), and that the velocity error is pressure-independent. This remarkable feature distinguishes pressure-robust mixed methods from classical mixed methods. Interestingly, something similar can be observed*

for the discrete pressure. According to (4.4c), the discrete pressure is the best approximation of the continuous pressure in $L^2(\Omega)$ up to an additive error that is only velocity-dependent. This property has been rarely emphasized so far in the context of mixed finite element methods for the (Navier–) Stokes equations. Moreover, the inverse of the discrete inf-sup constant β_h enters only the pressure estimates. In addition, it occurs only in the part of the error bound which is scaled by ν and therefore this term is usually small. In the velocity estimates, the constant C_F for an appropriate Fortin interpolant replaces the classical constant $1/\beta_h$.

The error estimates show that for pressure-robust mixed methods there holds an invariance principle, similar to the continuous problem, see Lemma 2.10.

LEMMA 4.6. *Let the finite element spaces $\mathbf{X}_h \subset \mathbf{X}$ and $Y \subset Y_h$ fulfill the discrete inf-sup stability (3.2) and $\nabla \cdot \mathbf{X}_h \subset Y_h$. Then, for the unique discrete solution (\mathbf{u}_h, p_h) of (3.1) holds the following discrete fundamental invariance property: changing the right-hand side $\mathbf{f} \rightarrow \mathbf{f} + \nabla\psi$ with $\mathbf{f} \in L^2(\Omega)^d$ and $\psi \in H^1(\Omega)/\mathbb{R}$ leads to a change of the discrete solution in the form $(\mathbf{u}_h, p_h) \rightarrow (\mathbf{u}_h, p_h + \pi_{Y_h}\psi)$.*

Proof. The continuous and discrete solution operators $(\mathbf{f}, g) \rightarrow (\mathbf{u}, p)$ and $(\mathbf{f}, g) \rightarrow (\mathbf{u}_h, p_h)$ are linear. Hence, it suffices to study (2.1) and (3.1) for the right-hand side $(\nabla\psi, 0)$. The solutions of these special continuous and discrete problems are also denoted by (\mathbf{u}, p) and (\mathbf{u}_h, p_h) . Due to Corollary 2.9 it holds $\mathbb{P}(\nabla\psi) \equiv \mathbf{0}$, and the stability estimates from the Lemmata 2.8 and 4.2 yield $\mathbf{u} \equiv \mathbf{0}$ and $\mathbf{u}_h \equiv \mathbf{0}$. Moreover, the continuous fundamental invariance property from Lemma 2.10 gives $(\mathbf{u}, p) = (\mathbf{0}, \psi)$. Since $\|\nabla(\mathbf{u} - \mathbf{u}_h)\|_{L^2(\Omega)} = 0$, estimate (4.4b) allows to conclude that $(\mathbf{u}_h, p_h) = (\mathbf{0}, \pi_{Y_h}\psi)$, and the discrete fundamental invariance property is proven. \square

Altogether, it has been shown in this section that pressure-robust mixed methods possess a number of attractive properties.

4.2. The formal and the discrete vorticity equation. It has been shown that testing with a divergence-free test function in the continuous setting (2.9) or testing with a discretely divergence-free function in the discrete setting (3.4) allows one to derive elliptic problems that determine the velocity solution. Next, it will be argued that these elliptic problems indeed represent a formal vorticity equation and a discrete vorticity equation which characterize the difference between classical mixed methods and pressure-robust mixed methods.

The formal vorticity equation in the continuous setting. Here, the case $d = 3$ will be discussed; the two-dimensional case follows similar arguments. For an arbitrary divergence-free vector field $\mathbf{v} \in \mathbf{X}_{\text{div}} \cap C_0^\infty(\Omega)$, there exists a vector potential $\boldsymbol{\xi} \in C_0^\infty(\Omega)$ with $\mathbf{v} = \nabla \times \boldsymbol{\xi}$. Testing the momentum balance of (1.2) with \mathbf{v} , assuming that $(\mathbf{u}, p) \in \mathbf{H}^3(\Omega) \cap H^1(\Omega)$ and $\nabla \times \mathbf{f} \in L^2(\Omega)$, and applying integration by parts yields

$$(-\nu\Delta\mathbf{u}, \nabla \times \boldsymbol{\xi}) + (\nabla p, \nabla \times \boldsymbol{\xi}) = (\mathbf{f}, \nabla \times \boldsymbol{\xi}) \iff (-\nu\Delta\boldsymbol{\omega}, \boldsymbol{\xi}) = (\nabla \times \mathbf{f}, \boldsymbol{\xi}),$$

where the notation $\boldsymbol{\omega} := \nabla \times \mathbf{u}$ for the vorticity is used and the identity $\nabla \times (\nabla p) \equiv \mathbf{0}$ was applied. This equation shows that the vorticity satisfies formally, i.e., assuming sufficient regularity, the diffusion equation

$$(4.6) \quad -\nu\Delta\boldsymbol{\omega} = \nabla \times \mathbf{f}.$$

Note that the formal vorticity equation is derived from the strong form that corresponds to the weak velocity equation

$$(4.7) \quad a(\mathbf{u}, \mathbf{v}) = (\mathbf{f}, \mathbf{v}) = (\mathbb{P}(\mathbf{f}), \mathbf{v}) \quad \forall \mathbf{v} \in \mathbf{X}_{\text{div}},$$

which defines \mathbf{u} (together with the statement $-\nabla \cdot \mathbf{u} = g$) uniquely. This formal vorticity equation reflects perfectly the fundamental invariance property (1.4), since for the two forcings \mathbf{f} and $\mathbf{f} + \nabla\phi$ the same vorticity equation arises due to

$$\nabla \times (\mathbf{f} + \nabla\phi) = \nabla \times \mathbf{f}.$$

Therefore, the velocity \mathbf{u} and its vorticity $\boldsymbol{\omega}$ do not change, and the additional forcing $\nabla\phi$ only affects the pressure. In fact, the appearance of the Helmholtz projector $\mathbb{P}(\mathbf{f})$ in (4.7) corresponds to the dependence of the formal vorticity equation (4.6) on $\nabla \times \mathbf{f}$ (and not on \mathbf{f}). It should be noted that similar formal vorticity equations can also be derived for the time-dependent Navier–Stokes equations by testing with divergence-free vector fields.

REMARK 4.7. *The L^2 -orthogonality of gradient fields and divergence-free vector fields with compact support is equivalent to the vector calculus statements ‘gradient fields are irrotational’ and ‘curl fields are divergence-free’. Indeed, for $\mathbf{v} = \nabla \times \boldsymbol{\xi} \in \mathbf{X}_{\text{div}} \cap \mathbf{C}_0^\infty(\Omega)$, an integration by parts shows*

$$0 = \int_{\Omega} \nabla\phi \cdot \mathbf{v} \, d\mathbf{x} = \int_{\Omega} \nabla\phi \cdot \nabla \times \boldsymbol{\xi} \, d\mathbf{x} = \int_{\Omega} \underbrace{(\nabla \times \nabla\phi)}_{\equiv 0} \cdot \boldsymbol{\xi} \, d\mathbf{x} = - \int_{\Omega} \phi \underbrace{(\nabla \cdot (\nabla \times \boldsymbol{\xi}))}_{\equiv 0} \, d\mathbf{x}.$$

In classical mixed methods the L^2 -orthogonality between gradient fields and discretely divergence-free test functions is relaxed. This property is equivalent to a relaxation of ‘gradient fields are irrotational’.

REMARK 4.8. *The importance of the two operators divergence and curl for characterizing vector fields will be illustrated further with the following theorem from [8]: For a simply-connected bounded region $\Omega \subset \mathbb{R}^3$ with a surface $\partial\Omega$ consisting of a union of a finite number of disjoint closed C^2 surfaces, there is a uniquely defined vector field $\mathbf{v} \in L^2(\Omega)^d$, which fulfills*

$$\nabla \cdot \mathbf{v} = g \text{ in } \Omega, \quad \nabla \times \mathbf{v} = \boldsymbol{\omega} \text{ in } \Omega, \quad \mathbf{v} \cdot \mathbf{n} = 0 \text{ in } \partial\Omega,$$

for given $g \in L_0^2(\Omega)$ and $\boldsymbol{\omega} \in C^1(\Omega)^3$ with $\nabla \cdot \boldsymbol{\omega} = 0$. The main message of this theorem is that information on the divergence and the curl of a vector field, together with some boundary data, determines the vector field completely. This result emphasizes the significance of the formal vorticity equation, since divergence and boundary data are always prescribed for the Navier–Stokes equations and only the curl of the velocity field is unknown.

Discrete vorticity equations for classical and pressure-robust mixed methods. In (conforming) mixed finite element methods for the Stokes equations, the discrete velocity solution is determined by

$$a(\mathbf{u}_h, \mathbf{v}_h) = (\mathbf{f}, \mathbf{v}_h)$$

for all $\mathbf{v}_h \in \mathbf{X}_{h,\text{div}}$. Introducing a discrete Helmholtz projector $\mathbb{P}_h : L^2(\Omega)^d \rightarrow \mathbf{X}_{h,\text{div}}$, defined as the L^2 -projection onto $\mathbf{X}_{h,\text{div}}$, this formulation can be written as

$$(4.8) \quad a(\mathbf{u}_h, \mathbf{v}_h) = (\mathbb{P}_h(\mathbf{f}), \mathbf{v}_h)$$

for all $\mathbf{v}_h \in \mathbf{X}_{h,\text{div}}$. Similarly to the continuous setting, cf. Remark 4.7, where (4.7) is understood as a formal weak vorticity equation, testing with a (discretely) divergence-free vector field is considered as a weak application of a curl operator, which yields the *discrete vorticity equation* (4.8).

In the case of pressure-robust methods with $\mathbf{X}_{h,\text{div}} \subset \mathbf{X}_{\text{div}}$ there obviously holds $\mathbb{P}_h(\nabla\phi) = \mathbf{0}$ for all $\phi \in H^1(\Omega)$, and the discrete vorticity equation

$$(4.9) \quad a(\mathbf{u}_h, \mathbf{v}_h) = -\nu(\Delta\mathbf{u}, \mathbf{v}_h)$$

for all $\mathbf{v}_h \in \mathbf{X}_{h,\text{div}}$ is *pressure-independent*.

In contrast, in the case of classical mixed methods with $\mathbf{X}_{h,\text{div}} \not\subset \mathbf{X}_{\text{div}}$, one has for all $\mathbf{v}_h \in \mathbf{X}_{h,\text{div}}$

$$(4.10) \quad a(\mathbf{u}_h, \mathbf{v}_h) = (\mathbb{P}_h(\mathbf{f}), \mathbf{v}_h) = -\nu(\Delta\mathbf{u}, \mathbf{v}_h) + (\mathbb{P}_h(\nabla p), \mathbf{v}_h),$$

and one obtains with the definition of \mathbb{P}_h , integration by parts, $(\pi_{Y_h} p, \nabla \cdot \mathbf{v}_h) = 0$, and the approximation estimate for the L^2 -projection (assuming that p is sufficiently regular)

$$|(\mathbb{P}_h(\nabla p), \mathbf{v}_h)| = |(\nabla p, \mathbf{v}_h)| = |(p, \nabla \cdot \mathbf{v}_h)| = |(p - \pi_{Y_h} p, \nabla \cdot \mathbf{v}_h)| \leq Ch^k |p|_{H^k(\Omega)} \|\nabla \cdot \mathbf{v}_h\|_{L^2(\Omega)}.$$

Compared with (4.9), equation (4.10) contains the additional term $(\mathbb{P}_h(\nabla p), \mathbf{v}_h)$ with $\mathbf{v}_h \in \mathbf{X}_{h,\text{div}}$. It is this term that distinguishes *pressure-robust mixed methods* from *classical mixed methods*. It can be understood as a *pressure-dependent* consistency error of the discrete vorticity equation of classical mixed methods. Of course, this consistency error vanishes with optimal order, whenever p is regular enough. However, it can be arbitrarily large, depending on the given flow problem.

REMARK 4.9. *Testing a vector field \mathbf{w} with a smooth compactly supported divergence-free vector field $\mathbf{v} = \nabla \times \boldsymbol{\xi} \in \mathbf{X}_{\text{div}}$ equals the application of a distributional curl operator $\mathbf{C}_0^\infty(\Omega) \rightarrow \mathbb{R}$ to the vector field \mathbf{w}*

$$(\mathbf{w}, \mathbf{v}) = (\mathbf{w}, \nabla \times \boldsymbol{\xi}).$$

This distributional curl operator vanishes for all $\mathbf{w} = \nabla\phi$.

Similarly, one can define a discrete distributional curl operator $\mathbf{C}_0^\infty(\Omega) \rightarrow \mathbb{R}$ by

$$(\mathbf{w}, \mathbb{P}_h(\nabla \times \boldsymbol{\xi})).$$

Then, the discrete distributional curl of pressure-robust mixed methods vanishes for all $\mathbf{w} = \nabla\phi$, while for the discrete distributional curl operator of classical mixed methods there holds

$$|(\nabla\phi, \mathbb{P}_h(\nabla \times \boldsymbol{\xi}))| \leq \mathcal{O}(h^k) |\phi|_{H^k(\Omega)}.$$

REMARK 4.10. *In Lemma 4.6 it was shown that pressure-robust mixed methods satisfy a fundamental invariance property, which is in perfect analogy to the continuous result from Lemma 2.10. However, for classical mixed methods there also holds a (much weaker) discrete fundamental invariance property, which is equivalent to the statement that the discrete curl operator of classical mixed methods fulfills $\nabla_h \times \nabla\phi \equiv \mathcal{O}(h^k) |\phi|_{H^k(\Omega)}$: changing $\mathbf{f} \rightarrow \mathbf{f} + \nabla\psi_h$ by some discrete $\psi_h \in Y_h$ implies that $(\mathbf{u}_h, p_h) \rightarrow (\mathbf{u}_h, p_h + \psi_h)$. For discontinuous pressure spaces Y_h , the expression $\nabla\psi_h$ is to be understood as a discrete distributional gradient $\mathbf{v}_h \rightarrow -(\psi_h, \nabla \cdot \mathbf{v}_h)$.*

4.3. A tool to develop divergence-free elements: the de Rham Complex. During the past 30 years, the construction of de Rham sub-complexes consisting of finite element spaces has been an invaluable tool to develop stable finite element pairs for problems in porous media flow,

electromagnetics, and linear elasticity [5, 6, 19, 56]. The key idea of this program is to mimic the algebraic and topological properties found at the continuous level to obtain mixed finite element spaces with enhanced stability properties and that preserve physical quantities of interest. The culmination of these ideas and tools is the finite element exterior calculus framework [5, 6], where canonical finite element spaces are developed in arbitrary dimensions for the Hodge Laplacian. However, only recently have these tools and ideas been applied to the Navier–Stokes problem to obtain divergence-free finite element pairs.

To explain the main ideas, it is first recalled that the two-dimensional de Rham complex with minimal L^2 smoothness is given by the sequence of mappings

$$(4.11) \quad \mathbb{R} \longrightarrow H^1(\Omega) \xrightarrow{\mathbf{curl}} \mathbf{H}(\operatorname{div}, \Omega) \xrightarrow{\operatorname{div}} L^2(\Omega) \longrightarrow 0,$$

where $\mathbf{curl} := (\partial/\partial x_2, -\partial/\partial x_1)^t$ denotes the vector curl operator. If the domain Ω is simply connected, then this complex is exact, that is, the range of each operator is the kernel of the succeeding one [37]. In particular, the exactness of the complex implies that (i) if $z \in H^1(\Omega)$ is curl-free, then z is constant; (ii) if $\mathbf{v} \in \mathbf{H}(\operatorname{div}, \Omega)$ is solenoidal, then $\mathbf{v} = \mathbf{curl} z$ for some $z \in H^1(\Omega)$; and (iii) the mapping $\mathbf{H}(\operatorname{div}, \Omega) \rightarrow L^2(\Omega)$ is a surjection.

A finite element sub-complex of (4.11) consists of finite element spaces $\Upsilon_h \subset H^1(\Omega)$, $\mathbf{W}_h \subset \mathbf{H}(\operatorname{div}, \Omega)$ and $Q_h \subset L^2(\Omega)$ satisfying the relations

$$(4.12) \quad \mathbb{R} \longrightarrow \Upsilon_h \xrightarrow{\mathbf{curl}} \mathbf{W}_h \xrightarrow{\operatorname{div}} Q_h \longrightarrow 0.$$

It is well-known that standard conforming finite element spaces form a discrete complex of (4.11) [6, 56]. For example, one may take Υ_h to be the Lagrange finite element space, \mathbf{W}_h to be either the Raviart–Thomas or Brezzi–Douglas–Marini finite element spaces, and Q_h to be the space of discontinuous piecewise polynomials [17, 66]. Similar to the continuous setting, the sub-complex (4.12) is exact provided the domain is simply connected; as a result, the finite element pairs $\Upsilon_h \times \mathbf{W}_h$ and $\mathbf{W}_h \times Q_h$ form stable finite element pairs with respect to the curl and divergence operator, respectively. For example, the exactness property of the sub-complex implies that $\operatorname{div} : \mathbf{W}_h \rightarrow Q_h$ is a surjection, and simple arguments show that this surjection has a bounded right-inverse independent of h . From this result, one easily deduces the inf-sup condition: $\sup_{\mathbf{w} \in \mathbf{W}_h} (\operatorname{div} \mathbf{w}, q) / \|\mathbf{w}\|_{H(\operatorname{div}; \Omega)} \geq \beta \|q\|_{L^2(\Omega)}$, $\forall q \in Q_h$.

While the complex (4.11) and its discrete counterpart are useful in the study of several problems, it is not suitable for the Stokes problem due to the minimal smoothness of the Hilbert spaces. Instead, a smooth de Rham complex (or Stokes complex) has been proposed [31, 40, 55]:

$$(4.13) \quad \mathbb{R} \longrightarrow H^2(\Omega) \xrightarrow{\mathbf{curl}} \mathbf{H}^1(\Omega) \xrightarrow{\operatorname{div}} L^2(\Omega) \longrightarrow 0.$$

Again, this complex is exact provided Ω is simply connected [37]. In particular all divergence-free $\mathbf{H}^1(\Omega)$ functions satisfy the relation $\mathbf{v} = \mathbf{curl} z$ for some $z \in H^2(\Omega)$, where z is often referred to as the stream-function if \mathbf{v} models an incompressible fluid. Moreover, the mapping $\operatorname{div} : \mathbf{H}^1(\Omega) \rightarrow L^2(\Omega)$ is a surjection, implying the continuous inf-sup condition (1.3).

Similar to the previous setting, one can obtain stable finite element pairs by considering sub-complexes of (4.13) consisting of finite element spaces:

$$(4.14) \quad \mathbb{R} \longrightarrow \Sigma_h \xrightarrow{\mathbf{curl}} \mathbf{X}_h \xrightarrow{\operatorname{div}} Y_h \longrightarrow 0,$$

where $\Sigma_h \subset H^2(\Omega)$, $\mathbf{X}_h \subset \mathbf{H}^1(\Omega)$ and $Y_h \subset L^2(\Omega)$. If the discrete complex (4.14) is exact, then the finite element pair $\mathbf{X}_h \times Y_h$ satisfies the discrete inf-sup condition provided this mapping has a bounded right-inverse. The mappings in (4.14) then imply that $\operatorname{div} \mathbf{X}_h = W_h$, and thus, the finite element pair yields divergence-free approximations. A useful feature of this methodology is that the complex (4.14) provides a guiding tool to develop the pair $\mathbf{X}_h \times Y_h$ satisfying these properties, in particular, the $H^2(\Omega)$ -conforming relatives that dictates the local and global properties of these spaces. As far as we are aware, every divergence-free finite element pair has a H^2 relative satisfying (4.14).

As an example for the derivation of divergence-free pairs from H^2 -conforming finite element spaces, the Hsieh–Clough–Tocher (HCT) finite element will be considered. To describe this space, let \mathcal{T}_h denote a shape regular, conforming simplicial triangulation of $\Omega \subset \mathbb{R}^2$. For a simplex $T \in \mathcal{T}_h$, let $\{K_r^{(T)}\}_{r=1}^3$ denote the three sub-triangles obtained by performing a barycenter refinement on T , and set $\mathcal{M}_h := \{K_r^{(T)} : T \in \mathcal{T}_h\}$. The HCT space Σ_h^{HCT} is defined as the space of globally H^2 piecewise cubic polynomials with respect to the (refined) mesh \mathcal{M}_h . Denoting by \mathcal{V}_h and \mathcal{E}_h the set of vertices and edges in the original mesh \mathcal{T}_h , one can show that any function $z \in \Sigma_h^{HCT}$ is uniquely determined by the constraint $z|_T \in H^2(T)$ for all $T \in \mathcal{T}_h$, and the values $z(a)$, $\nabla z(a)$, and $\int_e \frac{\partial z}{\partial \mathbf{n}_e} ds$ over all $a \in \mathcal{V}_h$ and $e \in \mathcal{E}_h$ (cf. [24] and Figure 4.1, row 1). Here, $\frac{\partial z}{\partial \mathbf{n}_e} := \nabla z \cdot \mathbf{n}_e$ and \mathbf{n}_e denotes the outward unit normal of the edge e . It follows that the dimension of this space is $\dim \Sigma_h^{HCT} = 3|\mathcal{V}_h| + |\mathcal{E}_h|$, where $|\mathcal{S}|$ denotes the cardinality of a set \mathcal{S} .

The definition of the HCT space and its properties naturally lead to finite element spaces satisfying (4.14). In particular, since differentiation lowers polynomial degree and global continuity by 1, one may take \mathbf{X}_h^{HCT} to be the space of globally H^1 piecewise quadratic, vector-valued polynomials with respect to \mathcal{M}_h , and take Y_h^{HCT} to be the space of (discontinuous) piecewise linear polynomials with respect to \mathcal{M}_h . The inclusions $\mathbf{curl} \Sigma_h^{HCT} \subset \mathbf{X}_h^{HCT}$ and $\operatorname{div} \mathbf{X}_h^{HCT} \subset Y_h^{HCT}$ are immediate, and thus these spaces satisfy (4.14).

To verify that the finite element spaces Σ_h^{HCT} , \mathbf{X}_h^{HCT} and Y_h^{HCT} inherit the exactness property, one first observes that if $\mathbf{v} \in \mathbf{X}_h^{HCT} \subset \mathbf{H}^1(\Omega)$ is divergence-free, then $\mathbf{v} = \mathbf{curl} z = (\partial z / \partial x_2, -\partial z / \partial x_1)^t$ for some $z \in H^2(\Omega)$ due to the exactness property of the complex (4.13). Using the definitions of the curl operator and of \mathbf{X}_h^{HCT} , one deduces that both $\partial z / \partial x_1$ and $\partial z / \partial x_2$ are piecewise quadratic polynomials, and therefore z is a piecewise cubic polynomial. Moreover, the condition $\mathbf{curl} z \in \mathbf{H}^1(\Omega)$ implies that $z \in H^2(\Omega)$, and therefore $z \in \Sigma_h^{HCT}$.

Thus, to verify the exactness of the sub-complex (4.14) and to show that $\mathbf{X}_h \times Y_h$ forms a stable finite element pair for the Stokes problem, it suffices to show that $\operatorname{div} \mathbf{X}_h^{HCT} \rightarrow Y_h^{HCT}$ is a surjection with a bounded right-inverse. This surjection property can be achieved by a simple counting argument. Indeed, since $\operatorname{div} \mathbf{X}_h^{HCT} \subseteq W_h^{HCT}$, it suffices to show that the dimension of $\operatorname{div} \mathbf{X}_h^{HCT}$ and Y_h^{HCT} are the same. Since the finite element space Y_h^{HCT} consists of piecewise linear polynomials with respect to \mathcal{M}_h , and since the dimension of the space of linear polynomials in two dimensions is three, one has $\dim Y_h^{HCT} = 3|\mathcal{M}_h| = 9|\mathcal{T}_h|$. Moreover, any function $\mathbf{v} \in \mathbf{X}_h^{HCT}$ is uniquely determined by its values at the vertices of \mathcal{M}_h and its mean over all edges in \mathcal{M}_h [24]. Since the number of vertices in the refined mesh \mathcal{M}_h is $|\mathcal{V}_h| + |\mathcal{T}_h|$, and the number of edges in \mathcal{M}_h is $|\mathcal{E}_h| + 3|\mathcal{T}_h|$, one has $\dim \mathbf{X}_h^{HCT} = 2(|\mathcal{V}_h| + |\mathcal{E}_h| + 4|\mathcal{T}_h|)$. Therefore by the rank-nullity theorem

and Euler's formula $|\mathcal{V}_h| + |\mathcal{J}_h| - |\mathcal{E}_h| = 1$ one obtains

$$\begin{aligned} \dim(\operatorname{div} \mathbf{X}_h^{HCT}) &= \dim \mathbf{X}_h^{HCT} - \dim \mathbf{curl} \Sigma_h^{HCT} = \dim \mathbf{X}_h^{HCT} - \dim \Sigma_h^{HCT} + 1 \\ &= 2(|\mathcal{V}_h| + |\mathcal{E}_h| + 4|\mathcal{J}_h|) - (3|\mathcal{V}_h| + |\mathcal{E}_h|) + (|\mathcal{V}_h| + |\mathcal{J}_h| - |\mathcal{E}_h|) = 9|\mathcal{J}_h| \\ &= \dim Y_h^{HCT}. \end{aligned}$$

Thus, the sub-complex with the finite element spaces Σ_h^{HCT} , \mathbf{X}_h^{HCT} , and Y_h^{HCT} is exact. Moreover, using a macro-element technique [7], one can show that the surjection $\operatorname{div} \mathbf{X}_h \rightarrow Y_h$ has a bounded right-inverse independent of h , and therefore the discrete inf-sup condition (3.2) is uniformly satisfied. For the Stokes equations, one obtains the Scott–Vogelius pair of spaces $\mathcal{P}_2/\mathcal{P}_1^{\operatorname{disc}} = \mathbf{V}_h^{HCT}/W_h^{HCT}$ [7, 68] on a barycenter-refined mesh.

The given example is not limited to the Hsieh–Clough–Tocher element; one may start with any $H^2(\Omega)$ -conforming finite element space to derive a stable divergence-free finite element pair for the Stokes problem. Examples of $H^2(\Omega)$ spaces include the Morgan–Scott element [57], the Argyris element [24], the rational Zienkiewicz element [24], and the Bogner–Fox–Schmit rectangular element [24]. These $H^2(\Omega)$ finite element spaces were used to derive stable divergence-free finite element pairs in [31, 40, 69]; these finite element spaces and their H^2 -conforming relative are summarized in Figure 4.1.

While the development of divergence-free, two-dimensional Stokes elements has reached a stage of maturity, the three-dimensional case is considerably more challenging, and several issues remain to be resolved. To explain the added difficulties, as before the de Rham complex with minimal L^2 smoothness is stated:

$$(4.15) \quad \mathbb{R} \longrightarrow H^1(\Omega) \xrightarrow{\operatorname{grad}} \mathbf{H}(\mathbf{curl}; \Omega) \xrightarrow{\mathbf{curl}} \mathbf{H}(\operatorname{div}; \Omega) \xrightarrow{\operatorname{div}} L^2(\Omega) \longrightarrow 0,$$

where $\mathbf{H}(\mathbf{curl}; \Omega)$ denotes the space of square-integrable vector-valued functions whose curl is in $L^2(\Omega)$. Similar to the two-dimensional case, classical families of finite element spaces form a sub-complex of (4.15) that inherit the cohomology of the sequence.

Based on the complex (4.15) one may construct complexes with enhanced smoothness that are suitable for the Stokes problem. However, due to the additional space and differential operator in the three-dimensional case, different Stokes complexes may be considered. For example, the complex

$$(4.16) \quad \mathbb{R} \longrightarrow H^2(\Omega) \xrightarrow{\operatorname{grad}} \mathbf{H}^1(\mathbf{curl}; \Omega) \xrightarrow{\mathbf{curl}} \mathbf{H}^1(\Omega) \xrightarrow{\operatorname{div}} L^2(\Omega) \longrightarrow 0,$$

with $\mathbf{H}^1(\mathbf{curl}; \Omega) = \{\mathbf{v} \in \mathbf{H}^1(\Omega); \mathbf{curl} \mathbf{v} \in \mathbf{H}^1(\Omega)\}$ was proposed in [59, 70] to develop conforming and non-conforming divergence-free elements. Due to the high regularity of the spaces, the polynomial order becomes exceedingly high. For example, the lowest degree H^2 -conforming piecewise polynomial space is nine; as a result, the lowest order velocity space based on this construction is six [59], which may limit the practical use of these elements. On the other hand, one could consider the quintic composite elements (also known as macro elements) documented in [46] as the H^2 -conforming finite element space. This element is most likely related to the Scott–Vogelius pair $\mathcal{P}_3/\mathcal{P}_2^{\operatorname{disc}}$ on barycenter refined triangulations studied in [77]. However, the corresponding $\mathbf{H}^1(\mathbf{curl}; \Omega)$ conforming element completing the sequence (4.16) is missing in the literature.

Alternatively, the complex

$$(4.17) \quad \mathbb{R} \longrightarrow H^1(\Omega) \xrightarrow{\operatorname{grad}} \Phi \xrightarrow{\mathbf{curl}} \mathbf{H}^1(\Omega) \xrightarrow{\operatorname{div}} L^2(\Omega) \longrightarrow 0,$$

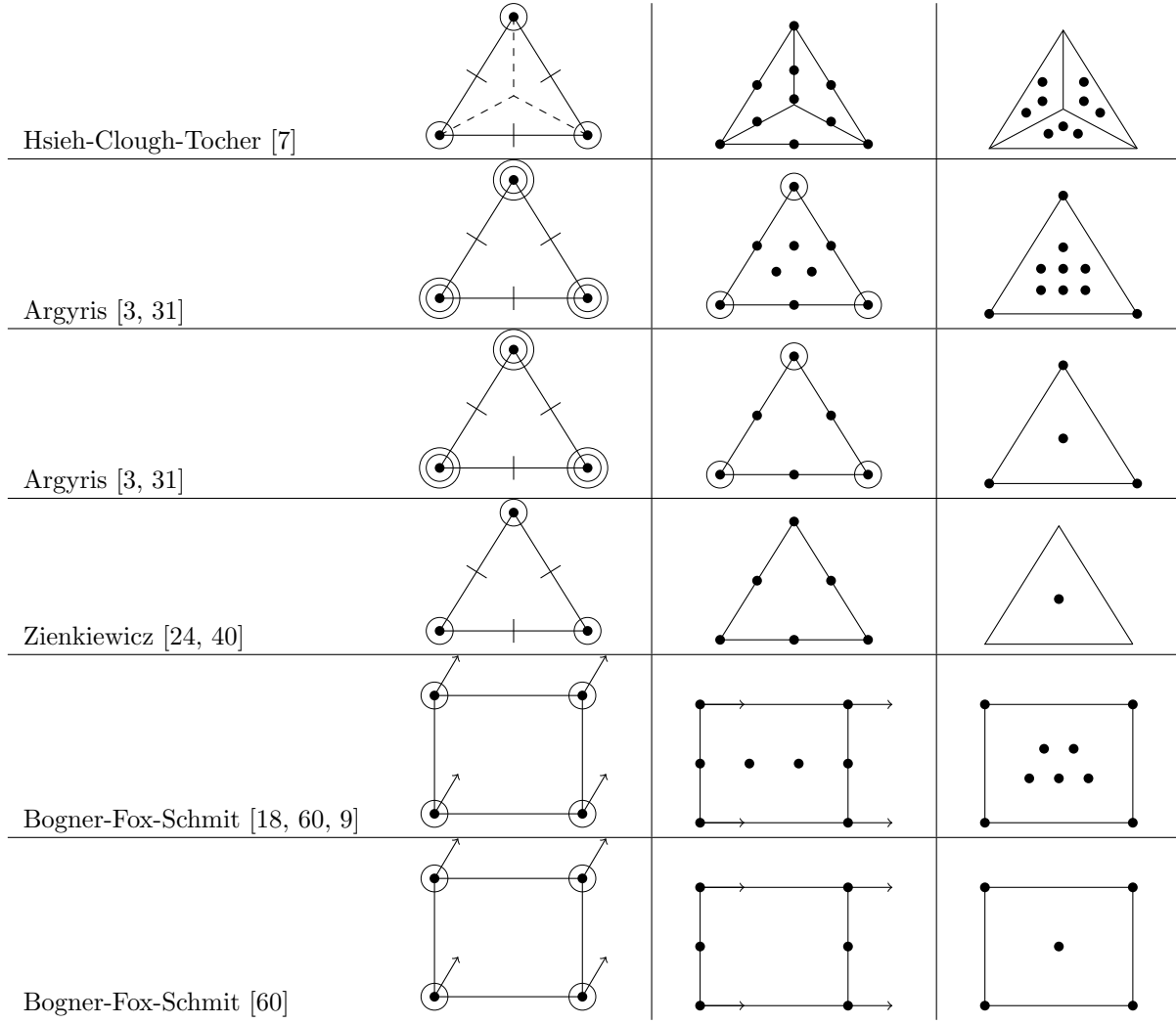


FIG. 4.1. H^2 -conforming finite element space Σ_h (left), velocity space \mathbf{X}_h (middle), and pressure space Y_h (right) satisfying the exact complex (4.14). Small and large circles denote first and second derivative degrees of freedom (d.o.f.s), respectively, solid points denote function d.o.f.s, arrows denote directional derivative d.o.f.s, and lines without arrows denote normal derivative d.o.f.s.

with $\Phi := \{\mathbf{v} \in \mathbf{L}^2(\Omega) : \mathbf{curl} \mathbf{v} \in \mathbf{H}^1(\Omega)\}$ was recently proposed in [30] to derive stable pairs in an isogeometric framework. On the other hand, as far as we are aware, there does not exist finite element spaces conforming to the complex (4.17).

Constructions of divergence-free finite elements obtained in different ways can be found, e.g., in [78, 79].

4.4. $\mathbf{H}(\text{div})$ -conforming finite element methods. Recently, to bypass the difficulty of constructing conforming, inf-sup stable, and divergence-free spaces, finite element methods for the Stokes problem that use strictly $\mathbf{H}(\text{div}, \Omega)$ -conforming bases have been proposed [25, 39, 45, 55,

70, 73, 74, 76]. Before presenting these schemes, a criterion to ensure that a finite element space is a subspace of $\mathbf{H}(\text{div}, \Omega)$ is reviewed.

As before, \mathcal{T}_h denotes a shape-regular triangulation of Ω . Let \mathcal{E}_h be the set of (open) edges ($d = 2$) or faces ($d = 3$) of the mesh. The set of boundary edges/faces is denoted by $\mathcal{E}_h^B \subset \mathcal{E}_h$, i.e., $e \in \mathcal{E}_h^B$ if $e \cap \partial\Omega \neq \emptyset$, and $\mathcal{E}_h^I := \mathcal{E}_h \setminus \mathcal{E}_h^B$ is the set of interior edges/faces.

LEMMA 4.11. *Let \mathbf{W}_h denote a space of piecewise polynomials with respect to the partition \mathcal{T}_h . Then $\mathbf{W}_h \subset \mathbf{H}(\text{div}, \Omega)$ provided the normal components (but not necessarily the tangential components) of functions in this space are continuous across all inter-element boundaries $e \in \mathcal{E}_h^I$.*

Proof. Let $\mathbf{w}_h \in \mathbf{W}_h$ and suppose that the normal component of \mathbf{w}_h is continuous across each $e \in \mathcal{E}_h^I$. Set $\rho_h \in L^2(\Omega)$ such that $\rho_h|_T = \nabla \cdot \mathbf{w}_h|_T$ for all $T \in \mathcal{T}_h$. Applying the divergence theorem element-wise yields for any $\psi \in C_0^\infty(\Omega)$,

$$\begin{aligned} - \int_{\Omega} \nabla \psi \cdot \mathbf{w}_h \, d\mathbf{x} &= - \sum_{T \in \mathcal{T}_h} \int_T \nabla \psi \cdot \mathbf{w}_h \, d\mathbf{x} = \sum_{T \in \mathcal{T}_h} \left(\int_{T \in \mathcal{T}_h} \psi (\nabla \cdot \mathbf{w}_h) \, d\mathbf{x} - \int_{\partial T} (\mathbf{w}_h \cdot \mathbf{n}_T) \psi \, ds \right) \\ &= \int_{\Omega} \rho_h \psi \, d\mathbf{x} - \sum_{T \in \mathcal{T}_h} \int_{\partial T} (\mathbf{w}_h \cdot \mathbf{n}_T) \psi \, ds. \end{aligned}$$

Since the normal component of \mathbf{w}_h is continuous, and since ψ vanishes on $\partial\Omega$, the boundary integrals vanish, and the statement of the lemma follows from Definition 2.3. \square

Two canonical $\mathbf{H}(\text{div}, \Omega)$ -conforming finite element spaces satisfying this criterion include the Raviart–Thomas space of order $k \geq 0$ [58, 66]:

$$(4.18a) \quad \text{RT}_k := \{\mathbf{w}_h \in \mathbf{H}_0(\text{div}, \Omega) : \mathbf{w}_h|_T \in \text{RT}_k(T), \forall T \in \mathcal{T}_h\},$$

and the Brezzi–Douglas–Marini (BDM) space of degree $k \geq 1$:

$$(4.18b) \quad \text{BDM}_k := \{\mathbf{w}_h \in \mathbf{H}_0(\text{div}, \Omega) : \mathbf{w}_h|_T \in \mathcal{P}_k(T), \forall T \in \mathcal{T}_h\}.$$

Here, $\mathbf{H}_0(\text{div}, \Omega) = \{\mathbf{v} \in \mathbf{H}(\text{div}, \Omega) : \mathbf{v} \cdot \mathbf{n}|_{\partial\Omega} = 0\}$, and $\text{RT}_k(T) := \mathcal{P}_k(T) + \mathbf{x}\mathcal{P}_k(T)$ is the local Raviart–Thomas space. Both of these spaces form inf-sup stable pairs with appropriate pressure spaces, and consequently, lead to stable discretizations for second order elliptic problems.

To make this last statement precise, denote by Q_h the space of discontinuous piecewise polynomials of degree k if $\mathbf{W}_h = \text{RT}_k$ or $k - 1$ if $\mathbf{W}_h = \text{BDM}_k$ and with vanishing mean. Then the finite element pair $\mathbf{W}_h \times Q_h$ is inf-sup stable in the sense

$$(4.19) \quad \inf_{q_h \in Q_h \setminus \{0\}} \sup_{\mathbf{w}_h \in \mathbf{W}_h \setminus \{0\}} \frac{\int_{\Omega} (\nabla \cdot \mathbf{w}_h) q_h \, d\mathbf{x}}{\|\mathbf{w}_h\|_{\mathbf{H}(\text{div}, \Omega)} \|q_h\|_{L^2(\Omega)}} \geq \beta_h,$$

with $\beta_h > 0$ uniformly bounded from below. Moreover, it is easy to see from their definitions that the inclusion $\nabla \cdot \mathbf{W}_h \subseteq Q_h$ is satisfied; as a result, the discretely divergence-free functions are globally divergence-free pointwise, i.e., $\{\mathbf{w}_h \in \mathbf{W}_h : \int_{\Omega} (\nabla \cdot \mathbf{w}_h) q_h \, d\mathbf{x} = 0, \forall q_h \in Q_h\} = \{\mathbf{w}_h \in \mathbf{W}_h : \nabla \cdot \mathbf{w}_h \equiv 0\}$.

While these spaces are inf-sup stable with respect to the $\mathbf{H}(\text{div}, \Omega)$ norm and the discretely divergence-free functions are solenoidal, the spaces are not directly applicable for the Stokes problem due to their lack of smoothness. In particular, since the Raviart–Thomas and BDM spaces satisfy the non-inclusion $\mathbf{W}_h \not\subset \mathbf{H}_0^1(\Omega)$, i.e., these spaces are non-conforming with respect to $\mathbf{H}_0^1(\Omega)$, the finite element method for the Stokes problem (3.1) is not well-defined since the gradients of functions

in \mathbf{W}_h do not exist globally. Furthermore, if the gradients in the formulation (3.1) are replaced by the piecewise defined counterpart, the resulting method, even if non-singular, is not convergent since the method is inconsistent in the sense that

$$-\int_{\Omega} \Delta \mathbf{v} \cdot \mathbf{w}_h \, d\mathbf{x} \neq a(\mathbf{v}, \mathbf{w}_h)$$

for general functions $\mathbf{v} \in \mathbf{H}^2(\Omega) \cap \mathbf{H}_0^1(\Omega)$ and $\mathbf{w}_h \in \mathbf{W}_h$. As such, modifications of the method are needed to ensure that the discrete problem is stable and consistent, yet still preserve the divergence-free property. Generally speaking, this is achieved in two ways: (i) modify the bilinear forms in (3.1) or (ii) modify the $\mathbf{H}(\text{div}, \Omega)$ spaces to impose tangential continuity in some weak sense.

In the first case, using techniques found in discontinuous Galerkin methods, the bilinear form $a(\cdot, \cdot)$ in (3.1) is modified to ensure that the form is consistent with the Laplace operator. Here, the symmetric interior penalty arguments given in [73, 74] are presented, although different discontinuous Galerkin techniques are available [25]. For simplicity it is assumed that $\Omega \subset \mathbb{R}^2$, however the arguments generalize quite naturally to the three-dimensional case. Let $\mathbf{w}_h \in \mathbf{W}_h \subset \mathbf{H}(\text{div}, \Omega)$ be an arbitrary function in the Raviart–Thomas or BDM space, and assume that the velocity solution of the Stokes problem \mathbf{u} is sufficiently smooth. Then it follows from Green’s theorem that

$$-\int_T \Delta \mathbf{u} \cdot \mathbf{w}_h \, d\mathbf{x} = \int_T \nabla \mathbf{u} : \nabla \mathbf{w}_h \, d\mathbf{x} - \int_{\partial T} \frac{\partial \mathbf{u}}{\partial \mathbf{n}_T} \cdot \mathbf{w}_h \, ds,$$

where $\frac{\partial \mathbf{u}}{\partial \mathbf{n}_T} := \nabla \mathbf{u} \mathbf{n}_T$. Let $\boldsymbol{\tau}_T$ denote the tangential unit vector of ∂T , obtained by rotating \mathbf{n}_T by 90 degrees counter-clockwise. Due to the vector identity $\mathbf{v} = (\mathbf{v} \cdot \mathbf{n}_T) \mathbf{n}_T + (\mathbf{v} \cdot \boldsymbol{\tau}_T) \boldsymbol{\tau}_T$ and summing over $T \in \mathcal{T}_h$, there holds

$$\begin{aligned} -\int_{\Omega} \Delta \mathbf{u} \cdot \mathbf{w}_h \, d\mathbf{x} &= \int_{\Omega} \nabla_h \mathbf{u} : \nabla_h \mathbf{w}_h \, d\mathbf{x} - \sum_{T \in \mathcal{T}_h} \int_{\partial T} \left(\frac{\partial(\mathbf{u} \cdot \mathbf{n}_T)}{\partial \mathbf{n}_T} (\mathbf{w}_h \cdot \mathbf{n}_T) + \frac{\partial(\mathbf{u} \cdot \boldsymbol{\tau}_T)}{\partial \mathbf{n}_T} (\mathbf{w}_h \cdot \boldsymbol{\tau}_T) \right) ds \\ (4.20) \quad &= \int_{\Omega} \nabla_h \mathbf{u} : \nabla_h \mathbf{w}_h \, d\mathbf{x} - \sum_{T \in \mathcal{T}_h} \int_{\partial T} \frac{\partial(\mathbf{u} \cdot \boldsymbol{\tau}_T)}{\partial \mathbf{n}_T} (\mathbf{w}_h \cdot \boldsymbol{\tau}_T) \, ds, \end{aligned}$$

where ∇_h denotes the piecewise gradient operator, and the normal continuity of \mathbf{w}_h was used to derive the second equality.

The sum of boundary integrals is now written as a sum of integrals over edges of the triangulation. Let $e \in \mathcal{E}_h^I$ with $e = \partial T_+ \cap \partial T_-$ with $T_{\pm} \in \mathcal{T}_h$. For a piecewise smooth vector-valued function \mathbf{w} the average and jump of \mathbf{w} across e , respectively, are defined as

$$\{\{\varepsilon(\mathbf{w})\}\}_e := \frac{1}{2} \left(\frac{\partial(\mathbf{w}_+ \cdot \boldsymbol{\tau}_{T_+})}{\partial \mathbf{n}_{T_+}} + \frac{\partial(\mathbf{w}_- \cdot \boldsymbol{\tau}_{T_-})}{\partial \mathbf{n}_{T_-}} \right), \quad \llbracket \mathbf{w} \rrbracket_{\tau}|_e := \mathbf{w}_+ \cdot \boldsymbol{\tau}_{T_+} + \mathbf{w}_- \cdot \boldsymbol{\tau}_{T_-},$$

where $\mathbf{w}_{\pm} = \mathbf{w}|_{T_{\pm}}$. For a boundary edge $e \in \mathcal{E}_h^B$ with $e = \partial T \cap \partial \Omega$ these operators are given by

$$\{\{\varepsilon(\mathbf{w})\}\}_e := \frac{\partial(\mathbf{w} \cdot \boldsymbol{\tau}_T)}{\partial \mathbf{n}_T}, \quad \llbracket \mathbf{w} \rrbracket_{\tau}|_e := \mathbf{w} \cdot \boldsymbol{\tau}_T.$$

Combining (4.20) with the algebraic identity $ab - cd = \frac{1}{2}(a - c)(b + d) + \frac{1}{2}(a + c)(b - d)$, and noting that the jump of \mathbf{u} vanishes on all edges, yields

$$-\int_{\Omega} \Delta \mathbf{u} \cdot \mathbf{w}_h \, d\mathbf{x} = \int_{\Omega} \nabla_h \mathbf{u} : \nabla_h \mathbf{w}_h \, d\mathbf{x} - \sum_{e \in \mathcal{E}_h} \int_e \{\{\varepsilon(\mathbf{u})\}\} \llbracket \mathbf{w}_h \rrbracket_{\tau} \, ds \quad \forall \mathbf{w}_h \in \mathbf{W}_h.$$

While the right-hand side of (4.20) induces a consistent bilinear form for the Laplace operator, it has two undesirable properties. First, the right-hand side is non-symmetric with respect to \mathbf{u} and \mathbf{w}_h , which is in strong contrast to the self-adjoint property of the Laplacian. Second, the form induced by (4.20) restricted to $\mathbf{W}_h \times \mathbf{W}_h$ is non-coercive, again, in contrast to the Laplace operator. A simple fix to address these issues is to exploit the jump-free property of \mathbf{u} and amend this identity with two trivial terms:

$$(4.21) \quad \begin{aligned} - \int_{\Omega} \Delta \mathbf{u} \cdot \mathbf{w}_h \, d\mathbf{x} &= \int_{\Omega} \nabla_h \mathbf{u} : \nabla_h \mathbf{w}_h \, d\mathbf{x} \\ &- \sum_{e \in \mathcal{E}_h} \left(\int_e \{\{\varepsilon(\mathbf{u})\}\} \|\mathbf{w}_h\|_{\tau} \, ds + \int_e \{\{\mathbf{w}_h\}\} \|\mathbf{u}\|_{\tau} \, ds - \frac{\sigma}{h_e} \int_e \|\mathbf{u}\|_{\tau} \|\mathbf{w}_h\|_{\tau} \, ds \right) \\ &=: a_h(\mathbf{u}, \mathbf{w}_h) \quad \forall \mathbf{w}_h \in \mathbf{X}_h, \end{aligned}$$

where $h_e = \text{diam}(e)$ and $\sigma > 0$ is some parameter. In the literature, the edge terms in the bilinear form $a_h(\cdot, \cdot)$, going from left to right, are commonly referred to (for obvious reasons) as consistency terms, symmetry terms, and penalization terms, respectively. The choice of the penalization parameter σ is dictated by the next lemma.

LEMMA 4.12 ([74]). *There exists $\sigma_0 > 0$ depending only on the shape regularity of \mathcal{T}_h such that for $\sigma \geq \sigma_0$, there holds*

$$\frac{1}{2} \|\mathbf{w}_h\|_{1,h}^2 \leq a_h(\mathbf{w}_h, \mathbf{w}_h) \quad \forall \mathbf{w}_h \in \mathbf{W}_h,$$

where the discrete \mathbf{H}^1 -norm is defined as

$$\|\mathbf{w}\|_{1,h}^2 := \sum_{T \in \mathcal{T}_h} \|\nabla \mathbf{w}\|_{L^2(T)}^2 + \sum_{e \in \mathcal{E}_h} h_e \|\{\{\varepsilon(\mathbf{w})\}\}\|_{L^2(e)}^2 + \sum_{e \in \mathcal{E}_h} h_e^{-1} \|\llbracket \mathbf{w} \rrbracket_{\tau}\|_{L^2(e)}^2.$$

Moreover, there holds for all $\mathbf{w}_h \in \mathbf{W}_h$ and $\mathbf{v} \in \mathbf{H}^s(\Omega)$ with $s > 3/2$,

$$a_h(\mathbf{v}, \mathbf{w}_h) \leq (1 + \sigma) \|\mathbf{v}\|_{1,h} \|\mathbf{w}_h\|_{1,h}.$$

This derivation of the bilinear form $a_h(\cdot, \cdot)$ motivates the finite element method for the Stokes problem using $\mathbf{H}(\text{div}, \Omega)$ -conforming elements: Find $(\mathbf{u}_h, p_h) \in \mathbf{W}_h \times Q_h$ satisfying

$$(4.22a) \quad a_h(\mathbf{u}_h, \mathbf{w}_h) + b(\mathbf{w}_h, p_h) = (\mathbf{f}, \mathbf{w}_h) \quad \forall \mathbf{w}_h \in \mathbf{W}_h,$$

$$(4.22b) \quad b(\mathbf{u}_h, q_h) = (g, q_h) \quad \forall q_h \in Q_h.$$

From the derivation of the bilinear form $a_h(\cdot, \cdot)$, one immediately sees that the method is consistent provided \mathbf{u} is sufficiently smooth (e.g., $\mathbf{u} \in \mathbf{H}^s(\Omega)$ with $s > 3/2$); in particular, if one interchanges \mathbf{u}_h with \mathbf{u} in (4.22), then the two statements are still satisfied. Furthermore, a combination of (4.19) and scaling arguments show that the inf-sup condition is satisfied on $\mathbf{W}_h \times Q_h$ with respect to the discrete \mathbf{H}^1 -norm:

$$\inf_{q_h \in Q_h \setminus \{0\}} \sup_{\mathbf{w}_h \in \mathbf{W}_h \setminus \{0\}} \frac{\int_{\Omega} (\nabla \cdot \mathbf{w}_h) q_h}{\|\mathbf{w}_h\|_{1,h} \|q_h\|_{L^2(\Omega)}} \geq \beta_h,$$

with β_h uniformly bounded. Therefore, in light of Lemma 4.12, and by slightly generalizing the framework of Section 3, one concludes that if σ is sufficiently large, then there exists a unique solution to (4.22). Moreover, by approximation properties of the finite element spaces (cf. (4.18)), and since the discretely divergence-free functions are globally divergence-free pointwise, the errors satisfy

$$\begin{aligned} \|\mathbf{u} - \mathbf{u}_h\|_{1,h} &\leq C \inf_{\mathbf{w}_h \in \mathbf{W}_h} \|\mathbf{u} - \mathbf{w}_h\|_{1,h} \leq Ch^{\ell-1} \|\mathbf{u}\|_{H^\ell(\Omega)}, \\ \|p - p_h\|_{L^2(\Omega)} &\leq C \left(\inf_{q_h \in Q_h} \|p - q_h\|_{L^2(\Omega)} + \nu \|\mathbf{u} - \mathbf{u}_h\|_{1,h} \right) \leq C (h^m \|p\|_{H^m(\Omega)} + \nu h^{\ell-1} \|\mathbf{u}\|_{H^\ell(\Omega)}), \end{aligned}$$

where $\ell = \min\{s, k + 1\}$ and $\mathbf{u} \in \mathbf{H}^s(\Omega)$. If $p \in H^r(\Omega)$ and if $\mathbf{W}_h \times Q_h$ is the Raviart–Thomas pair, then $m = \min\{r, k + 1\}$. If $\mathbf{W}_h \times Q_h$ is the BDM pair, then $m = \min\{r, k\}$.

Another class of $\mathbf{H}(\text{div}, \Omega)$ -conforming methods for the Stokes problem modifies the Raviart–Thomas and BDM spaces locally with divergence-free vector fields such that the resulting spaces possess weak tangential continuity [39, 55, 70, 76]. The reasoning behind this approach is that, if the spaces are augmented with divergence-free vector fields, then the inf-sup condition (4.19) is satisfied and discretely divergence-free functions are still globally divergence-free. To be precise, the local spaces of these elements, in two dimensions, are of the form [39, 40]

$$(4.23) \quad \hat{\mathbf{W}}(T) = \mathbf{W}(T) + \mathbf{curl}(b_T S(T)), \quad \text{with} \quad \mathbf{curl} q := \begin{pmatrix} \partial q / \partial x_2 \\ -\partial q / \partial x_1 \end{pmatrix},$$

where b_T is the cubic bubble function (i.e., the product of the three barycentric coordinates of T), $S(T)$ is some auxiliary space, and $\mathbf{W}(T)$ is the local space of \mathbf{W}_h , that is, $\mathbf{W}(T) = \mathcal{P}_k(T)$ if \mathbf{W}_h is the BDM space or $\mathbf{W}(T) = \text{RT}_k(T)$ if it is the Raviart–Thomas space. Clearly one has $\text{div} \hat{\mathbf{W}}(T) = \text{div} \mathbf{W}(T)$, indicating that the range of the divergence operator acting on the augmented space is preserved.

As an example, reference [55] takes $\mathbf{W}(T)$ to be the local, lowest order Raviart–Thomas space $\text{RT}_0(T)$, and the auxiliary space to be the space of piecewise linear polynomials, $S(T) = \mathcal{P}_1(T)$. It is easy to see in this case, that the sum in (4.23) is direct, and thus, the dimension of the local augmented space is $\dim \hat{\mathbf{W}}(T) = \dim \text{RT}_0(T) + \dim \mathbf{curl}(b_T \mathcal{P}_1(T)) = \dim \text{RT}_0(T) + \dim \mathcal{P}_1(T) = 3 + 3 = 6$. In addition to the property $\text{div} \hat{\mathbf{W}}(T) = \text{div} \text{RT}_0(T) = \mathcal{P}_0(T)$, the normal component of functions in $\hat{\mathbf{W}}(T)$ are constant on the boundary of T . Indeed, if $\mathbf{w}_h = \mathbf{w}_0 + \mathbf{curl}(b_T q_h) \in \hat{\mathbf{W}}(T)$ with $\mathbf{w}_0 \in \text{RT}_0(T)$ and $q_h \in \mathcal{P}_1(T)$, then by properties of $\text{RT}_0(T)$, the curl operator, and b_T ,

$$\mathbf{w}_h \cdot \mathbf{n}_e|_e = \mathbf{w}_0 \cdot \mathbf{n}_e|_e + \frac{\partial(q_h b_T)}{\partial \boldsymbol{\tau}_e}|_e = \mathbf{w}_0 \cdot \mathbf{n}_e|_e \in \mathcal{P}_0(e).$$

On the only other hand, the tangential component is generally cubic.

In [55] it is shown that a function $\mathbf{w}_h \in \hat{\mathbf{W}}(T)$ is uniquely determined by the six values

$$\int_e \mathbf{w}_h ds \quad e \subset \partial T,$$

or equivalently,

$$(4.24) \quad \int_e \mathbf{w}_h \cdot \mathbf{n}_e ds, \quad \int_e \mathbf{w}_h \cdot \boldsymbol{\tau}_e ds \quad e \subset \partial T.$$

The global space $\hat{\mathbf{W}}_h$ induced by the local space and degrees of freedom (4.24) is the space of L^2 -functions that are (i) locally in $\hat{\mathbf{W}}(T)$ on each $T \in \mathcal{T}_h$; (ii) continuous with respect to (4.24) on each $e \in \mathcal{E}_h^I$; and (iii) vanish on (4.24) for $e \subset \partial\Omega$.

Since the normal component of $\mathbf{w}_h \in \hat{\mathbf{W}}_h$ is constant on edges, the first set of degrees of freedom given in (4.24) implies that the normal component of \mathbf{w}_h is continuous across interior edges; thus, $\hat{\mathbf{W}}_h \subset \mathbf{H}(\text{div}, \Omega)$ (cf. Lemma 4.11), and the finite element space can be written as

$$\hat{\mathbf{W}}_h = \left\{ \mathbf{w}_h \in \mathbf{H}_0(\text{div}; \Omega) : \mathbf{w}_h|_T \in \hat{\mathbf{W}}(T), \int_e [[\mathbf{w}_h]]_\tau ds = 0 \forall e \in \mathcal{E}_h \right\}.$$

The pressure space is the space of discontinuous constants with vanishing mean

$$Q_h = \{q_h \in L_0^2(\Omega) : q|_T \in \mathcal{P}_0(T) \forall T \in \mathcal{T}_h\}.$$

Due to the high polynomial degree of the tangential component, the condition $\int_e [[\mathbf{w}_h]]_\tau ds = 0$ is not sufficient to ensure that $[[\mathbf{w}_h]]_\tau = 0$ on interior edges. As a result the global space is not \mathbf{H}^1 -conforming: $\hat{\mathbf{W}}_h \not\subset \mathbf{H}^1(\Omega)$; nonetheless, there does hold

$$(4.25) \quad \int_e |[[\mathbf{w}_h]]_\tau|^2 ds \leq Ch \|\nabla_h \mathbf{w}_h\|_{L^2(\omega_e)}^2 \quad \forall \mathbf{w}_h \in \hat{\mathbf{W}}_h,$$

where ω_e denotes the set of triangles with e as an edge. One concludes from this estimate that, although the space is not globally conforming, it does possess a weak type of continuity across edges.

The finite element method for the Stokes problem utilizing these spaces has the same form as (4.22), but with \mathbf{W}_h replaced by $\hat{\mathbf{W}}_h$, and with the bilinear form $a_h(\cdot, \cdot)$ defined as

$$a_h(\mathbf{w}, \mathbf{v}) = \int_\Omega \nabla_h \mathbf{w} : \nabla_h \mathbf{v} dx.$$

From the previous arguments, one concludes that this form is not consistent with the Laplace operator since $\hat{\mathbf{W}}_h$ is not globally continuous. However, one can exploit the weak continuity of $\hat{\mathbf{W}}_h$ to show

$$\left| - \int_\Omega (\Delta \mathbf{u}) \cdot \mathbf{v}_h dx - a_h(\mathbf{u}, \mathbf{v}_h) \right| \leq Ch \|\mathbf{u}\|_{H^2(\Omega)} \|\nabla_h \mathbf{v}_h\|_{L^2(\Omega)} \quad \forall \mathbf{v}_h \in \hat{\mathbf{W}}_h.$$

Using this result, it can be proved that there exists a unique solution to the finite element method and the errors satisfy

$$\begin{aligned} \|\nabla_h(\mathbf{u} - \mathbf{u}_h)\|_{L^2(\Omega)} &\leq Ch \|\mathbf{u}\|_{H^2(\Omega)}, \\ \|p - p_h\|_{L^2(\Omega)} &\leq Ch(\|p\|_{H^1(\Omega)} + \nu \|\mathbf{u}\|_{H^2(\Omega)}). \end{aligned}$$

5. Improving the pressure-robustness of standard mixed finite elements. The (vast) majority of finite element codes contains only standard finite element methods such that the use of standard mixed methods is a straightforward option for the discretization of incompressible flow problems. Hence, approaches for improving the pressure-robustness of standard mixed methods are of great interest. There are essentially two approaches for this purpose. Both modify the bilinear form of the momentum equation of the finite element problem. The grad-div stabilization

adds a penalization with respect to the continuity equation. This method can be applied to any standard mixed method. It just reduces the lack of pressure-robustness but it does not remove it. The second method chooses appropriate test functions for some terms of the finite element formulation to reestablish properties from the continuous equation in the finite element problem, e.g., the fundamental invariance property (1.4). This rather new approach is currently known to be applicable to a number of mixed methods with discontinuous pressure. It leads to pressure-robust discretizations. For the sake of completeness, a post-processing technique for low order pairs of finite element spaces that do not satisfy the discrete inf-sup condition will be briefly discussed.

5.1. Grad-div stabilization. Grad-div stabilization is probably the most popular technique for improving the pressure-robustness of pairs of finite element spaces which do not satisfy the continuity equation in a sufficiently strong sense. In practice, it is usually applied in the case $\nabla \cdot \mathbf{u} = 0$ and the discussion herein will be restricted to this case. An extension to $\nabla \cdot \mathbf{u} = g$ is possible with additional technical details. For $g = 0$, the insufficient satisfaction of the continuity equation means that the finite element solution is not divergence-free in the sense of Definition 2.3.

The grad-div stabilization arises from adding $\mathbf{0} = -\gamma \nabla(\nabla \cdot \mathbf{u})$ to the continuous momentum equation. Applying integration by parts in deriving the weak formulation of the equation and replacing then the infinite-dimensional spaces with finite element spaces leads to the term $\gamma(\nabla \cdot \mathbf{u}_h, \nabla \cdot \mathbf{v}_h)$ in the finite element formulation. As it was discussed throughout this paper, $\nabla \cdot \mathbf{u}_h \neq 0$ in most common finite element choices, such as the Taylor–Hood pair of spaces, and so this ‘grad-div term’ is non-zero and does have an effect on the discrete solution.

Grad-div stabilization was first introduced in [33] and it has been widely studied over the past decade. It is now well known that it penalizes for lack of mass conservation, can improve solution accuracy for simulations of Stokes and Navier–Stokes equations by reducing the effect of the pressure on the velocity error [48, 63, 61, 62], and it can improve conditioning of discrete systems [38] and convergence of iterative solvers [13, 15, 20, 41]. It has also been shown to improve solution accuracy for related coupled multiphysics problems [29, 36, 44, 54, 71]. Some recent studies have considered the optimal choice of the parameter γ . Although $\gamma = \mathcal{O}(1)$ is often a good choice with Taylor–Hood elements, some guidelines are given in [43] for potentially better choices, depending on the pair of finite element spaces, the mesh structure, the relative size of the pressure to the size of the velocity, and whether or not the sequence of weakly divergence-free subspaces of the discrete velocity spaces has an optimal approximation property.

To see the effect of grad-div stabilization, consider again the discrete Stokes system (1.2), but now with a grad-div term and with $g = 0$. Assuming that (\mathbf{X}_h, Y_h) satisfies the discrete inf-sup condition (3.2), the grad-div stabilized Stokes system takes the form: Find $\mathbf{u}_h \in \mathbf{X}_{h,\text{div}}$ such that

$$(5.1) \quad a(\mathbf{u}_h, \mathbf{v}_h) + \gamma(\nabla \cdot \mathbf{u}_h, \nabla \cdot \mathbf{v}_h) = (\mathbf{f}, \mathbf{v}_h) \quad \forall \mathbf{v}_h \in \mathbf{X}_{h,\text{div}},$$

where the bilinear form $a(\cdot, \cdot)$ is given in (2.1a). Since $a(\cdot, \cdot)$ is positive definite and the term $\gamma(\nabla \cdot \mathbf{u}_h, \nabla \cdot \mathbf{v}_h)$ is positive semidefinite, the existence and uniqueness of a solution of the grad-div stabilized discrete Stokes system follows directly from the lemma of Lax–Milgram.

First, it will be shown that the *grad-div stabilization penalizes the divergence error*. This fact can be seen immediately from an a priori estimate found by taking $\mathbf{v}_h = \mathbf{u}_h$ in (5.1). Applying the estimate for the dual pairing yields

$$\begin{aligned} \nu \|\nabla \mathbf{u}_h\|_{L^2(\Omega)}^2 + \gamma \|\nabla \cdot \mathbf{u}_h\|_{L^2(\Omega)}^2 &= (\mathbf{f}, \mathbf{u}_h) \leq \|\mathbf{f}\|_{H^{-1}(\Omega)} \|\nabla \mathbf{u}_h\|_{L^2(\Omega)} \\ &\leq \frac{\nu^{-1}}{2} \|\mathbf{f}\|_{H^{-1}(\Omega)}^2 + \frac{\nu}{2} \|\nabla \mathbf{u}_h\|_{L^2(\Omega)}^2. \end{aligned}$$

Reducing this estimate gives

$$(5.2) \quad \nu \|\nabla \mathbf{u}_h\|_{L^2(\Omega)}^2 + 2\gamma \|\nabla \cdot \mathbf{u}_h\|_{L^2(\Omega)}^2 \leq \nu^{-1} \|\mathbf{f}\|_{H^{-1}(\Omega)}^2.$$

Since \mathbf{f} is given, the right-hand side is a fixed constant independent of γ . Thus taking γ larger forces the divergence error to become smaller, since (5.2) implies that $\|\nabla \cdot \mathbf{u}_h\|_{L^2(\Omega)} \leq \mathcal{O}(\gamma^{-1/2})$.

Estimate (5.2) can be refined to obtain a stronger scaling with γ , following [36]. Denote by \mathbf{V}_h the weakly divergence-free subspace of \mathbf{X}_h , i.e.,

$$\mathbf{V}_h := \{\mathbf{v}_h \in \mathbf{X}_h : \|\nabla \cdot \mathbf{v}_h\|_{L^2(\Omega)} = 0\},$$

and let \mathbf{V}_h^\perp be its orthogonal complement in $\mathbf{X}_{h,\text{div}}$ with respect to the inner product induced by $a(\cdot, \cdot)$. It is shown in [36] that for $\mathbf{v}_h^r \in \mathbf{V}_h^\perp$,

$$\|\nabla \mathbf{v}_h^r\|_{L^2(\Omega)} \leq C(h) \|\nabla \cdot \mathbf{v}_h^r\|_{L^2(\Omega)},$$

with $C(h)$ potentially depending inversely on h . However, on certain types of meshes and element degrees, it can be even independent of h [37, 53]. Orthogonally decomposing the solution into $\mathbf{u}_h = \mathbf{u}_h^0 + \mathbf{u}_h^r$ with $\mathbf{u}_h^0 \in \mathbf{V}_h$ and $\mathbf{u}_h^r \in \mathbf{V}_h^\perp$, choosing now $\mathbf{v}_h = \mathbf{u}_h^r$ in (5.1) and using $a(\mathbf{u}_h^0, \mathbf{u}_h^r) = 0$ and $\nabla \cdot \mathbf{u}_h^0 = 0$ gives

$$\nu \|\nabla \mathbf{u}_h^r\|_{L^2(\Omega)}^2 + \gamma \|\nabla \cdot \mathbf{u}_h^r\|_{L^2(\Omega)}^2 \leq \|\mathbf{f}\|_{-1} \|\nabla \mathbf{u}_h^r\|_{L^2(\Omega)} \leq C(h) \|\mathbf{f}\|_{H^{-1}(\Omega)} \|\nabla \cdot \mathbf{u}_h^r\|_{L^2(\Omega)},$$

and consequently

$$\|\nabla \cdot \mathbf{u}_h\|_{L^2(\Omega)} = \|\nabla \cdot \mathbf{u}_h^r\|_{L^2(\Omega)} \leq C(h, \nu^{-1}, \mathbf{f}) \gamma^{-1}.$$

Hence, on a fixed mesh, one can expect first order convergence to zero of the divergence error as γ^{-1} goes to zero.

Now, it will be discussed that the *grad-div stabilization can reduce the effect of the pressure on the velocity error*. The error estimate without grad-div stabilization for the Galerkin discretization is given in (3.5). It shall be emphasized once more that if the pressure p is large or complex, then the second term on the right-hand side of (3.5) becomes the dominant term of the error bound. This term represents the best approximation error of the pressure scaled by ν^{-1} . Note that for the Navier–Stokes equations and other related problems, error estimates will often have this same pressure term [47], and so similar issues occur there as well.

The finite element error analysis starts by deriving an error equation for the grad-div stabilized finite element method (5.1) by subtracting the scheme from the weak form of the Stokes equation (2.1a)

$$\nu(\nabla \mathbf{e}, \nabla \mathbf{v}_h) + \gamma(\nabla \cdot \mathbf{e}, \nabla \cdot \mathbf{v}_h) = (p, \nabla \cdot \mathbf{v}_h) = (p - q_h, \nabla \cdot \mathbf{v}_h) \quad \forall \mathbf{v}_h \in \mathbf{X}_{h,\text{div}},$$

where $\mathbf{e} = \mathbf{u} - \mathbf{u}_h$ and q_h is arbitrary in Y_h . For arbitrary $I_h \mathbf{u} \in \mathbf{X}_{h,\text{div}}$, the error is decomposed into $\mathbf{e} = (\mathbf{u} - I_h \mathbf{u}) - (\mathbf{u}_h - I_h \mathbf{u}) =: \boldsymbol{\eta} - \boldsymbol{\phi}_h$. Then choosing $\mathbf{v}_h = \boldsymbol{\phi}_h$ provides

$$\nu \|\nabla \boldsymbol{\phi}_h\|_{L^2(\Omega)}^2 + \gamma \|\nabla \cdot \boldsymbol{\phi}_h\|_{L^2(\Omega)}^2 = -(p - q_h, \nabla \cdot \boldsymbol{\phi}_h) + \gamma(\nabla \cdot \boldsymbol{\eta}, \nabla \cdot \boldsymbol{\phi}_h) + \nu(\nabla \boldsymbol{\eta}, \nabla \boldsymbol{\phi}_h),$$

which immediately reduces with Cauchy–Schwarz and Young’s inequalities to

$$\nu \|\nabla \boldsymbol{\phi}_h\|_{L^2(\Omega)}^2 + \gamma \|\nabla \cdot \boldsymbol{\phi}_h\|_{L^2(\Omega)}^2 \leq 2(p - q_h, \nabla \cdot \boldsymbol{\phi}_h) + \gamma \|\nabla \cdot \boldsymbol{\eta}\|_{L^2(\Omega)}^2 + \nu \|\nabla \boldsymbol{\eta}\|_{L^2(\Omega)}^2.$$

Next, the pressure is majorized by using again Cauchy–Schwarz and Young’s inequalities

$$2(p - q_h, \nabla \cdot \boldsymbol{\phi}_h) \leq 2\gamma^{-1} \|p - q_h\|_{L^2(\Omega)}^2 + \frac{\gamma}{2} \|\nabla \cdot \boldsymbol{\phi}_h\|_{L^2(\Omega)}^2.$$

An estimate of this form is not possible for the Galerkin discretization considered in Section 3. Inserting this estimate and applying the triangle inequality yields

$$(5.3) \quad \|\nabla(\mathbf{u} - \mathbf{u}_h)\|_{L^2(\Omega)}^2 + \frac{\gamma}{2\nu} \|\nabla \cdot (\mathbf{u} - \mathbf{u}_h)\|_{L^2(\Omega)}^2 \\ \leq \frac{4}{\gamma\nu} \inf_{q_h \in Y_h} \|p - q_h\|_{L^2(\Omega)}^2 + \inf_{I_h \mathbf{u} \in \mathbf{X}_{h,\text{div}}} \left(4\|\nabla(\mathbf{u} - I_h \mathbf{u})\|_{L^2(\Omega)}^2 + \frac{3\gamma}{\nu} \|\nabla \cdot (\mathbf{u} - I_h \mathbf{u})\|_{L^2(\Omega)}^2 \right).$$

Comparing this estimate to (3.5) and considering the choice $\gamma > \nu$, then the scaling of the velocity error (in the \mathbf{H}^1 norm) with the best approximation error of the pressure is reduced from ν^{-1} to $\nu^{-1/2}\gamma^{-1/2}$. Thus if the best approximation error of the pressure is the dominant source of the velocity error, grad-div stabilization can reduce the velocity error, sometimes substantially depending on the relative size of the pressure approximation error to the velocity approximation error.

In some finite element settings, the weakly divergence-free subspace \mathbf{V}_h of the velocity space has optimal approximation properties in the sense of

$$\inf_{I_h \mathbf{v} \in \mathbf{V}_h} \|\nabla(\mathbf{v} - I_h \mathbf{v})\|_{L^2(\Omega)} \leq C \inf_{I_h \mathbf{v} \in \mathbf{X}_h} \|\nabla(\mathbf{v} - I_h \mathbf{v})\|_{L^2(\Omega)}$$

holding when $\nabla \cdot \mathbf{v} = 0$. For example, this holds for $\mathbf{X}_h = \mathcal{P}_k$ with $k = d$ on barycenter-refined triangular/tetrahedral meshes [65, 77]. In such cases, the error analysis for the grad-div stabilized discretization can be modified by taking $I_h \mathbf{u} \in \mathbf{V}_h$, which leads to $\|\nabla \cdot \boldsymbol{\eta}\|_{L^2(\Omega)} = 0$, and provides the modified error estimate

$$(5.4) \quad \|\nabla(\mathbf{u} - \mathbf{u}_h)\|_{L^2(\Omega)}^2 + \frac{\gamma}{\nu} \|\nabla \cdot (\mathbf{u} - \mathbf{u}_h)\|_{L^2(\Omega)}^2 \\ \leq C \left(\frac{1}{\gamma\nu} \inf_{q_h \in Y_h} \|p - q_h\|_{L^2(\Omega)}^2 + \inf_{I_h \mathbf{u} \in \mathbf{X}_h} \|\nabla(\mathbf{u} - I_h \mathbf{u})\|_{L^2(\Omega)}^2 \right).$$

This estimate is better than (5.3) in the sense that one can take in (5.4) large values of γ without increasing the error bound at all. The best approximation error in $\mathbf{X}_{h,\text{div}}$ appearing in (5.3) can be estimated with the best approximation error in \mathbf{X}_h using (4.2). Since $\mathbf{V}_h \subset \mathbf{X}_{h,\text{div}}$, the constant in (5.4) will potentially be bigger than the constant which is introduced by applying (4.2) to (5.3). But on the other hand one can take γ arbitrarily large (up to where the condition number of the linear system of equations becomes prohibitively large) and essentially completely remove the impact of the pressure on the velocity error.

Proposals for the choice of the stability parameter γ in practice rely on equilibrating the terms in the error bound containing γ . For instance, if both infima on the right-hand side of (5.3) are asymptotically of the same order, then this approach leads to $\gamma = \mathcal{O}(1)$ with respect to the mesh width. A careful study of optimal choices of γ with respect to error bounds in different norms and of the dependence of γ on norms of the solution of the Stokes problem can be found in [43]. In this paper, the analytical results were supported with comprehensive numerical studies. It turns out that for each concrete example an appropriate choice typically depends on several aspects such that a good choice is usually a priori not clear.

In summary, grad-div stabilization is a popular, simple, and rather well understood technique for improving the pressure-robustness of any mixed method. However, it is not a complete remedy in the sense that a pressure-robust method is not constructed in this way, see also Example 6.2.

5.2. Using appropriate reconstructions of test functions. This section shows that an appropriate modification of the test functions might lead to *pressure-robust* mixed methods. This recent and quite general approach was introduced in [49, 50, 2], and it is based on well-understood inf-sup stable mixed methods. The modifications of the standard mixed methods are not severe, and in the case of the Stokes equations, the stiffness matrix is even unchanged.

The approach is based on the observation that test and trial functions play a quite different role. Changing the velocity test functions by using an $\mathbf{H}(\text{div})$ -conforming velocity reconstruction operator, one establishes the L^2 -orthogonality between discretely divergence-free test functions and arbitrary gradient fields. In this way, one obtains the discrete counterpart of the Helmholtz–Hodge decomposition, Lemma 2.6, which is relaxed in classical mixed methods. Then, also the fundamental invariance property (1.4) is recovered. In addition, one obtains a discrete vorticity equation which is close to equation (4.9) for pressure-robust mixed methods with $\mathbf{X}_{h,\text{div}} \subset \mathbf{X}_{\text{div}}$. The price to pay is an additional velocity-dependent consistency error, which is however of sufficiently high order.

While the approach was originally presented and analyzed for the first-order non-conforming Crouzeix–Raviart element, it will be presented here for the conforming pair of finite element spaces $\mathbf{X}_h/Y_h = \mathcal{P}_2^{\text{bubble}}/\mathcal{P}_1^{\text{disc}}$, to have a better comparison with the results from Section 3. Besides the discrete spaces \mathbf{X}_h and Y_h , the construction of the method needs the first order Raviart–Thomas space $\mathbf{R}_h := \text{RT}_1$, which is a $\mathbf{H}(\text{div})$ -conforming space (cf. Section 4.4). Important properties of \mathbf{R}_h utilized for the construction of the method are:

- for all $\mathbf{v}_h \in \mathbf{R}_h, e \subset \partial T, T \in \mathcal{T}_h$ it holds that $\mathbf{v}_h|_e \in \mathcal{P}_1(e)$,
- for all $q \in \mathcal{P}_1(e)$ it is $\int_e q [\mathbf{v}_h \cdot \mathbf{n}_e]_{\tau} ds = 0$,
- for all $\mathbf{v}_h \in \mathbf{R}_h$ it holds $\nabla \cdot \mathbf{v}_h \in Y_h$.

The construction of the method requires the definition of a velocity reconstruction operator $\Pi_h : \mathbf{X} \rightarrow \mathbf{R}_h$ satisfying the following properties:

$$(5.5) \quad \int_T (\mathbf{v} - \Pi_h \mathbf{v}) d\mathbf{x} = 0, \quad \forall \mathbf{v} \in \mathbf{X}, \forall T \in \mathcal{T}_h,$$

$$(5.6) \quad \int_e (\mathbf{v} - \Pi_h \mathbf{v}) \cdot \mathbf{n}_e q_h ds = 0, \quad \forall \mathbf{v} \in \mathbf{X}, \forall q_h \in \mathcal{P}_1(e),$$

$$(5.7) \quad \|\Pi_h \mathbf{v} - \mathbf{v}\|_{L^2(T)} \leq Ch_T^m |\mathbf{v}|_{H^m(T)}, \quad m = 0, 1, 2,$$

with a constant C depending only on the angles of T . By this definition, the reconstruction operator is just the standard Fortin interpolator for the RT_1 element. Using the product rule, integration by parts, (5.5), (5.6), $\nabla q_h|_T$ is constant, and once more integration by parts gives for $\mathbf{v} \in \mathbf{X}$, for all $T \in \mathcal{T}_h$ and all $q_h \in Y_h$

$$(5.8) \quad \begin{aligned} \int_T \nabla \cdot \mathbf{v} q_h d\mathbf{x} &= \int_T \nabla \cdot (\mathbf{v} q_h) d\mathbf{x} - \int_T \nabla q_h \cdot \mathbf{v} d\mathbf{x} = \int_{\partial T} q_h \mathbf{v} \cdot \mathbf{n}_T ds - \int_T \nabla q_h \cdot \mathbf{v} d\mathbf{x} \\ &= \int_{\partial T} q_h (\Pi_h \mathbf{v}) \cdot \mathbf{n}_T ds - \int_T \nabla q_h \cdot (\Pi_h \mathbf{v}) d\mathbf{x} = \int_T \nabla \cdot (\Pi_h \mathbf{v}) q_h d\mathbf{x}. \end{aligned}$$

Consequently, it holds that

$$(5.9) \quad \nabla \cdot (\Pi_h \mathbf{v}) = \pi_{Y_h}(\nabla \cdot \mathbf{v}).$$

In particular, for discretely divergence-free vector fields $\mathbf{v}_h \in \mathbf{X}_{h,\text{div}}$ the left-hand side of (5.8) vanishes such that from (5.9) it follows that such fields are mapped to divergence-free ones in the sense of $\mathbf{H}(\text{div})$.

Now, the modified scheme reads as follows: Find $(\mathbf{u}_h, p_h) \in \mathbf{X}_h \times Y_h$ such that for all $(\mathbf{v}_h, q_h) \in \mathbf{X}_h \times Y_h$

$$(5.10a) \quad a(\mathbf{u}_h, \mathbf{v}_h) + b(\mathbf{v}_h, p_h) = (\mathbf{f}, \Pi_h \mathbf{v}_h),$$

$$(5.10b) \quad b(\mathbf{u}_h, q_h) = (g, q_h).$$

LEMMA 5.1. *Let $\mathbf{u} \in H^3(\Omega)^d$ and $\mathbf{v} \in \mathbf{X}$, then it holds*

$$(5.11) \quad |(\Delta \mathbf{u}, \Pi_h \mathbf{v}) + (\nabla \mathbf{u}, \nabla \mathbf{v})| \leq C \sum_{T \in \mathcal{T}_h} h_T^2 |\mathbf{u}|_{H^3(T)} |\mathbf{v}|_{H^1(T)}.$$

Proof. Using integration by parts, (5.5), the Cauchy–Schwarz inequality, and interpolation estimates for both factors, e.g., (5.7) yields

$$\begin{aligned} (\Delta \mathbf{u}, \Pi_h \mathbf{v}) + (\nabla \mathbf{u}, \nabla \mathbf{v}) &= (\Delta \mathbf{u}, \Pi_h \mathbf{v} - \mathbf{v}) + (\nabla \mathbf{u}, \nabla \mathbf{v}) + (\Delta \mathbf{u}, \mathbf{v}) \\ &= (\Delta \mathbf{u} - \pi_{\mathcal{P}_0(T)} \Delta \mathbf{u}, \Pi_h \mathbf{v} - \mathbf{v}) \leq C \sum_{T \in \mathcal{T}_h} h_T^2 |\mathbf{u}|_{H^3(T)} |\mathbf{v}|_{H^1(T)}. \end{aligned}$$

□

THEOREM 5.2. *Assume that the solution of the Stokes equations (2.1) satisfies $\mathbf{u} \in \mathbf{H}^3(\Omega)$ and $p \in H^2(\Omega)$. Let the finite element problem (5.10) be discretized with $\mathcal{P}_2^{\text{bubble}}/\mathcal{P}_1^{\text{disc}}$, then the following error bounds hold*

$$(5.12) \quad \|\nabla(\mathbf{u} - \mathbf{u}_h)\|_{L^2(\Omega)} \leq 2(1 + C_F) \inf_{\mathbf{w}_h \in \mathbf{X}_h} \|\nabla(\mathbf{u} - \mathbf{w}_h)\|_{L^2(\Omega)} + Ch^2 |\mathbf{u}|_{H^3(\Omega)},$$

$$(5.13) \quad \|\pi_{Y_h} p - p_h\|_{L^2(\Omega)} \leq \frac{\nu}{\beta_h} \left(2(1 + C_F) \inf_{\mathbf{w}_h \in \mathbf{X}_h} \|\nabla(\mathbf{u} - \mathbf{w}_h)\|_{L^2(\Omega)} + Ch^2 |\mathbf{u}|_{H^3(\Omega)} \right),$$

$$(5.14) \quad \begin{aligned} \|p - p_h\|_{L^2(\Omega)} &\leq \inf_{q_h \in Y_h} \|p - q_h\|_{L^2(\Omega)} \\ &\quad + \frac{\nu}{\beta_h} \left(2(1 + C_F) \inf_{\mathbf{w}_h \in \mathbf{X}_h} \|\nabla(\mathbf{u} - \mathbf{w}_h)\|_{L^2(\Omega)} + Ch^2 |\mathbf{u}|_{H^3(\Omega)} \right). \end{aligned}$$

Proof. Because of $\mathbf{u}_h \in \mathbf{X}_{h,\text{div}}(g)$ it holds for an arbitrary $\mathbf{w}_h \in \mathbf{X}_{h,\text{div}}(g)$ that $\mathbf{v}_h^0 := \mathbf{u}_h - \mathbf{w}_h \in \mathbf{X}_{h,\text{div}}$. Since $C_0^\infty(\Omega)$ is dense in $H^2(\Omega)$ and $\Pi_h \mathbf{v}_h^0 \in \mathbf{H}(\text{div})$, one gets from (2.2) that $(\nabla p, \Pi_h \mathbf{v}_h^0) = 0$. Using this property, after having applied (5.10a), gives

$$\begin{aligned} \nu \|\nabla \mathbf{v}_h^0\|_{L^2(\Omega)}^2 &= a(\mathbf{v}_h^0, \mathbf{v}_h^0) = a(\mathbf{u}_h, \mathbf{v}_h^0) - a(\mathbf{w}_h, \mathbf{v}_h^0) = (-\nu \Delta \mathbf{u} + \nabla p, \Pi_h \mathbf{v}_h^0) - a(\mathbf{w}_h, \mathbf{v}_h^0) \\ &= a(\mathbf{u} - \mathbf{w}_h, \mathbf{v}_h^0) - \nu ((\Delta \mathbf{u}, \Pi_h \mathbf{v}_h^0) + (\nabla \mathbf{u}, \nabla \mathbf{v}_h^0)). \end{aligned}$$

Using (5.11) and the Cauchy–Schwarz inequality yields

$$\nu \|\nabla \mathbf{v}_h^0\|_{L^2(\Omega)}^2 \leq \nu \|\nabla(\mathbf{u} - \mathbf{w}_h)\|_{L^2(\Omega)} \|\nabla \mathbf{v}_h^0\|_{L^2(\Omega)} + \nu Ch^2 |\mathbf{u}|_{H^3(\Omega)} \|\nabla \mathbf{v}_h^0\|_{L^2(\Omega)},$$

such that

$$\|\nabla \mathbf{v}_h^0\|_{L^2(\Omega)} \leq \inf_{\mathbf{w}_h \in \mathbf{X}_{h,\text{div}}(g)} \|\mathbf{u} - \mathbf{w}_h\|_{L^2(\Omega)} + Ch^2 |\mathbf{u}|_{H^3(\Omega)}.$$

With the triangle inequality it follows that

$$\|\nabla(\mathbf{u} - \mathbf{u}_h)\|_{L^2(\Omega)} \leq \|\nabla(\mathbf{u} - \mathbf{w}_h)\|_{L^2(\Omega)} + \|\nabla \mathbf{v}_h^0\|_{L^2(\Omega)}.$$

Inserting now the estimate for $\|\nabla \mathbf{v}_h^0\|_{L^2(\Omega)}$, noting that \mathbf{w}_h was chosen to be arbitrary, and applying (4.2) finishes the proof of estimate (5.12).

To proof (5.13), consider an arbitrary function $\mathbf{v}_h \in \mathbf{X}_h$. It is $\nabla \cdot \Pi_h \mathbf{v}_h \in Y_h$ and from the definition of the L^2 -projection and (5.8) it follows that

$$(5.15) \quad (p, \nabla \cdot \Pi_h \mathbf{v}_h) = (\pi_{Y_h} p, \nabla \cdot \Pi_h \mathbf{v}_h) = (\pi_{Y_h} p, \nabla \cdot \mathbf{v}_h).$$

Using now (5.10a), integration by parts, and (5.15) yields

$$\begin{aligned} (\pi_{Y_h} p - p_h, \nabla \cdot \mathbf{v}_h) &= (\pi_{Y_h} p, \nabla \cdot \mathbf{v}_h) + (\mathbf{f}, \Pi_h \mathbf{v}_h) - a(\mathbf{u}_h, \mathbf{v}_h) \\ &= (\pi_{Y_h} p, \nabla \cdot \mathbf{v}_h) + (\nabla p, \Pi_h \mathbf{v}_h) - (\nu \Delta \mathbf{u}, \Pi_h \mathbf{v}_h) - a(\mathbf{u}_h, \mathbf{v}_h) \\ &= (\pi_{Y_h} p, \nabla \cdot \mathbf{v}_h) - (p, \nabla \cdot \Pi_h \mathbf{v}_h) - (\nu \Delta \mathbf{u}, \Pi_h \mathbf{v}_h) - a(\mathbf{u}_h, \mathbf{v}_h) \\ &= -(\nu \Delta \mathbf{u}, \Pi_h \mathbf{v}_h) - a(\mathbf{u}_h, \mathbf{v}_h) \\ &= -(\nu \Delta \mathbf{u}, \Pi_h \mathbf{v}_h) - a(\mathbf{u}, \mathbf{v}_h) - a(\mathbf{u}_h - \mathbf{u}, \mathbf{v}_h). \end{aligned}$$

Inserting this expression in the discrete inf-sup condition (3.2) and applying the triangle and the Cauchy–Schwarz inequalities and (5.11) gives

$$\begin{aligned} \|\pi_{Y_h} p - p_h\| &\leq \frac{\nu}{\beta_h} \left(\|\nabla(\mathbf{u} - \mathbf{u}_h)\|_{L^2(\Omega)} + \sup_{\mathbf{0} \neq \mathbf{v}_h \in \mathbf{X}_h} \frac{|(\Delta \mathbf{u}, \Pi_h \mathbf{v}_h) + (\nabla \mathbf{u}, \nabla \mathbf{v}_h)|}{\|\nabla \mathbf{v}_h\|_{L^2(\Omega)}} \right) \\ &\leq \frac{\nu}{\beta_h} (\|\nabla(\mathbf{u} - \mathbf{u}_h)\|_{L^2(\Omega)} + Ch^2 |\mathbf{u}|_{H^3(\Omega)}). \end{aligned}$$

The proof of (5.13) is finished by inserting (5.12).

Estimate (5.14) is a direct consequence of the triangle inequality

$$\|p - p_h\|_{L^2(\Omega)} \leq \|p - \pi_{Y_h} p\|_{L^2(\Omega)} + \|\pi_{Y_h} p - p_h\|_{L^2(\Omega)},$$

estimate (5.13), and the observation that the L^2 -projection is the best approximation in the $L^2(\Omega)$ norm. \square

The error estimates above show that, in order to get pressure-robustness, the inclusion $\mathbf{X}_{h,\text{div}} \subset \mathbf{X}_{\text{div}}$ is not needed. In fact, for the incompressible Stokes equations a lack of pressure-robustness can only evolve in the discretization of the right hand side term $(\mathbf{f}, \mathbf{v}_h)$. The key idea is to repair the L^2 scalar product, in order to achieve that discretely divergence-free vector fields become orthogonal to gradient fields. For more complex flows than the incompressible Stokes equations, one has to repair this kind of L^2 -orthogonality in every term of the discrete weak formulation, where some force is tested in the L^2 sense with a test function \mathbf{v}_h . This issue concerns also the nonlinear convection term $(\mathbf{u}_h \cdot \nabla) \mathbf{u}_h$ and the Coriolis force term, see [50, 51]. So far, the approach could be generalized to mixed discretizations of arbitrarily high order on triangles, tetrahedra, squares, and cuboids, if the discrete pressures are discontinuous [2].

REMARK 5.3. *Instead of $\mathbf{R}_h = \text{RT}_1$ one can also use $\mathbf{R}_h := \text{BDM}_2$ and its standard Fortin interpolator Π_h . This approach has the advantage of a possibly smaller consistency error and it leaves quadratic test functions untouched. In other words, only the non-quadratic bubble functions*

have to be modified. This version of the reconstruction was used in the numerical examples below. Similarly, the test functions of the lowest order Bernardi–Raugel element were reconstructed into $\mathbf{R}_h := \text{BDM}_1$ with the associated standard Fortin interpolator, which only affects the normal-weighted face bubbles.

5.3. Post-processing of low order velocity fields computed with non-inf-sup stable methods. An approach for post-processing a finite element solution in such a way that one obtains a divergence-free solution in $\mathbf{H}(\text{div})$ was proposed for certain stabilized discretizations in [10, 11, 12]. In these paper, two-dimensional problems were considered which were discretized with \mathcal{P}_1 finite elements for the velocity and \mathcal{P}_0 or \mathcal{P}_1 finite elements for the pressure. The stabilization with respect to the discrete inf-sup condition is based on jumps of $\nabla \mathbf{u}_h$ or p_h across the edges of the mesh cells. The basic idea of this approach consists of adding a correction from $\text{RT}_0(\mathcal{J}_h)$ to \mathbf{u}_h so that the resulting discrete velocity is divergence-free. The concrete form of the correction depends on the stabilization used. It can be shown that the divergence-free velocity field converges with optimal order in appropriate norms.

6. Numerical studies. This section presents a couple of examples which illustrate situations in which the methods discussed in the previous sections are beneficial, but also situations where standard methods work equally well.

EXAMPLE 6.1. Example 1.1 – Example 1.3 with appropriate reconstructions of test functions. In Examples 1.1 – 1.3 the dependence of the velocity error on the viscosity for the standard non-conforming Crouzeix–Raviart finite element discretization $\mathcal{P}_1^{\text{CR}}/\mathcal{P}_0$ was clearly seen. As mentioned at the beginning of Section 5.2, a reconstruction of the test function can be applied for this pair of finite element spaces, see [50]. In the case of the Stokes equations, this reconstruction is performed only on the right-hand side. For the Navier–Stokes equations, the test function in the convective term, and if present, also the term with the Coriolis force, have to be reconstructed, see [16]. For the Crouzeix–Raviart finite element, the reconstructed test function is a projection onto a Raviart–Thomas function of order zero (RT_0). Applying this reconstruction, one obtains the results presented in Figure 6.1. One can see that in all cases the velocity fields are recovered up to round-off errors.

EXAMPLE 6.2. Grad-div stabilization. The effect of using the grad-div stabilization described in Section 5.1 will be illustrated for the Stokes equations with the prescribed solution

$$\mathbf{u} = 200 \begin{pmatrix} x^2(1-x)^2y(1-y)(1-2y) \\ -x(1-x)(1-2x)y^2(1-y)^2 \end{pmatrix}, \quad p = 10 \left(\left(x - \frac{1}{2} \right)^3 y^2 + (1-x)^3 \left(y - \frac{1}{2} \right)^3 \right),$$

see Figure 6.2. The velocity field has the form of a large vortex. Note that for the flow problem from Example 1.1, the second infimum in the error bound (5.3) vanishes such that $\gamma \rightarrow \infty$ leads to the ideal computed velocity field. This situation is not representative for the general case.

Here, only a few results will be presented. The simulations were performed with the Taylor–Hood pair of spaces $\mathcal{P}_2/\mathcal{P}_1$. The unstructured initial grid depicted in Figure 6.2 was refined four times leading to 36,546 degrees of freedom (d.o.f.) for the velocity and 4,688 d.o.f. for the pressure. In this situation, the error estimate (5.3) for $\|\nabla(\mathbf{u} - \mathbf{u}_h)\|_{L^2(\Omega)}^2$ applies. Both infima in the error bound are of the same order, hence their equilibration leads to the choice $\gamma = \mathcal{O}(1)$ with respect to the mesh width. The analysis from [43] shows that the optimal choice of γ depends on norms of the solution. Since the prescribed solution does not depend on the viscosity, the optimal stabilization parameter should be independent of ν . A representative result is presented in Figure 6.3. It can be

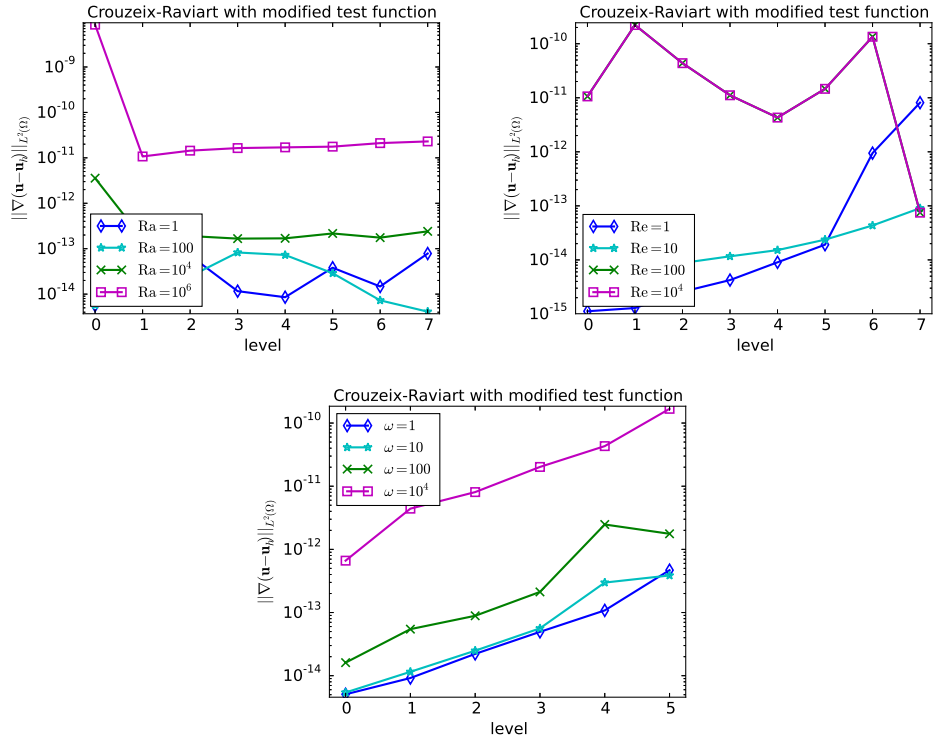


FIG. 6.1. Example 6.1. Crouzeix–Raviart pair of spaces with reconstructed test function, Examples 1.1 – 1.3.

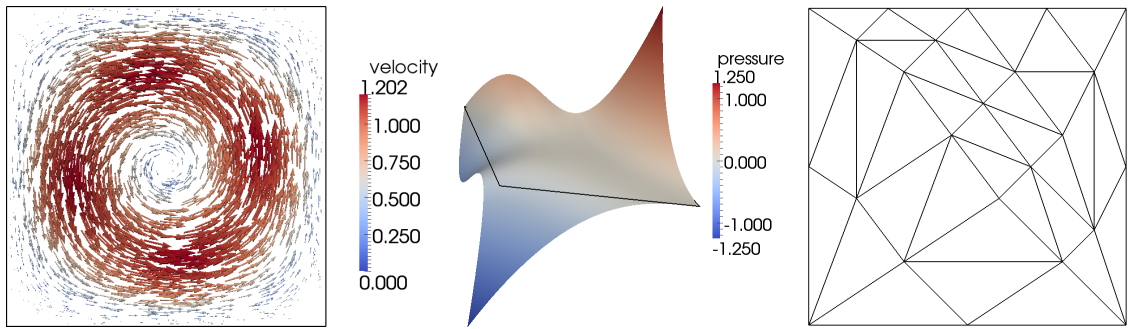


FIG. 6.2. Example 6.2. Velocity, pressure, initial grid (level 0).

seen that for $\nu = 1$ one gets for a wide range of γ approximately the same results. Only for large γ , the divergence error decreases but at the same time $\|\nabla(\mathbf{u} - \mathbf{u}_h)\|_{L^2(\Omega)}^2$ increases. For smaller values of ν , one observes that the optimal stabilization parameter with respect to $\|\nabla(\mathbf{u} - \mathbf{u}_h)\|_{L^2(\Omega)}^2$ is contained in $[0.03, 0.08]$. The impact on the error $\|\nabla \cdot \mathbf{u}_h\|_{L^2(\Omega)}^2$ is much higher for small ν . In particular in the case $\nu = 10^{-6}$, very large values of γ lead to almost divergence-free solutions with

only a slightly larger velocity error compared with the optimal parameter for $\|\nabla(\mathbf{u} - \mathbf{u}_h)\|_{L^2(\Omega)}^2$. However, it shall be emphasized that large contributions of the grad-div stabilization result in linear systems of equations with large condition numbers [62].

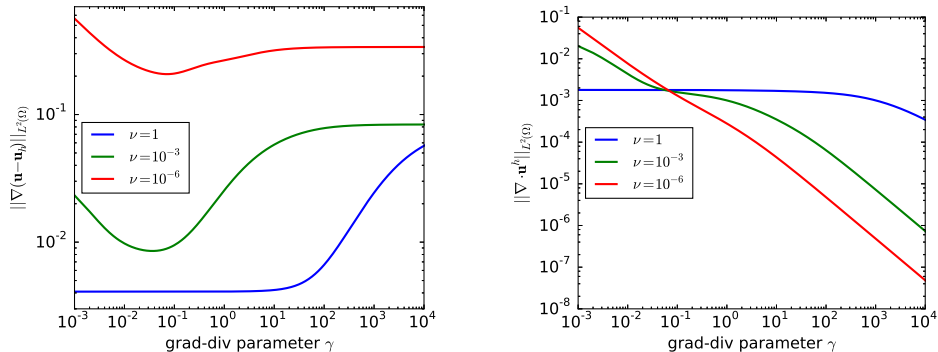


FIG. 6.3. *Example 6.2. Errors for a wide range of stabilization parameters.*

The presented result illustrates the final comment of Section 5.1 quite well: the grad-div stabilization might improve the pressure-robustness in certain situations but it is not a remedy. For this reason, the presentation of more numerical results will be omitted here. Instead it is referred to the comprehensive numerical studies in [43].

EXAMPLE 6.3. Natural convection in a triangular cavity. In natural convection problems, the flow is driven by the temperature. Here, a model consisting of a coupled system of the Stokes equations and of a convection-diffusion equation for the temperature will be considered:

$$(6.1) \quad -\Delta \mathbf{u} + \nabla p = \text{Ra} \mathbf{e}_j \theta,$$

$$(6.2) \quad \nabla \cdot \mathbf{u} = 0,$$

$$(6.3) \quad -\Delta \theta + \mathbf{u} \cdot \nabla \theta = 0,$$

with θ representing temperature, and \mathbf{e}_j being a unit vector pointing in the direction opposite to gravity. Simulations were performed with the Rayleigh number $\text{Ra} = 10^6$. Models of this type can be used for the simulation of fluids like silicon oil.

Natural convection problems defined on the unit square are standard test problems. To present a different setup, the domain Ω was chosen to be the right triangle with vertices $(0, 0)$, $(1, 0)$ and $(0, 1)$. The boundary is considered to be solid walls. Thus, homogeneous Dirichlet boundary conditions for the velocity are prescribed on the walls. For the temperature, a sinusoidal heat source is enforced on the bottom boundary with a Dirichlet condition, the left wall is set to a constant temperature of zero, and the hypotenuse wall is perfectly insulated so that a Neumann boundary condition is appropriate. A diagram of the domain and the boundary conditions is given in Figure 6.4. This figure shows also the initial triangulation (level 0) used in the simulations.

Besides presenting plots of the numerical solutions, the Nusselt number defined by

$$\text{Nu} = \int_{\partial\Omega \cap \{y=0\}} \nabla T \cdot \mathbf{n} \, ds$$

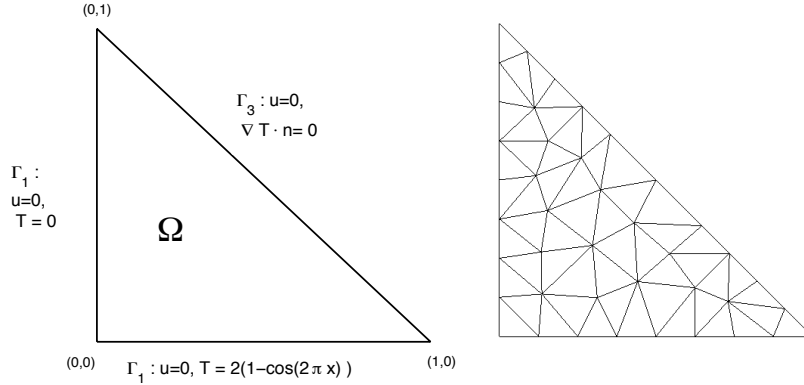


FIG. 6.4. *Example 6.3. Left: domain and boundary conditions for the natural convection problem in a triangular cavity; right: initial triangulation (level 0).*

will be studied. Extrapolating results obtained with higher order discretizations, one finds $\text{Nu} \approx 24.535$.

First, results for a low order discretization will be presented. For the Stokes equations, the Bernardi–Raugel element $\mathcal{P}_1^{\text{BR}}/\mathcal{P}_0$ [14] was used and for the temperature the \mathcal{P}_1 finite element. The velocity space in the Bernardi–Raugel element consists of \mathcal{P}_1 functions which are enriched with edge bubble functions. For this element, a reconstruction of the test function as described in Section 5.2 and Remark 5.3 can be constructed.

For the methods that use a reconstruction of the test functions, the discrete velocity fields are not weakly divergence-free. In order to enforce this property, one has to apply a projection operator which maps the discretely divergence-free velocity field to a divergence-free velocity field. To this end, the same operator Π_h can be employed which was used for reconstructing the test functions. The desired divergence-free property follows from (5.9). This reconstruction was applied to \mathbf{u} in (6.3).

Computed solutions obtained without and with this reconstruction are depicted in Figures 6.5 – 6.7. The Nusselt numbers and the divergence of the discrete velocity are given in Table 6.1. The velocity fields computed using the method with reconstruction is much smoother on coarse grids. Also the temperature is somewhat smoother. The computed pressure fields look similar for both methods. With respect to the Nusselt number, generally the results of the method with reconstruction are more accurate. Altogether, the use of an appropriately reconstructed test function in the Bernardi–Raugel pair of spaces led to a clear improvement of the accuracy of the computed results compared with the standard method.

As higher order discretizations, the Taylor–Hood pair $\mathcal{P}_2/\mathcal{P}_1$, the Scott–Vogelius pair $\mathcal{P}_2/\mathcal{P}_1^{\text{disc}}$ [68], and the pair $\mathcal{P}_2^{\text{bubble}}/\mathcal{P}_1^{\text{disc}}$ from [26] were considered. In the $\mathcal{P}_2^{\text{bubble}}/\mathcal{P}_1^{\text{disc}}$ finite element, the velocity space consists of \mathcal{P}_2 functions and an enrichment with mesh cell bubbles. The reconstruction of the test function for this pair is described in Section 5.2 and Remark 5.3. As for the Bernardi–Raugel element with reconstruction, the reconstruction is also applied to \mathbf{u} in (6.3). For applying the Scott–Vogelius pair, an additional barycentric refinement of the grids was applied to guarantee the satisfaction of the discrete inf-sup condition (3.2), see [65]. Since $Y_h = \mathcal{P}_1^{\text{disc}} = \nabla \cdot \mathcal{P}_2 = \mathbf{X}_h$,

TABLE 6.1
Example 6.3. Nusselt number obtained with the Bernardi–Raugel element $\mathcal{P}_1^{\text{BR}}/\mathcal{P}_0$.

level	d.o.f.	standard	with reconstruction
0	271	not conv.	11.828
1	947	14.016	13.870
2	3317	17.232	20.935
3	13115	21.955	23.665
4	51697	23.664	24.238
reference			24.535

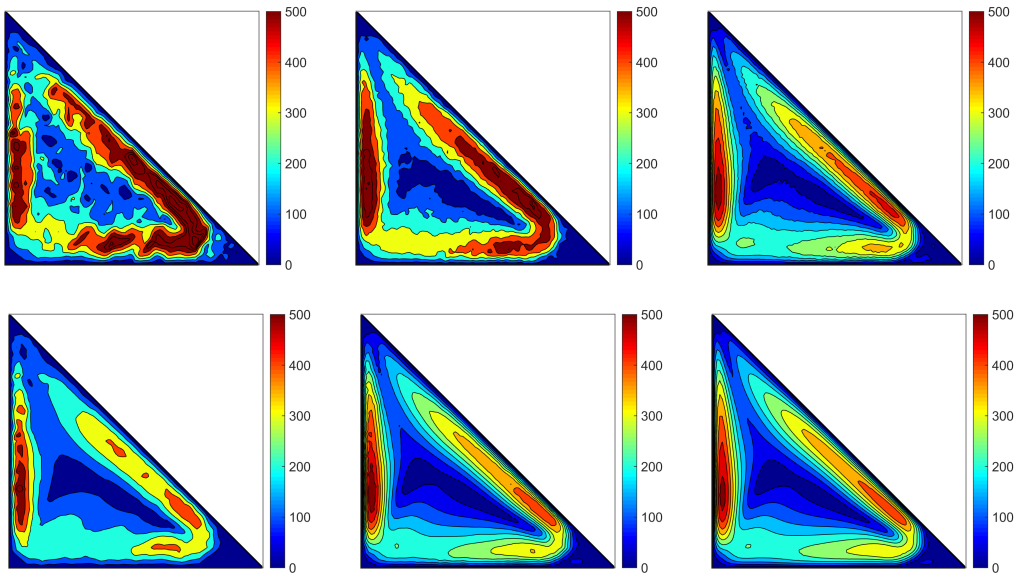


FIG. 6.5. *Example 6.3. Absolute value of the velocity (speed) obtained with the Bernardi–Raugel element $\mathcal{P}_1^{\text{BR}}/\mathcal{P}_0$ on levels 1 to 3; top: standard formulation; bottom: with reconstruction of the test function.*

the use of the Scott–Vogelius pair gives divergence-free velocity fields in the sense of Definition 2.3. For all higher order discretizations, the temperature was discretized with the \mathcal{P}_2 finite element.

The computed velocity fields for the higher order discretizations are presented in Figure 6.8. Only for the grids with the smallest number of degrees of freedom, small differences can be observed. In this case, the velocity obtained with the Taylor–Hood pair seems to be the least accurate. The situation is similar for the temperature. With respect to the pressure, there are only small differences between the different methods, which is the same situation as for the low order discretizations. For the sake of brevity, the presentation of the pressures computed by the higher-order methods is omitted.

To obtain a reference value for the Nusselt number, simulations with the Taylor–Hood and Scott–Vogelius finite elements were performed on very fine meshes and the numbers were extrapolated by Aitken extrapolation, see Table 6.2. Both methods agree on the first two digits. For

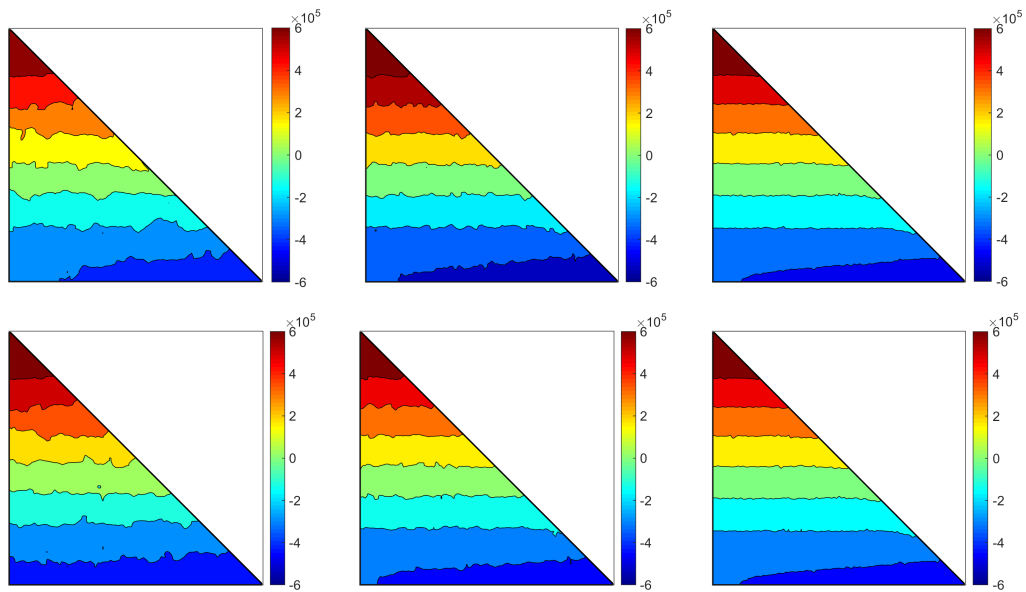


FIG. 6.6. Example 6.3. Pressure obtained with the Bernardi–Raugel element $\mathcal{P}_1^{\text{BR}}/\mathcal{P}_0$ on levels 1 to 3; top: standard formulation; bottom: with reconstruction of the test function.

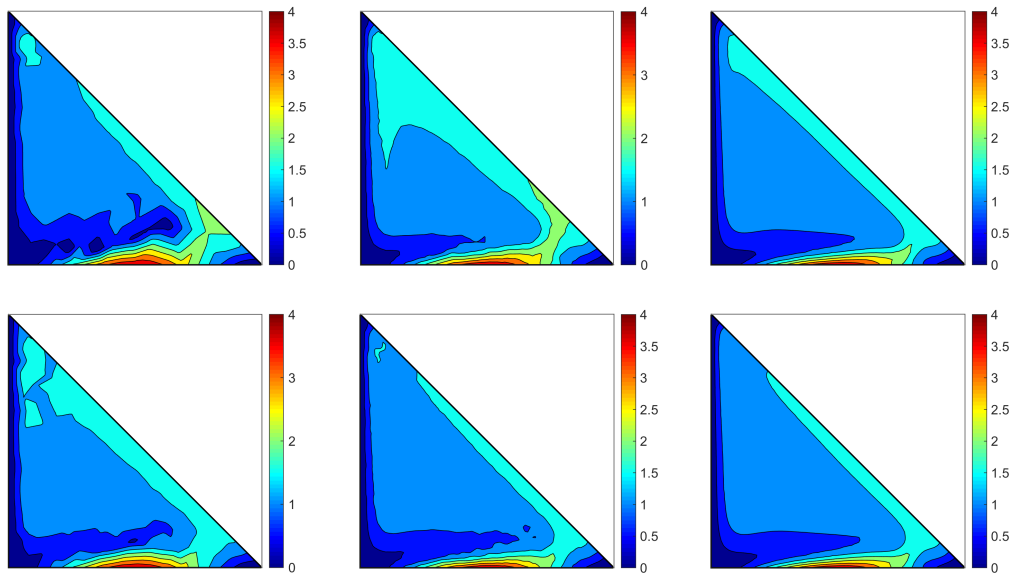


FIG. 6.7. Example 6.3. Temperature obtained with the Bernardi–Raugel element $\mathcal{P}_1^{\text{BR}}/\mathcal{P}_0$ on levels 1 to 3; top: standard formulation; bottom: with reconstruction of the test function.

TABLE 6.2

Example 6.3. Nusselt number obtained with $\mathcal{P}_2/\mathcal{P}_1$, $\mathcal{P}_2/\mathcal{P}_1^{\text{disc}}$, $\mathcal{P}_2^{\text{bubble}}/\mathcal{P}_1^{\text{disc}}$, $\mathcal{P}_2^{\text{bubble}}/\mathcal{P}_1^{\text{disc}}$ with reconstructed test function.

level	$\mathcal{P}_2/\mathcal{P}_1$		$\mathcal{P}_2/\mathcal{P}_1^{\text{disc}}$		$\mathcal{P}_2^{\text{bubble}}/\mathcal{P}_1^{\text{disc}}$ std./reco.		
	d.o.f.	Nu	d.o.f.	Nu	d.o.f.	Nu	Nu
0	446	0.074	1539	10.318	675	5.778	6.240
1	1551	16.105	5829	17.867	2469	13.850	13.765
2	5414	20.748	21333	21.967	8869	20.261	20.254
3	21361	23.475	86409	23.918	35561	23.460	23.461
4	84108	24.183	344685	24.333	141149	24.184	24.184
5	332757	24.427	1373127	24.471			
6	1325912	24.501					
extrapolation		24.537		24.533			

a similar number of degrees of freedom, more accurate Nusselt numbers were obtained with the Taylor–Hood pair of spaces compared with the Scott–Vogelius pair. The application of the reconstruction for $\mathcal{P}_2^{\text{bubble}}/\mathcal{P}_1^{\text{disc}}$ had only a minor effect on the computed Nusselt numbers.

Altogether, with the standard Taylor–Hood pair of spaces $\mathcal{P}_2/\mathcal{P}_1$ good results were obtained, except on grids with very few degrees of freedom. Apart of getting a divergence-free solution, there is no advantage to use the Scott–Vogelius pair for this problem. There was also no advantage to apply a reconstruction of the test function for the $\mathcal{P}_2^{\text{bubble}}/\mathcal{P}_1^{\text{disc}}$ pair of spaces. Possibly, the almost linear pressure, which can be resolved well by all discrete piecewise linear pressure spaces, is a reason that only minor differences for the higher order methods could be observed. However, it will be shown in Example 6.5 that a divergence-free solution might be very important if the scalar quantity possesses certain restrictions arising from the physics of the problem.

EXAMPLE 6.4. Flow over a forward facing step with Coriolis force. As already mentioned in Example 1.3 flows with strong Coriolis forces appear in several applications. The simplest model for such a flow has the form

$$-\nu\Delta\mathbf{u} + \nabla p + 2\boldsymbol{\omega} \times \mathbf{u} = \mathbf{f}, \quad \nabla \cdot \mathbf{u} = 0,$$

where $\boldsymbol{\omega}$ is a constant angular velocity vector. A two-dimensional example with $\boldsymbol{\omega} = (0, 0, \omega)^T$ will be considered. Since

$$\nabla \times (\boldsymbol{\omega} \times \mathbf{u}) = \boldsymbol{\omega} \begin{pmatrix} -\partial_z u_1 \\ -\partial_z u_2 \\ \nabla \cdot \mathbf{u} \end{pmatrix} = \mathbf{0},$$

$(\boldsymbol{\omega} \times \mathbf{u})$ is conservative, which implies that there is a function ϕ satisfying $\boldsymbol{\omega} \nabla \phi = \boldsymbol{\omega} \times \mathbf{u}$. Thus, changing the magnitude ω of the Coriolis force will change only the pressure solution, i.e., $p \rightarrow p + \omega\phi$, and not the velocity solution.

This problem was considered in the domain $\Omega = (0, 4) \times (0, 2) \setminus [2, 4] \times [0, 1]$, see Figure 6.9. The inlet is situated at $x = 0$ and the outlet at $x = 4$. Dirichlet boundary conditions were prescribed on the entire boundary, where the volume preserving parabolic inflow and outflow profiles were given by

$$\mathbf{u}_{\text{in}} = \begin{pmatrix} y(2-y)/2 \\ 0 \end{pmatrix}, \quad \mathbf{u}_{\text{out}} = \begin{pmatrix} 4(2-y)(y-1) \\ 0 \end{pmatrix},$$

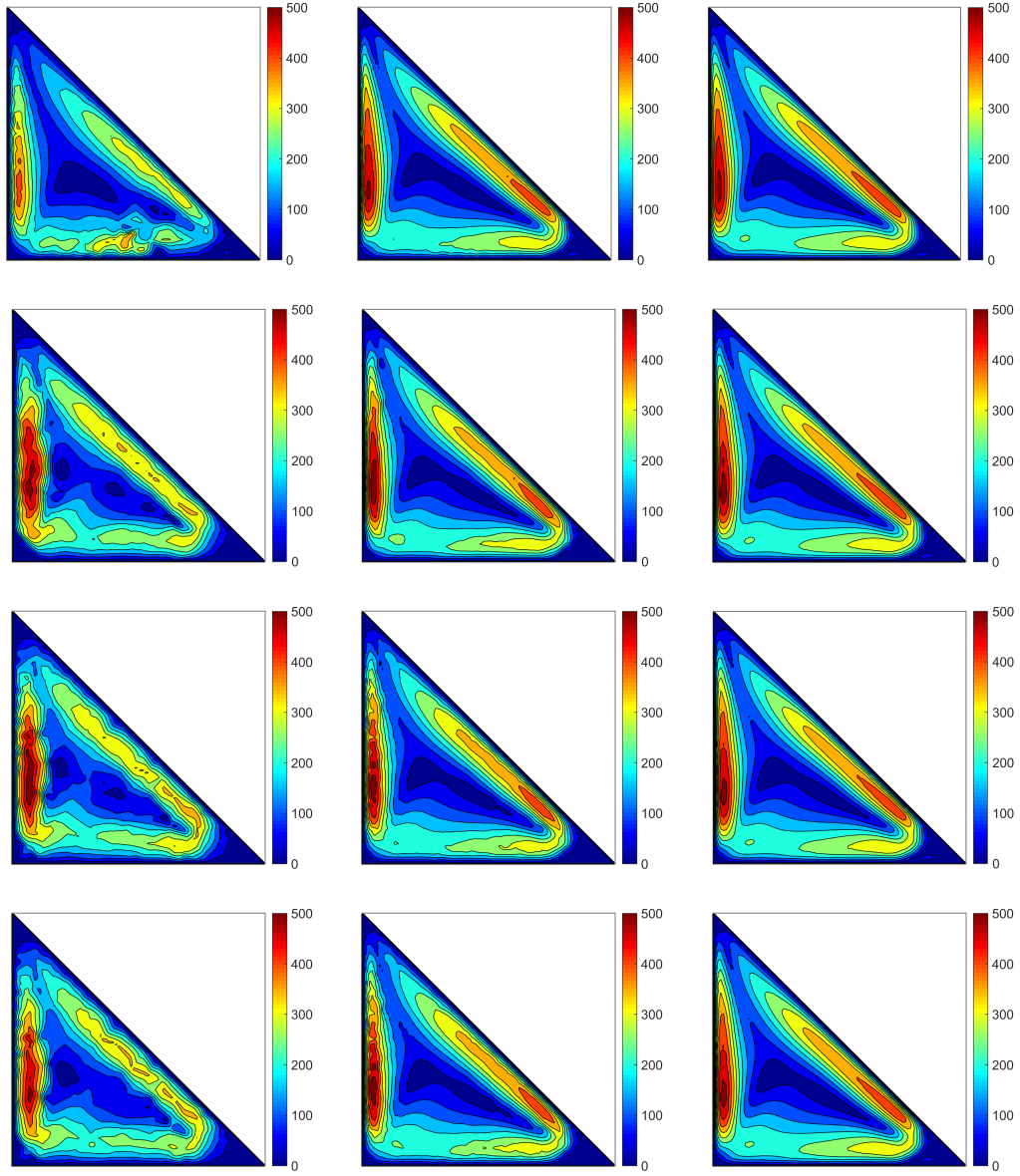


FIG. 6.8. *Example 6.3. Absolute value of the velocity (speed); top to bottom: $\mathcal{P}_2/\mathcal{P}_1$ (levels 1 to 3), $\mathcal{P}_2/\mathcal{P}_1^{\text{disc}}$ (levels 0 to 2 with barycentric refinement), $\mathcal{P}_2^{\text{bubble}}/\mathcal{P}_1^{\text{disc}}$ (levels 0 to 2), $\mathcal{P}_2^{\text{bubble}}/\mathcal{P}_1^{\text{disc}}$ with reconstructed test function (levels 0 to 2).*

and no-slip conditions were used at all other parts of the boundary. Simulations were performed with $\nu = 0.01$ and $\omega = 100$. The initial grid is depicted in Figure 6.9. For the Scott–Vogelius pair of finite element spaces, a barycentric refinement of all grid levels was applied.

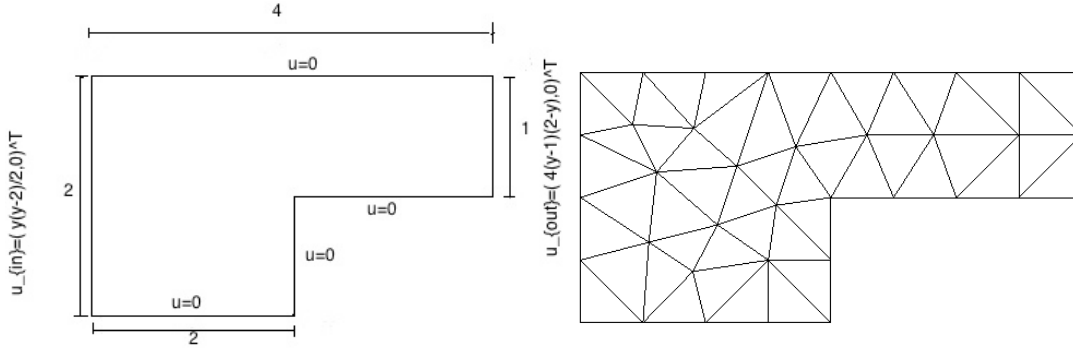


FIG. 6.9. Example 6.4. Domain and boundary conditions and coarsest mesh (level 0).

Computed solutions obtained on coarse grids are presented in Figures 6.10 – 6.12. The positive effect of using the formulation with reconstructed test function and Coriolis force term can be observed clearly, not only for the low order Bernardi–Raugel element $\mathcal{P}_1^{\text{BR}}/\mathcal{P}_0$ but also for the higher order $\mathcal{P}_2^{\text{bubble}}/\mathcal{P}_1^{\text{disc}}$ pair of spaces, Figures 6.10 and 6.11. Also the solutions computed with the divergence-free Scott–Vogelius finite element are considerably more accurate than the solutions obtained with the Taylor–Hood element on grids with a comparable number of degrees of freedom, Figure 6.12. Note that due to the barycentric refinement, the number of degrees of freedom for the Scott–Vogelius element on level l is approximately the same as for the Taylor–Hood element on level $l - 1$.

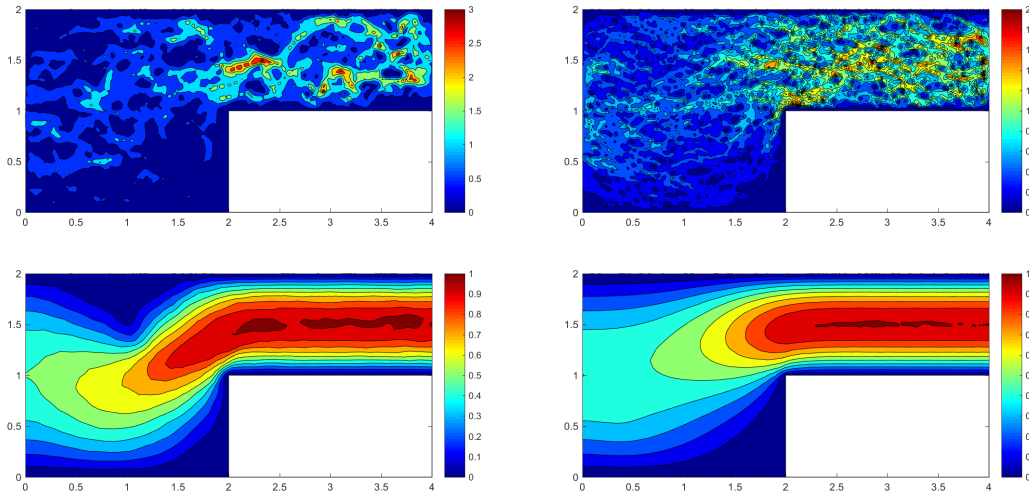


FIG. 6.10. Example 6.4. Absolute value of the velocity (speed) obtained with the Bernardi–Raugel element $\mathcal{P}_1^{\text{BR}}/\mathcal{P}_0$ on refinement levels 2 and 3; top: standard formulation; bottom: with reconstruction of the test function.

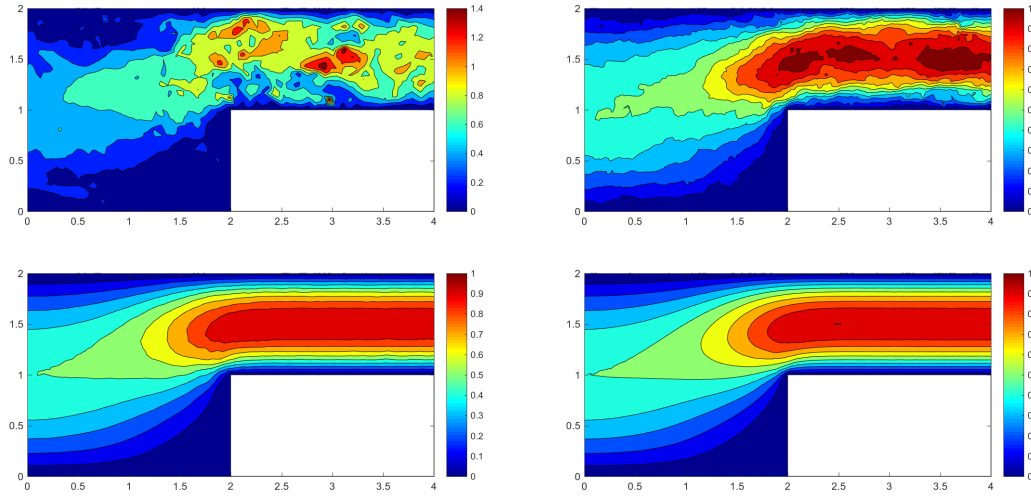


FIG. 6.11. *Example 6.4.* Absolute value of the velocity (speed) obtained with $\mathcal{P}_2^{\text{bubble}}/\mathcal{P}_1^{\text{disc}}$ on refinement levels 1 and 2; top: standard formulation; bottom: with reconstruction of the test function.

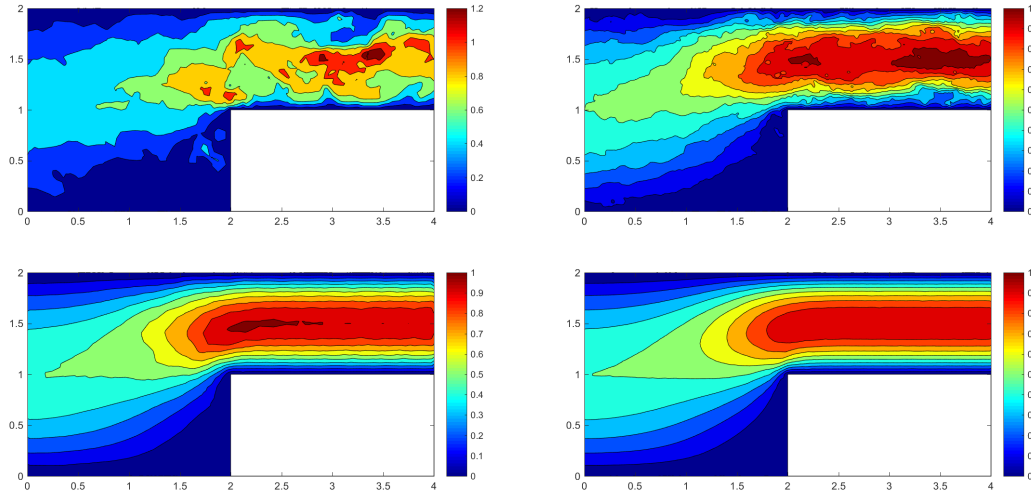


FIG. 6.12. *Example 6.4.* Absolute value of the velocity (speed) obtained with the Taylor-Hood element on refinement levels 1 and 2 (top) and the Scott-Vogelius element on refinement levels 0 and 1 (bottom).

Altogether, this example shows clearly the benefit which might be achieved if pressure-robust discretizations are used for simulations of flows with Coriolis forces.

EXAMPLE 6.5. Convection-dominated transport of a passive scalar. The final example demonstrates that divergence-free discrete velocity fields might be also of advantage in coupled problems. To this end, consider the transport of a passive scalar, e.g., temperature, through a domain with a

flow field which is governed by the Stokes equations

$$(6.4) \quad -\nu \Delta \mathbf{u} + \nabla p = \mathbf{0},$$

$$(6.5) \quad \nabla \cdot \mathbf{u} = 0,$$

$$(6.6) \quad -\varepsilon \Delta \theta + \mathbf{u} \cdot \nabla \theta = 0.$$

The domain and the boundary conditions for the velocity are the same as in Example 6.4. At the inlet, the constant temperature $\theta = 1$ is prescribed and on all other boundaries a free temperature flux $-\varepsilon \nabla \theta \cdot \mathbf{n} = 0$. Together with (6.6) it follows that $\theta = 1$ is the solution for the temperature field. Simulations were performed with the coefficients $\nu = 0.01$ and $\varepsilon = 10^{-6}$. The same initial grid was used as presented in Figure 6.9.

The Stokes equations were discretized either by the Bernardi–Raugel element $\mathcal{P}_1^{\text{BR}}/\mathcal{P}_0$, the $\mathcal{P}_2^{\text{bubble}}/\mathcal{P}_1^{\text{disc}}$ element, or the Taylor–Hood element. Equation (6.6) for the temperature is a convection-dominated equation. It is well known that stabilizations are necessary for discretizing this type of system. There are numerous proposals, e.g., see [67]. However, there are only a few stabilized methods that satisfy a discrete maximum principle, which is an important property in many applications to guarantee that numerical solutions have meaningful physical values. One of these discretizations is the exponentially-fitted Voronoi finite volume method from [34, 35]. This method satisfies the discrete maximum principle on Delaunay grids (the used grids are of this type) and for divergence-free convection fields.

The computation of weakly divergence-free fields for the methods that use a reconstruction of the test functions is described in Example 6.3.

Figure 6.13 and Table 6.3 present results of the numerical simulations. The velocity field is of the same form as in Example 6.4. Since there is no Coriolis force, visually there appear almost no differences of the velocity fields computed with the different discretizations (presentation omitted for the sake of brevity). However, the violation of the divergence constraint causes (strong) spurious oscillations of the discrete temperature in all cases where the discrete velocity fields are not divergence-free. In contrast, the methods with divergence-free velocity fields compute the temperature with exact accuracy on all grid levels.

TABLE 6.3
Example 6.5. Minimal and maximal temperature.

level	$\mathcal{P}_1^{\text{BR}}/\mathcal{P}_0$		$\mathcal{P}_2^{\text{bubble}}/\mathcal{P}_1^{\text{disc}}$		$\mathcal{P}_2/\mathcal{P}_1$	$\mathcal{P}_2/\mathcal{P}_1^{\text{disc}}$
	std.	reco.	std.	reco.		
0	0.550/1.331	1.000/1.000	0.942/2.071	1.000/1.000	0.881/1.930	1.000/1.000
1	0.273/6.343	1.000/1.000	0.875/1.319	1.000/1.000	0.828/1.640	1.000/1.000
2	0.408/2.997	1.000/1.000	0.948/1.037	1.000/1.000	0.773/1.052	1.000/1.000
3	0.582/2.761	1.000/1.000	0.993/1.005	1.000/1.000	0.955/1.030	1.000/1.000
4	0.827/1.415	1.000/1.000	0.993/1.002	1.000/1.000	0.909/1.017	1.000/1.000

7. Outlook. This paper has provided a thorough review of the state of the art methods and numerical analysis for the enforcement of the divergence constraint in mixed finite element methods for equations that model incompressible flows, with a special emphasis on the Stokes equations with possibly non-vanishing divergence of the velocity field. Although a significant amount of progress has been achieved, in particular in the past decade, these methods have not reached large scale and widespread use. As already discussed in Section 4.3, there remain several open problems related to

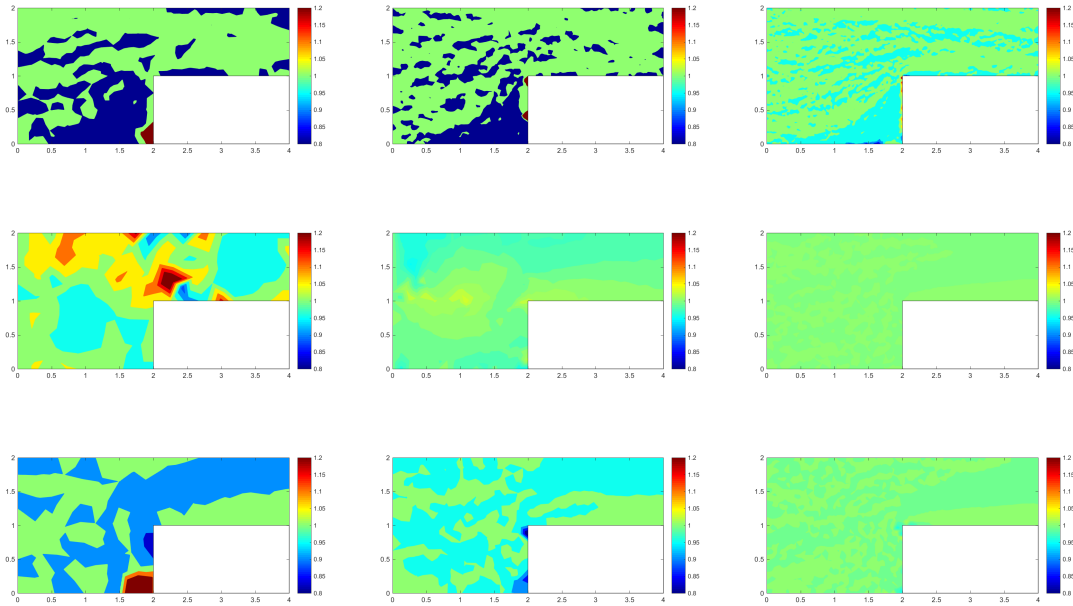


FIG. 6.13. *Example 6.5. Concentration obtained with a Voronoi finite volume method and velocity fields by the Bernardi–Raugel element $\mathcal{P}_1^{\text{BR}}/\mathcal{P}_0$ on refinement levels 2–4 (top), the $\mathcal{P}_2^{\text{bubble}}/\mathcal{P}_1^{\text{disc}}$ on refinement levels 1–3 (middle), or the Taylor–Hood element on refinement levels 1–3 (bottom).*

de Rham complexes in the three-dimensional case. Further, since the concentration here was mainly on the Stokes equations, additional important details can arise when Coriolis forces are present, for the Navier–Stokes equations, and for multi-physics systems. This concerns all methods discussed, but especially all discussed pressure-robust discretizations that are only $\mathbf{H}(\text{div})$ -conforming and the methods that apply $\mathbf{H}(\text{div})$ -conforming velocity reconstructions, see Section 5.2 and Section 5 in [50].

Another important open problem is the development of efficient linear solvers for large-scale computations with divergence-free elements. Most linear solvers used in large-scale Navier–Stokes codes seem tailored to low order elements, and are less effective when used with divergence-free elements, due to the pressure matrices being much larger. However, these larger pressure matrices are very sparse, and this can likely be exploited. Furthermore, divergence-free elements usually have a macro-element structure in the mesh, which seems to provide a natural framework to develop multigrid preconditioners.

REFERENCES

- [1] M. Ainsworth and W. Dörfler. Reliable a posteriori error control for nonconformal finite element approximation of Stokes flow. *Math. Comp.*, 74(252):1599–1619 (electronic), 2005.
- [2] Alexander Linke, Gunar Matthies, and Lutz Tobiska. Robust arbitrary order mixed finite element methods for the incompressible stokes equations with pressure independent velocity errors. *ESAIM: M2AN*, 2015. to appear.

- [3] J. Argyris, I. Fried, and D. Scharpf. The TUBA family of plate elements for the matrix displacement method. *Aero. J. Roy. Aero. Soc.*, 72:701–709, 1968.
- [4] D. N. Arnold, F. Brezzi, and M. Fortin. A stable finite element for the Stokes equations. *Calcolo*, 21(4):337–344 (1985), 1984.
- [5] D. N. Arnold, R. S. Falk, and R. Winther. Finite element exterior calculus, homological techniques, and applications. *Acta Numer.*, 15:1–155, 2006.
- [6] D. N. Arnold, R. S. Falk, and R. Winther. Finite element exterior calculus: from Hodge theory to numerical stability. *Bull. Amer. Math. Soc. (N.S.)*, 47(2):281–354, 2010.
- [7] D. N. Arnold and J. Qin. Quadratic velocity/linear pressure Stokes elements. In R. Vichnevetsky, D. Knight, and G. Richter, editors, *Advances in Computer Methods for Partial Differential Equations VII*, pages 28–34. IMACS, 1992.
- [8] G. Auchmuty and J. C. Alexander. L^2 -well-posedness of 3D div-curl boundary value problems. *Quart. Appl. Math.*, 63(3):479–508, 2005.
- [9] T. M. Austin, T. A. Manteuffel, and S. McCormick. A robust multilevel approach for minimizing $\mathbf{H}(\text{div})$ -dominated functionals in an \mathbf{H}^1 -conforming finite element space. *Numer. Linear Algebra Appl.*, 11(2-3):115–140, 2004.
- [10] G. R. Barrenechea and F. Valentin. Consistent local projection stabilized finite element methods. *SIAM J. Numer. Anal.*, 48(5):1801–1825, 2010.
- [11] G. R. Barrenechea and F. Valentin. A residual local projection method for the Oseen equation. *Comput. Methods Appl. Mech. Engrg.*, 199(29-32):1906–1921, 2010.
- [12] G. R. Barrenechea and F. Valentin. Beyond pressure stabilization: a low-order local projection method for the Oseen equation. *Internat. J. Numer. Methods Engrg.*, 86(7):801–815, 2011.
- [13] M. Benzi and M. A. Olshanskii. An augmented Lagrangian-based approach to the Oseen problem. *SIAM J. Sci. Comput.*, 28(6):2095–2113, 2006.
- [14] C. Bernardi and G. Raugel. Analysis of some finite elements for the Stokes problem. *Math. Comp.*, 44(169):71–79, 1985.
- [15] S. Börm and S. Le Borne. \mathcal{H} -LU factorization in preconditioners for augmented Lagrangian and grad-div stabilized saddle point systems. *Internat. J. Numer. Methods Fluids*, 68(1):83–98, 2012.
- [16] C. Brennecke, A. Linke, C. Merdon, and J. Schöberl. Optimal and pressure-independent L^2 velocity error estimates for a modified Crouzeix-Raviart Stokes element with BDM reconstructions. *J. Comput. Math.*, 33(2):191–208, 2015.
- [17] F. Brezzi, J. Douglas, Jr., and L. D. Marini. Two families of mixed finite elements for second order elliptic problems. *Numer. Math.*, 47(2):217–235, 1985.
- [18] A. Buffa, C. de Falco, and G. Sangalli. IsoGeometric Analysis: stable elements for the 2D Stokes equation. *Internat. J. Numer. Methods Fluids*, 65(11-12):1407–1422, 2011.
- [19] A. Buffa, J. Rivas, G. Sangalli, and R. Vázquez. Isogeometric discrete differential forms in three dimensions. *SIAM J. Numer. Anal.*, 49(2):818–844, 2011.
- [20] Y. V. Bychenkov and E. V. Chizonkov. Optimization of one three-parameter method of solving an algebraic system of the Stokes type. *Russian J. Numer. Anal. Math. Modelling*, 14(5):429–440, 1999.
- [21] C. Carstensen and C. Merdon. Computational Survey on A Posteriori Error Estimators for the Crouzeix–Raviart Nonconforming Finite Element Method for the Stokes Problem. *Comput. Methods Appl. Math.*, 14(1):35–54, 2014.
- [22] M. A. Case, V. J. Ervin, A. Linke, and L. G. Rebholz. A connection between Scott-Vogelius and grad-div stabilized Taylor-Hood FE approximations of the Navier-Stokes equations. *SIAM J. Numer. Anal.*, 49(4):1461–1481, 2011.
- [23] E. Chizonkov and M. Olshanskii. On the domain geometry dependence of the LBB condition. *M2AN Math. Model. Numer. Anal.*, 34(5):935–951, 2000.
- [24] P. G. Ciarlet. *The finite element method for elliptic problems*. North-Holland Publishing Co., Amsterdam, 1978. Studies in Mathematics and its Applications, Vol. 4.
- [25] B. Cockburn, G. Kanschat, and D. Schötzau. A note on discontinuous Galerkin divergence-free solutions of the Navier-Stokes equations. *J. Sci. Comput.*, 31(1-2):61–73, 2007.
- [26] M. Crouzeix and P.-A. Raviart. Conforming and nonconforming finite element methods for solving the stationary Stokes equations. I. *Rev. Française Automat. Informat. Recherche Opérationnelle Sér. Rouge*, 7(R-3):33–75, 1973.
- [27] M. Dobrowolski. On the LBB constant on stretched domains. *Math. Nachr.*, 254/255:64–67, 2003.
- [28] M. Dobrowolski. On the LBB condition in the numerical analysis of the Stokes equations. *Appl. Numer. Math.*, 54(3-4):314–323, 2005.
- [29] O. Dorok, W. Grambow, and L. Tobiska. Aspects of finite element discretizations for solving the Boussinesq

- approximation of the Navier-Stokes Equations. Notes on Numerical Fluid Mechanics: Numerical Methods for the Navier-Stokes Equations. Proceedings of the International Workshop held at Heidelberg, October 1993, ed. by F.-K. Hebekker, R. Rannacher and G. Wittum, 47:50–61, 1994.
- [30] J. A. Evans and T. J. R. Hughes. Isogeometric divergence-conforming B-splines for the steady Navier-Stokes equations. Math. Models Methods Appl. Sci., 23(8):1421–1478, 2013.
- [31] R. S. Falk and M. Neilan. Stokes complexes and the construction of stable finite elements with pointwise mass conservation. SIAM J. Numer. Anal., 51(2):1308–1326, 2013.
- [32] M. Fortin. An analysis of the convergence of mixed finite element methods. RAIRO Anal. Numér., 11(4):341–354, iii, 1977.
- [33] L. P. Franca and T. J. R. Hughes. Two classes of mixed finite element methods. Comput. Methods Appl. Mech. Engrg., 69(1):89–129, 1988.
- [34] J. Fuhrmann, A. Linke, and H. Langmach. A numerical method for mass conservative coupling between fluid flow and solute transport. Appl. Numer. Math., 61(4):530–553, 2011.
- [35] J. Fuhrmann, A. Linke, C. Merdon, F. Neumann, T. Streckenbach, H. Baltruschat, and M. Khodayari. Inverse modeling of thin layer flow cells for detection of solubility, transport and reaction coefficients from experimental data. Preprint 2161, WIAS, Berlin, 2015.
- [36] K. J. Galvin, A. Linke, L. G. Rebholz, and N. E. Wilson. Stabilizing poor mass conservation in incompressible flow problems with large irrotational forcing and application to thermal convection. Comput. Methods Appl. Mech. Engrg., 237/240:166–176, 2012.
- [37] V. Girault and P.-A. Raviart. Finite element methods for Navier-Stokes equations, volume 5 of Springer Series in Computational Mathematics. Springer-Verlag, Berlin, 1986. Theory and algorithms.
- [38] R. Glowinski and P. Le Tallec. Augmented Lagrangian and operator-splitting methods in nonlinear mechanics, volume 9 of SIAM Studies in Applied Mathematics. Society for Industrial and Applied Mathematics (SIAM), Philadelphia, PA, 1989.
- [39] J. Guzmán and M. Neilan. A family of nonconforming elements for the Brinkman problem. IMA J. Numer. Anal., 32(4):1484–1508, 2012.
- [40] J. Guzmán and M. Neilan. Conforming and divergence-free Stokes elements on general triangular meshes. Math. Comp., 83(285):15–36, 2014.
- [41] T. Heister and G. Rapin. Efficient augmented Lagrangian-type preconditioning for the Oseen problem using grad-div stabilization. Internat. J. Numer. Methods Fluids, 71(1):118–134, 2013.
- [42] P. Hood and C. Taylor. Navier–Stokes equations using mixed interpolation. In J. T. Oden, R. H. Gallagher, O. C. Zienkiewicz, and C. Taylor, editors, Finite Element Methods in Flow Problems, pages 121–132. University of Alabama in Huntsville Press, 1974.
- [43] E. W. Jenkins, V. John, A. Linke, and L. G. Rebholz. On the parameter choice in grad-div stabilization for the Stokes equations. Adv. Comput. Math., 40(2):491–516, 2014.
- [44] V. John and A. Kindl. Numerical studies of finite element variational multiscale methods for turbulent flow simulations. Comput. Methods Appl. Mech. Engrg., 199(13-16):841–852, 2010.
- [45] G. Kanschat and N. Sharma. Divergence-conforming discontinuous Galerkin methods and C^0 interior penalty methods. SIAM J. Numer. Anal., 52(4):1822–1842, 2014.
- [46] M.-J. Lai and L. L. Schumaker. Spline functions on triangulations, volume 110 of Encyclopedia of Mathematics and its Applications. Cambridge University Press, Cambridge, 2007.
- [47] W. Layton. Introduction to the numerical analysis of incompressible viscous flows, volume 6 of Computational Science & Engineering. Society for Industrial and Applied Mathematics (SIAM), Philadelphia, PA, 2008. With a foreword by Max Gunzburger.
- [48] W. Layton, C. C. Manica, M. Neda, M. Olshanskii, and L. G. Rebholz. On the accuracy of the rotation form in simulations of the Navier-Stokes equations. J. Comput. Phys., 228(9):3433–3447, 2009.
- [49] A. Linke. A divergence-free velocity reconstruction for incompressible flows. C. R. Math. Acad. Sci. Paris, 350(17-18):837–840, 2012.
- [50] A. Linke. On the role of the Helmholtz decomposition in mixed methods for incompressible flows and a new variational crime. Comput. Methods Appl. Mech. Engrg., 268:782–800, 2014.
- [51] A. Linke and C. Merdon. On spurious oscillations due to irrotational forces in the Navier–Stokes momentum balance. Preprint 2132, WIAS, Berlin, 2015.
- [52] A. Linke, C. Merdon, and W. Wollner. Optimal L^2 velocity error estimate for a modified pressure-robust Crouzeix–Raviart Stokes element. Preprint 2140, WIAS, Berlin, 2015.
- [53] A. Linke, M. Neilan, L. Rebholz, and N. Wilson. Improving efficiency of coupled schemes for Navier-Stokes equations by a connection to grad-div stabilized projection methods. Submitted, 2014.
- [54] C. C. Manica, M. Neda, M. Olshanskii, and L. G. Rebholz. Enabling numerical accuracy of Navier-Stokes- α through deconvolution and enhanced stability. ESAIM Math. Model. Numer. Anal., 45(2):277–307, 2011.

- [55] K. A. Mardal, X.-C. Tai, and R. Winther. A robust finite element method for Darcy-Stokes flow. SIAM J. Numer. Anal., 40(5):1605–1631, 2002.
- [56] P. Monk. Finite element methods for Maxwell’s equations. Numerical Mathematics and Scientific Computation. Oxford University Press, New York, 2003.
- [57] J. Morgan and R. Scott. A nodal basis for C^1 piecewise polynomials of degree $n \geq 5$. Math. Comput., 29:736–740, 1975.
- [58] J.-C. Nédélec. Mixed finite elements in \mathbf{R}^3 . Numer. Math., 35(3):315–341, 1980.
- [59] M. Neilan. Discrete and conforming smooth de Rham complexes in three dimensions. Math. Comp., 84(295):2059–2081, 2015.
- [60] M. Neilan and D. Sap. Stokes elements on cubic meshes yielding divergence-free approximations. Calcolo, pages 1–21, 2015. to appear.
- [61] M. A. Olshanskii. A low order Galerkin finite element method for the Navier-Stokes equations of steady incompressible flow: a stabilization issue and iterative methods. Comput. Methods Appl. Mech. Engrg., 191(47-48):5515–5536, 2002.
- [62] M. A. Olshanskii, G. Lube, T. Heister, and J. Löwe. Grad-div stabilization and subgrid pressure models for the incompressible Navier-Stokes equations. Comput. Methods Appl. Mech. Engrg., 198(49-52):3975–3988, 2009.
- [63] M. A. Olshanskii and A. Reusken. Grad-div stabilization for Stokes equations. Math. Comp., 73(248):1699–1718, 2004.
- [64] J. Pedlosky. Geophysical Fluid Dynamics. Springer, New York, 1986.
- [65] J. Qin. On the Convergence of Some Low Order Mixed Finite Elements for Incompressible Fluids. PhD thesis, Department of Mathematics, Pennsylvania State University, 1994.
- [66] P.-A. Raviart and J. M. Thomas. A mixed finite element method for 2nd order elliptic problems. In Mathematical aspects of finite element methods (Proc. Conf., Consiglio Naz. delle Ricerche (C.N.R.), Rome, 1975), pages 292–315. Lecture Notes in Math., Vol. 606. Springer, Berlin, 1977.
- [67] H.-G. Roos, M. Stynes, and L. Tobiska. Robust numerical methods for singularly perturbed differential equations, volume 24 of Springer Series in Computational Mathematics. Springer-Verlag, Berlin, second edition, 2008. Convection-diffusion-reaction and flow problems.
- [68] L. R. Scott and M. Vogelius. Conforming finite element methods for incompressible and nearly incompressible continua. In Large-scale computations in fluid mechanics, Part 2 (La Jolla, Calif., 1983), volume 22 of Lectures in Appl. Math., pages 221–244. Amer. Math. Soc., Providence, RI, 1985.
- [69] L. R. Scott and M. Vogelius. Norm estimates for a maximal right inverse of the divergence operator in spaces of piecewise polynomials. RAIRO Modél. Math. Anal. Numér., 19(1):111–143, 1985.
- [70] X.-C. Tai and R. Winther. A discrete de Rham complex with enhanced smoothness. Calcolo, 43(4):287–306, 2006.
- [71] L. Tobiska and R. Verfürth. Analysis of a streamline diffusion finite element method for the Stokes and Navier-Stokes equations. SIAM J. Numer. Anal., 33(1):107–127, 1996.
- [72] M. Vogelius. A right-inverse for the divergence operator in spaces of piecewise polynomials. Application to the p -version of the finite element method. Numer. Math., 41(1):19–37, 1983.
- [73] J. Wang, Y. Wang, and X. Ye. A robust numerical method for Stokes equations based on divergence-free $H(\text{div})$ finite element methods. SIAM J. Sci. Comput., 31(4):2784–2802, 2009.
- [74] J. Wang and X. Ye. New finite element methods in computational fluid dynamics by $H(\text{div})$ elements. SIAM J. Numer. Anal., 45(3):1269–1286 (electronic), 2007.
- [75] M. Wohlmuth and M. Dobrowolski. Numerical analysis of Stokes equations with improved LBB dependency. Electron. Trans. Numer. Anal., 32:173–189, 2008.
- [76] X. Xie, J. Xu, and G. Xue. Uniformly-stable finite element methods for Darcy-Stokes-Brinkman models. J. Comput. Math., 26(3):437–455, 2008.
- [77] S. Zhang. A new family of stable mixed finite elements for the 3D Stokes equations. Math. Comp., 74(250):543–554, 2005.
- [78] S. Zhang. A family of $Q_{k+1,k} \times Q_{k,k+1}$ divergence-free finite elements on rectangular grids. SIAM J. Numer. Anal., 47(3):2090–2107, 2009.
- [79] S. Zhang. Quadratic divergence-free finite elements on Powell-Sabin tetrahedral grids. Calcolo, 48(3):211–244, 2011.